STARS

University of Central Florida
STARS

Electronic Theses and Dissertations, 2020-

2022

Hydrogen and Peer-to-Peer Energy Exchanges for Deep Decarbonization of Power Systems

Hamed Haggi
University of Central Florida

 Part of the Power and Energy Commons
Find similar works at: https://stars.library.ucf.edu/etd2020
University of Central Florida Libraries http://library.ucf.edu

This Doctoral Dissertation (Open Access) is brought to you for free and open access by STARS. It has been accepted for inclusion in Electronic Theses and Dissertations, 2020- by an authorized administrator of STARS. For more information, please contact STARS@ucf.edu.

STARS Citation
Haggi, Hamed, "Hydrogen and Peer-to-Peer Energy Exchanges for Deep Decarbonization of Power Systems" (2022). *Electronic Theses and Dissertations, 2020-*. 1211.
https://stars.library.ucf.edu/etd2020/1211

HYDROGEN AND PEER-TO-PEER ENERGY EXCHANGES FOR DEEP DECARBONIZATION OF POWER SYSTEMS

by

HAMED HAGGI
M.Sc. K. N. Toosi University of Technology, Tehran, Iran, 2018

A dissertation submitted in partial fulfilment of the requirements
for the degree of Doctor of Philosophy
in the Department of Electrical and Computer Engineering
in the College of Engineering and Computer Science
at the University of Central Florida
Orlando, Florida

Summer Term
2022

Major Professor: Wei Sun

© 2022 Hamed Haggi

ABSTRACT

Decreasing costs of renewable energy resources and net-zero emission energy production policy, set by U.S. government, are two preeminent factors that motivate power utilities to deploy more system- or consumer-centric distributed energy resources (DERs) to decarbonize electricity production. Since, deep energy decarbonization cannot be achieved without high penetration of renewable energy sources, utilities should develop and invest in new business models for power system operation and planning during the energy transition. Considering the pathways to deeply decarbonize power systems, first, this dissertation proposes a novel hierarchical peer-to-peer (P2P) energy market design in active distribution networks. The framework integrates the distributional locational marginal price to a multi-round double auction with average price mechanism to integrate the network usage charges into the bills of customers. Second, this dissertation investigates the role of grid-integrated hydrogen (H2) systems for improved utility operations and to supply fuel to transportation sector. Power quality concerns as well as risk of uncertain parameters are considered using conditional value at risk based epsilon constraint method. Third, this dissertation proposes a bi-level proactive rolling-horizon based scheduling of H2 systems in integrated distribution and transmission networks considering the flexibility of these assets as controllable load or generation, in addressing the utility operators' normal and emergency operation signals. Fourth, a detailed model is developed for grid-integrated Electrolyzer considering polarization curve and non-linear conversion efficiency of these assets in the P2P enabled distribution network. This framework shows that reasonable penetration of P2P energy exchanges can significantly lower the H2 production cost. Finally, this dissertation proposes a cyber-physical vulnerability assessment of P2P energy exchanges in an unbalanced active distribution networks. Simulation results of this dissertation show the effectiveness of the proposed frameworks.

I dedicate this dissertation to my dear family.

For their endless love, support and encouragement throughout these years.

ACKNOWLEDGMENTS

First and foremost, I would like to express my sincere gratitude to my Ph.D. advisor Dr. Wei Sun for his endless support and patience throughout these years. His guidance and immense knowledge helped me a lot in all the time of my research and writing of this dissertation. I will always be grateful to him for having faith in me, help me to become an independent researcher, and for providing me with many interesting research opportunities. My academic success would not have been possible without his help and support for sure.

I am also grateful to have had a unique opportunity in our Hydrogen demonstration project team. I feel really fortunate to do research under supervision of Dr. James M. Fenton (Professor and Director of FSEC Energy Research Center), Dr. Paul Brooker (Supervisor at Orlando Utilities Commission), and Dr. Adam Paxson (Electrolyzer Program Manager of Plug Power Company) who helped me to be a better researcher and team worker in a real interdisciplinary project. I will always remember our Monday project meetings since I have learned a lot regarding how to look at the real world challenges from different perspectives.

My sincere thanks also goes to my Ph.D. Committee: Dr. James M. Fenton, Dr. Qifeng Li, Dr. Aleksandar Dimitrovski, and Dr. Zhaomiao Guo for providing me insightful comments which improved the quality of my dissertation. Thank to their time for serving in my committee and their support in my academic life.

Last but not least, I would like to express my sincere gratitude for my parents Leila and Abbas, and also my brother Hesam. I truly believe that all of my accomplishments are the results of their never-ending love and support.

TABLE OF CONTENTS

LIST OF FIGURES

LIST OF TABLES

CHAPTER 1: INTRODUCTION

Background

Continued reliance on fossil fuels for supplying the power and transportation sectors' demand contribute to the global warming crisis. According to the U.S. Energy Information Administration, electricity production accounts for 33% of annual carbon dioxide (CO2) emissions in which 65% of this amount is produced by large-scale coal and natural gas power plants [3]. Following the current trajectory, the global temperature is estimated to rise more than 3 °C on average by the year 2050. To avoid additional damage to the environment and maintain the temperature rise below 2 °C [1] (presented in Fig. 1.1) U.S. as well as many other countries set a goal in which the power sector, especially utilities and generation companies must supply their electricity demand with green energy by 2035, and the transportation sector must be electrified completely by 2050 [4].

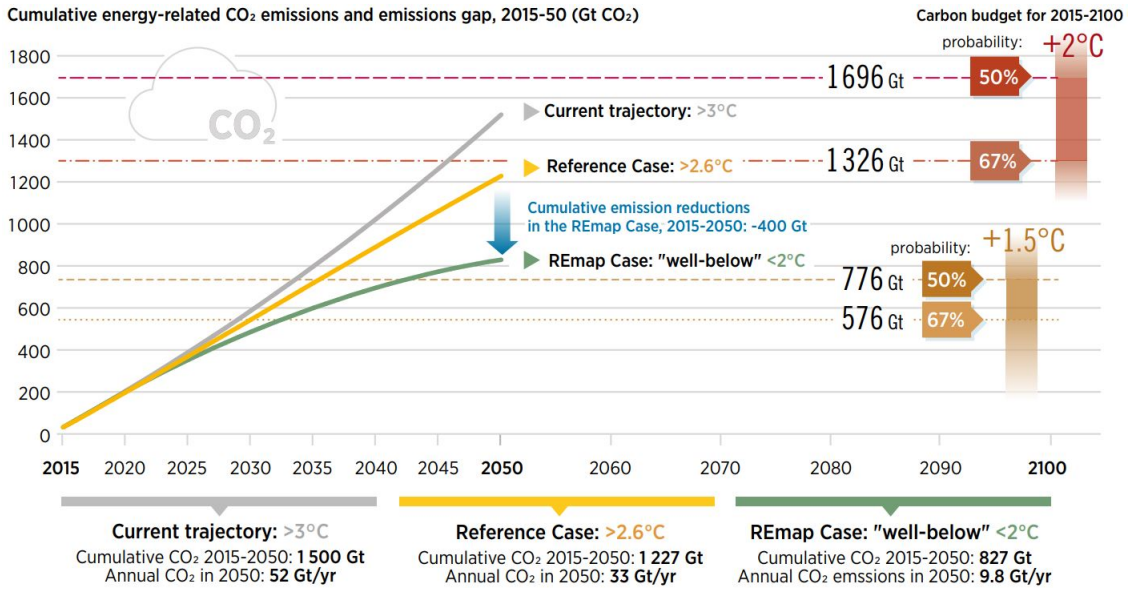

Figure 1.1. Temperature rise by the year 2050 for different cases: Following with current trajectory, reference case, and ideal case [1]

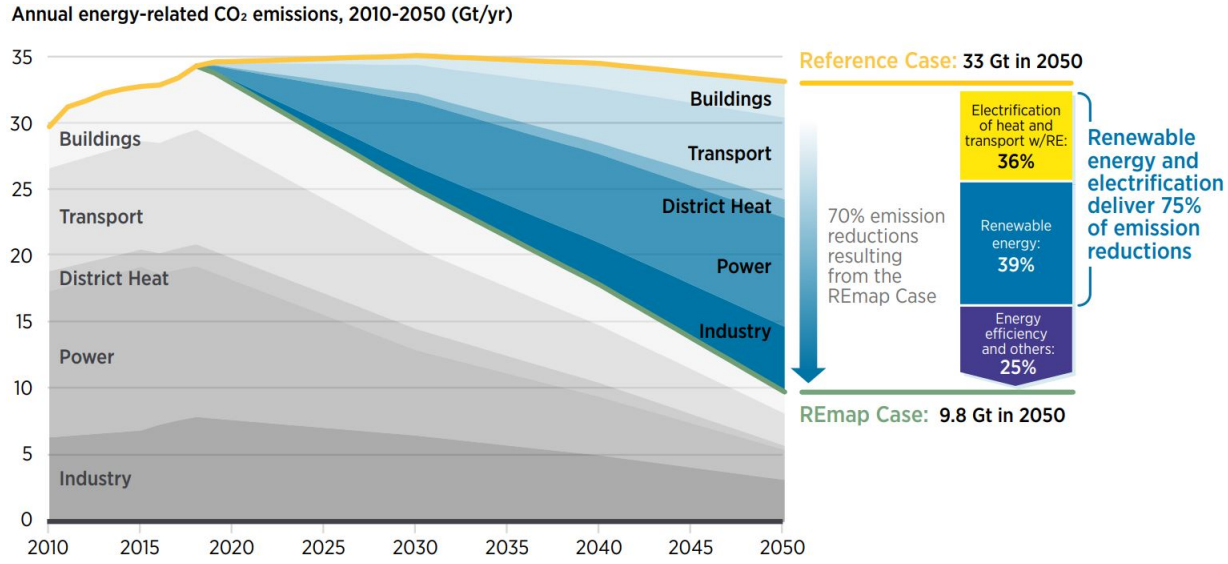

Figure 1.2. Emmission reduction using renewable energy and electrification by the year 2050 [1].

This goal results in eliminating the carbon footprints (as much as possible) by mid-century Fig. 1.2, a goal that generally is defined as ”Deep Decarbonization”. In the quest for power system deep decarbonization, different pathways must be considered to achieve the goal of net-zero emission energy production including government policies, priorities, realistic targets, and business models and cost targets [5]. More specifically, deep decarbonization requires 1) high penetration of distributed energy resources (DERs) such as wind, solar, storage, etc. to supply the current and forecasted electricity demand, 2) reductions in total energy consumption using more efficient smart grid technologies, 3) government support and policies by sending strong price incentives for using clean energy and penalties for carbon based electricity generation 4) realistic targets by considering the challenges of modern power systems' operation, planning, economic, and resilience.

Motivation and Challenges

Over the past decade, advancement in smart grid technologies results in significant reduction in capital costs of DERs and electricity bill reduction. According to the National Renewable Energy Lab's (NREL) reports the capital costs of these technologies will drop by 60%-70% by the year 2050 [6], accelerating the growing trend of utilizing utility-operated and small-scale consumer-centric DERs. This trend along with net-zero emission energy production policy motivates power utilities to supply the electricity demand by taking advantage of small-scale DERs. However, going forward, large-scale deployment of these DERs in distribution networks can impose significant technical challenges (such as bidirectional power flows, voltage fluctuations due to DERs power injection, congestion issues, etc.) since the current distribution systems' structure are not designed based on these challenges. In addition to the technical challenges, the business models in distribution systems are different from wholesale market due to the large number of agents. Furthermore, the current utility market designs cannot provide incentives to the small-scale DERs owners to share the energy with the grid.

Considering the pathways to deep decarbonization of power systems in both normal and emergency modes, long-term energy storage technologies are required for storing energy for longer duration since Li-ion and redox flow batteries are limited to their energy capacity [7]. For instance, a 4-hours duration battery cannot charge or discharge energy more than 4 hours with the maximum power rating. This renders utilities to use better energy storage technologies with longer duration. Recently, renewable H2 energy with its promising technical, economic, and environmental merits has demonstrated great potential for large deployment in distribution systems [8]. H2 energy can be produced, stored, and consumed using an electrolyzer, a reservoir tank, and fuel cell (FC) unit, respectively for improved utility operations. Apart from power sector, renewable H2 energy can be considered as a clean fuel for transportation sector especially heavy-duty road transport, deep

sea shipping and aviation. However, how and where to invest these technologies as well as market benefits of H2 energy while addressing policies and physical constraints of power networks are challenges that researchers pay attention.

Outline of the Dissertation

Considering the motivations and challenges discussed in the previous sections, Fig. 1.3 presents the outline of this dissertation which aims to provide decision making tools to overcome the challenges during the transition to carbon free power systems. The following paragraphs will specifically present the outline of this dissertation.

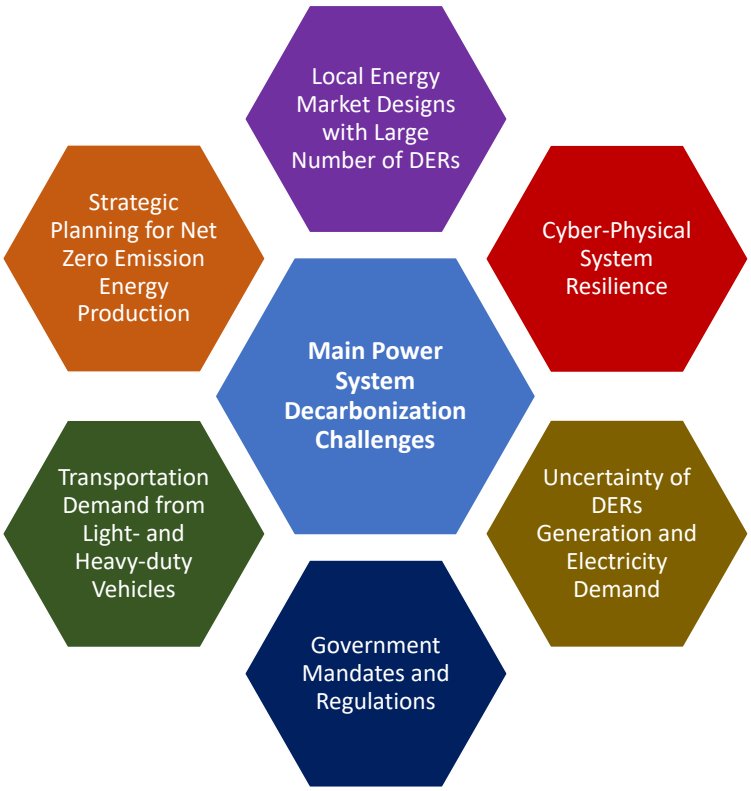

Figure 1.3. Power system deep decarbonization transition challenges.

Chapter 2 presents a comprehensive review for local energy markets with the focus on Peer-to-Peer energy trading in the first section. The business and physical layers as well as market settlement time aspects were compared. In the second section, a comprehensive review on techno-economic analysis of H2 systems with the focus on economic and resilience perspective is presented.

Chapter 3 proposes a multi-round double auction based Peer-to-Peer energy trading in active distribution networks. The entire distribution network clustered into multiple zones with transactions cleared at different levels, which decreases the additional costs for successful transactions, reduces the computational time, and increases the number of successful transactions. The proposed hierarchical framework considers distribution network physical constraints and present a strong budget balance market clearing mechanism for peers who successfully negotiate. Additionally, extra network usage costs for each transaction, such as power loss cost, voltage regulation cost, etc., into the payments of all prosumers and consumers, through distributional locational marginal component decomposition.

Chapter 4 proposes a multi-objective network-constrained framework for the day-ahead scheduling of hydrogen systems, including hydrogen production from water electrolysis by electrolyzers, hydrogen storage, stationary fuel cells, and fueling of fuel cell electric vehicles. This framework includes various physical constraints to ensure reliable operation and considers integrated demand response and conservation voltage reduction, and reactive power support from hydrogen systems for realistic day-ahead scheduling. It also incorporates the cooperative operation of PV units and hydrogen systems to supply power for water electrolysis from stationary hydrogen systems equipped with onsite PVs. Moreover, Conditional Value-at-Risk is applied to address the risk of PV output, H2 demand, loads, and market price.

Chapter 5 proposes a proactive rolling-horizon-based scheme for resilience-oriented operation of hydrogen systems in integrated distribution and transmission networks. The proposed framework

is a bi-level model in which the upper-level is focused on distribution system operation in both normal and emergency operation modes, and the lower-level problem accounts for the transmission network operation. To show the flexibility of H2 systems, capacity-based demand response signals are considered in both normal and emergency operation modes. Moreover, Unlike the batteries which can only charge and discharge energy based on maximum duration times and power ratings, H2 systems can be considered as the flexible long-term energy storage by storing H2 for days and supplying power to fuel cell in the case of *N-m* outages lasting for more than 10 hours. Moreover, H2 production cost based on water electrolysis and storage costs is calculated through distributional locational marginal.

Chapter 6 proposes a detailed model for grid-integrated electrolyzer operation based on polarization curves and variable efficiency under different operating conditions (different temperature, pressure, H2 demand, etc.). The model is integrated to an P2P enabled active distribution network under optimization framework. This study clearly shows that customer side DERs and accordingly P2P markets can contribute to the low-cost H2 production due to reducing the residential demand of customers, increasing the available capacity of renewables, and as a consequence reducing the distributional locational marginal price (DLMP) and H2 production cost.

Chapter 7 proposes a framework to assess the vulnerability of P2P energy exchanges to cyber-physical attacks in an unbalanced distribution network. In this study, a three phase P2P model is developed and integrated to Distflow model. various scenarios for vulnerability assessment of P2P energy exchanges considering adverse prosumers and consumers, who provide false information regarding the price and quantity with the goal of maximum financial benefit and system operation disruption, are considered.

Finally, Chapter 8 conclude the dissertation and presents the future works as potential extensions of these works.

CHAPTER 2: LITERATURE REVIEW

Peer-to-Peer Energy Trading Literature Review

The large-scale deployment of DERs and information and communication technologies (ICT) enables the emerging of pro-active consumers known as prosumers, with the capability of both producing and consuming energy in active distribution networks [9]. During certain times of a day, prosumers can sell their surplus energy to other consumers for monetary benefits, provision of ancillary services to the grid, etc. The energy exchange among prosumers and consumers could be enabled through peer-to-peer (P2P) energy trading. However, the distribution system operator (DSO) cannot manage large number of participants in the distribution energy market, due to the inaccessibility to real-time data and the behavior of market participants (e.g. offered prices, utilities of agents, and the amount of energy to be traded). Therefore, it is motivated to explore the possibility of building a P2P energy trading market under DSO's control.

The recent development of P2P market-oriented pragmatic projects include 1) design and modeling of the P2P market, e.g. Enerchain [10], NRGcoin [11], and P2P community energy trading with multi-time, multi-scale, and multi-qualities (P2P3M) [12]; and 2) implementation of control and ICT platform for prosumers, e.g. EMPOWER, Smart Watts, and Community First Village [13]. Besides practical P2P projects, research efforts on local energy market designs can be generally divided into three categories: 1) Business layer focusing on market structures and tools; 2) Physical layer; and 3) Market settlement time of local market with various considerations.

Business Layer

Different research studies in this layer can be categorized into two main directions: market structures and market tools.

Market Structure

There are various literature works on the market structure including, centralized, decentralized, and fully distributed designs. In the centralized design, DSO solves the optimal power flow (OPF) to obtain the optimal scheduling of DERs and clears the market with DLMP, derived from the duality analysis of network energy balance constraint, using second-order cone programming (SOCP) relaxation [14–16]. It is assumed that detailed information regarding agent behaviors, bid price, amount of energy to be traded, etc. must be accessible to system operators to schedule the generating units and DERs. Therefore, effective market mechanisms should be designed to extract this hidden information and consider consumers as price maker entities in local market designs.

On the other hand, decentralized and distributed designs address the challenges by sharing limited private information for decision-making. For instance, in [17], a decentralized DLMP-based market is presented considering a novel method for convergence acceleration by removing redundant Lagrangian multipliers. A market framework for decentralized congestion management using mobile distributed storage is presented in [18]. Alternating direction method of multipliers (ADMM) and dual decomposition are examples of fully distributed solution algorithms to solve DERs dispatching through sharing limited information among neighboring nodes [19, 20]. Besides, addressing the privacy of agents regarding the data sharing, the major concern of distributed techniques in local market designs is the convergence issue, which results in high computational time due to the potentially large number of market participants in the distribution network [21].

Market Tool

Recently, there has been preeminent attention on local energy markets based on P2P energy exchanges, which provides a platform for direct negotiations between prosumers and consumers. To this end, proper market mechanisms and structures are needed to enable this platform for agents. Research studies on P2P energy trading can be categorized into three different directions: a) Auction-based P2P markets; b) Game theory-based P2P markets; and c) Blockchain-based P2P markets; as well as the Hybrid methods combining both market structures and market tools, such as blockchain-based distributed P2P energy trading [22]. Each category is discussed below in details.

Auction-based P2P Market

An iterative double auction for enabling localized P2P electricity trading is proposed in [23] considering consortium blockchain technology. The major focus of this chapter is the balance between local generation units and local demand. However, not considering the network constraints may significantly affect the matching results between prosumers and consumers due to the physical limits of power system operation. To address this limitation, a decentralized P2P energy trading based on continuous double auction is proposed in [24], by considering the network's physical constraints. However, the proposed model fails to address the additional network charges which significantly affect matching results, such as the cost-saving of consumers and the profit of prosumers. Additionally, some agents may participate in the market with better prices, but due to communication delays, they may miss the opportunity to trade with more consumers/prosumers (e.g. the first-come-first-serve rule). Moreover, trading with neighboring agents as well as motivating agents to participate in the P2P market has not been addressed in the auction-based market designs and need proper mechanism to address the limitation of auction-based P2P designs.

Game theory-based P2P Market

Game theory is another market tool that affects/depends on the agents' decisions based on the action of other agents in P2P markets. The general form of this approach is known as the multi-leader multi-follower game. Considering the cooperative game theory approaches, a Stackelberg game is proposed for P2P energy trading in [25, 26], in which a unique and stable equilibrium can be achieved. Another Stackelberg game-theoretic approach for P2P energy trading in virtual microgrids is proposed in [27], considering load demand uncertainty and modeling the communication layer. Since game theory approaches depend on agents' behavior (leader-follower rule), a psychology-based motivational game-theoretic approach for P2P energy trading is investigated in [28] considering human behaviors. Apart from cooperative designs, a novel P2P energy sharing model as a non-cooperative game is proposed in [29] for energy sharing among buildings equipped with heating, ventilation, and air conditioning (HVAC) units and renewable energy units. The major deficiencies of the aforementioned research efforts are not considering the physical network constraints and additional costs associated with transactions, which significantly affect the P2P market outcomes. Additionally, game theory-based models heavily depend on iterative mechanisms to find the solution and render the model to converge in a longer time period for a system with large number of prosumers and consumers.

Blockchain-based P2P Market

Blockchain technology is another appropriate tool for P2P-based energy sharing mechanisms, with the characteristics of distributed data sharing among agents, privacy, and no need for a central entity. A comprehensive and systematic classification on P2P topics including different trading mechanisms, physical and communication layers, technical approaches, future blockchain-based P2P trading fundamentals, etc. is provided in [30]. P2P transactive energy exchange in local energy

markets is studied in [22] based on blockchain-based technologies. Consortium Blockchain-based energy trading to reduce cost and balance between load and generation for electric vehicles are presented in [23, 31, 32]. The aforementioned studies are mainly focused on the balance between generation and load without fully considering the network constraints and additional costs for each transaction. Although the transparency, privacy, and security of transactions increase by using blockchain technologies, trading mechanisms, grid constraints, and the role of prosumers and consumers on defining the matching price as well as additional costs must be addressed in blockchain-based P2P-based markets.

Hybrid Method-based P2P Market

The hybrid methods for P2P energy sharing are the combination of market tools and market structures. For instance, an iterative mechanism is introduced in [33] for peer and system-centric trading, with a strong assumption that DSO has the access to all required information about prosumers and consumers to clear the market. Additionally, consumers are considered as price taker entities in this method which neglects the role of consumers in P2P markets. Considering the flexibility of loads, authors of [34] propose a P2P local market for the joint trading of energy and uncertainty associated with local generation. This P2P model is proposed to trade forecasted PV power and uncertain power due to forecast error without considering grid constraints. Besides, different designs such as bilateral and auction-based P2P energy trading are reviewed in [35]. Bilateral contract-based designs are investigated in [36–38]. However, the hybrid methods presented in this section mainly follow the iterative process which significantly increases the computational time in distribution systems with a large number of market participants. Another factor that may increase the time of P2P matchings is the price adjusting factors, in which smaller values will increase the computational time.

Physical Grid Layer and Market Settlement Time

Besides price matching among peers, physical constraints of power systems like the voltage, power flows, etc. need to be considered for energy trading. The deficiencies of the iterative-based approaches have been explained in the previous sections. For auction-based P2P energy sharing, which is the more appropriate modeling since both prosumers and consumers can be considered as price maker entities, only [24] addresses network constraints. However, this study fails to address the additional costs associated with every transaction and consequently the revenue/payment of prosumers and consumers. Moreover, with the proposed method in [24], many P2P matchings satisfying the physical constraints may be subjected to rejection due to uneconomical reasons, e.g. the extra costs. On the other hand, many transactions could be finally rejected because of both uneconomical matchings and network constraint violations. Therefore, proper mechanisms are required for addressing these issues in auction-based P2P energy tradings, which have not been fully investigated yet.

Besides technical layer designs, the market settlement time of the aforementioned research efforts is another preeminent factor in designing P2P markets. The majority of papers are focused on the day-ahead operation of distribution network. However, P2P energy sharing depends on agents' participation, whose behaviors can change during the day. Besides, the uncertainty of loads and DERs must be modeled with high accuracy to ensure the reliable operation of the network. Considering the real-time aspect of P2P energy trading, iterative-based studies cannot be applicable due to the large number of agents' participation and price adjusting factors, which significantly increases the computational burden or the convergence time.

A large number of prosumers and consumers in P2P designs are equipped with IoT devices to share required information with each other or system operators. The information exchange happen through the communication layer of P2P designs and transactive energy markets. However, the communication and physical layers of P2P-enabled distribution network models are in danger of cyber-physical attacks. For instance, various data manipulation and false data injection attacks in power systems are reviewed in [39, 40]. A cooperative learning-based decentralized P2P energy trading market with considering cyber issues is proposed in [41]. In [42], a blockchain-based transactive energy market defense behavior against denial of service attacks is investigated. Cyber-physical security against data manipulation for transactive energy systems considering ventilation, heating, and air conditioning (HVAC) is analyzed in [43–45].

P2P energy trading frameworks presented in [46]- [30] are mainly focused on various market mechanisms, while some of them are focused on modeling the physical network constraints and transaction charges in balanced distribution networks. However, the real distribution networks are phase unbalanced, and proper modelling efforts are required to integrate P2P models to unbalanced systems. Moreover, these research studies are only focused on the normal operation of system, and neglect to consider the emergency operation in the case of disruptions such as natural disasters, cyber attacks, etc. Research works presented in [39]- [47] review the potential cyber-physical threats in highly DER penetrated power systems. Only in [43–45] the impact of false data injection on HVAC systems is investigated. There is no modelling effort for resilience-oriented P2P interactions in unbalanced network considering the physical constraints such as voltage, line loading, congestion, etc.

Techno-economic Analysis of H2 Systems Literature Review

H2 Systems Scheduling and Market Analysis in Normal Operation mode

Emission caused by fossil fuels and their impact on climate change has prompted the research in cleaner and sustainable energy form (e.g. photovoltaic (PV), wind, hydrogen (H2), etc.), for electricity generation. However, due to different penetration levels and the stochastic nature of these resources, new and challenging scenarios are emerging in the operation of power systems [48]. Among the aforementioned energy sources, H2 energy has demonstrated a great potential for large deployment in the future from economic, environmental, and technical viewpoints.

H2 energy can be produced, stored, and consumed using an electrolyzer, a reservoir tank, and fuel cell (FC) unit, respectively for assisting the power and transportation sectors. There are various technologies for water electrolysis such as alkaline, polymer electrolyte membrane (PEM), and solid oxide electrolysis, in which electricity is used to convert water into oxygen and hydrogen [49, 50]. The generated H2 can be stored in a reservoir tank, in the form of liquid or gas through high pressure. During off-peak generation, H2 energy can be converted into electricity using FC units, to supply loads or directly sold in the hydrogen market [51].

Different applications of H2 energy are, 1) power generation with stationary FC units; 2) transportation fuel for fuel cell electric vehicles (FCEVs), trucks and railways; 3) fuel for residential and commercial buildings (e.g. space and water heating); 4) feedstock for ammonia production, or at refineries, etc. More details regarding various applications of H2 energy can be found in [52] [53]. From an environmental aspect, using FCEVs over internal combustion engines and using distributed FC units rather than centralized power plants, are two main reasons that result in 16% CO_2 and 36% NOx emission reductions [53].

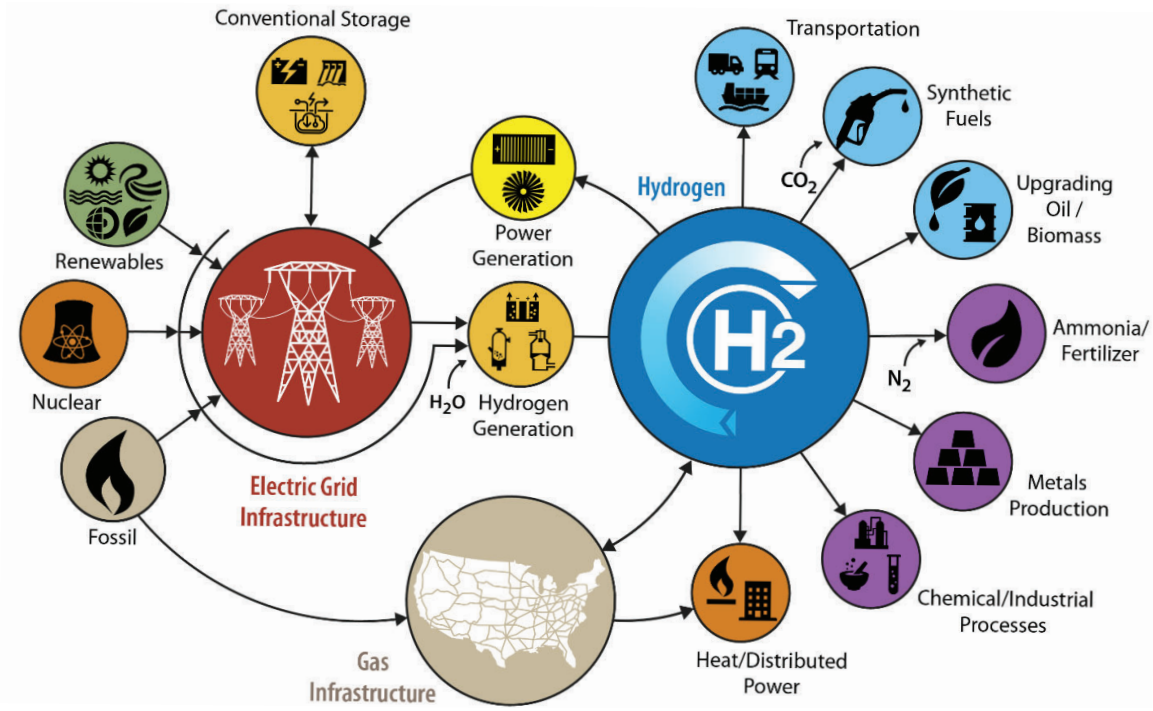

Figure 2.1. H2 energy applications in power in industry [2]

Research work in the literature has been focused on various aspects of H2 systems (HS), such as chemistry and material research of HSs' components, for use in the transportation sector, power system, etc. This chapter is mainly focusing on the operation scheduling and techno-economic analysis of HS. In this dissertation, it is assumed that HSs can be operated as 1) H2 fueling stations (to produce H2, store it, and supply the H2 demand of transportation sector) 2) long-term energy storage in which the H2 is produced by electrolyzer, store in reservoir tank, and be consumed by FC unit to assist the power grid from economical and technical aspects.

Centralized scheduling of distributed HFS under dynamic H2 pricing is proposed in [51] considering the capacity-based demand response (DR). A supervisory-based framework for optimal scheduling of distributed HFS is proposed in [54], in which the central entity uses the total reserved capacity to assist the grid operation. In [55], optimal operation management for centralized and

distributed electrolysis-based H2 generation and storage systems was developed to maximize the net revenue of private investors. In [56], an operating cost minimization model was proposed for scheduling H2 production to meet the H2 demand of HS. An economic feasibility study of selling H2 energy in the H2 market was investigated in [57] for the HSS integrated with the power grid. The techno-economic analysis and feasibility study of industrial plants including HSS were investigated in [58]. Another design framework is proposed in [59] considering the best design for HFS, in terms of the number of banks, size, and cost. Moreover, optimal scheduling of H2 storage to minimize cost and emission was studied in [60] considering DR and renewable energies. A capacity estimation framework for wind, FC, and solar was proposed in [61]. To address the uncertainty of renewables in HS operation, [62] proposed a multi-objective framework to address the power quality concerns as well as cost minimization for HS operation scheduling. In [63], an energy management framework considering fuel cell and combined heat and power technologies was proposed. A decentralized local energy market for electricity and H2 trading was proposed in [64] through a multiplayer game-based market clearing algorithm with the privacy preservation of market participants. Stochastic scheduling of H2 storage with wind and DR was investigated in [65, 66]. The authors proposed a distributed cooperative framework for wind and HFS operation using Nash bargaining theory in [67], considering uncertainties of wind power production and electricity price.

H2 Systems scheduling for Enhancing Resilience of Power Systems

Proliferation of DERs and smart grid technologies, have driven the power systems more complex and vulnerable to cyber-physical-human (CPH) threats and climate disasters [68] [69]. These threats can significantly affect the operation of power systems, especially distribution networks due to the radial topology, limited backup power, and overhead line outages [70]. To increase the system resilience and minimize the impact of these high-impact low-probability events on

power systems in both normal and emergency operation, proactive schemes must be considered by utilities, such as using flexible DERs (e.g. energy storage, microgrids, etc.), to provide backup power sources for delivering power especially to the critical loads.

Generally, the power systems resilience can be improved by proactive plans prior and after a disruption, survivability analysis, and restorative schemes. Since the scope of this dissertation is proactive scheduling plans, the authors only reviewed the related proactive and survivability research efforts in resilience enhancement topic (more details regarding the post-event and restoration part can be found in our previous work [70]). For instance, in [71], a stochastic model was developed for preparatory operation of distributed energy storage systems prior to hurricanes. Additionally, post-event decisions were also considered to enhance the resilience by restoring the critical loads. Authors of [72] proposed a two-stage adaptive robust approach to enhance the resilience by minimizing the damaging consequences using microgrids. In [73], both normal and emergency operation considering resilience cut for battery energy storage and microgrids were considered to improve the resilience of system. Moreover, uncertainties of loads and renewable generation were considered in their model. A proactive linearized plan was proposed in [74] using microgrids to cope with windstorms. Network reconfiguration, demand side management, etc. were considered to prevent load curtailment. Moreover, these authors' work was extended by considering both electric and gas networks [75].

System operators can schedule their assets, especially DERs, to prevent damages which may be caused by natural disasters or CPH threats. In the recent years, H2 energy is of great interest of researchers due to its environmental and technical merits in both power and transportation networks. To this end, different applications of H2 energy have been mainly focused on, 1) power generation by FC units for grid balancing purposes, 2) fuel for transportation sector by supplying the H2 demand of heavy duty trucks, fuel cell electric vehicles (FCEVs), and aviation sector, 3) feedstock for industry such as ammonia production, etc. [52]. For instance, authors of [54] proposed a model

in which distributed H2 fueling stations participate in reserve market based on their free capacity to increase the profit. In [51], H2 fueling stations (including electrolyzer and storage tank) were optimally scheduled considering the demand response signals with the aim of maximizing the total profit of private owner of these distributed fueling stations.

A design for onsite H2 production was proposed in [56] with the goal of minimizing the operational cost as well as supplying the H2 demand of fuel cell vehicles. A techno-economic feasibility analysis including H2 energy storage systems was investigated in [58]. A decentralized game theory-based local market for H2 and electricity trading considering the H2 vehicles demand was investigated in [64]. Authors of [67] proposed a distributed coordinated operation framework for wind and H2 fueling stations considering uncertainty of wind and electricity price.

CHAPTER 3: MULTI-ROUND DOUBLE AUCTION-ENABLED PEER-TO-PEER ENERGY EXCHANGE IN ACTIVE DISTRIBUTION NETWORKS [1]

Introduction

DERs, together with information and communication technologies, have transformed the traditional electricity consumers into proactive consumers, namely prosumers. Prosumers can exchange their surplus energy with consumers through peer-to-peer (P2P) energy sharing. In this chapter, the framework of P2P energy exchange in active distribution networks is developed using a multi-round double auction (MRDA) with average pricing mechanism (APM) integrated with distributional locational marginal price. The advantages of the proposed P2P framework include, 1) modeling and integration of the costs of voltage regulation, congestion, and power loss into the payments of agents for each transaction; 2) the entire distribution network clustered into multiple zones with transactions cleared at different levels, which decreases the additional costs for successful transactions, reduces the computational time, and increases the number of successful transactions; and 3) the matching algorithm encourages more prosumers and consumers to participate in P2P energy sharing and increases the efficiency and benefit from P2P market. The proposed MRDA-APM framework is validated by testing on the 33-node and 141-node distribution test systems. Simulation results demonstrate the effectiveness of the proposed mechanism for P2P energy exchange from both technical and computational viewpoints.

The major limitation of the market structure category is the computational time and hidden in-

[1] This chapter is prepared based on the paper presented at [76]:
Hamed Haggi and Wei Sun, "Multi-Round Double Auction-enabled Peer-to-Peer Energy Exchange in Active Distribution Networks," *IEEE Transactions on Smart Grid*, Vol. 12, No. 5, pp. 4403-4414, 2021.[Link]

formation accessibility. Since the studies in this category consider iterative-based approaches, computational time will be a major concern due to the large number of DERs in real distribution networks. This limitation can also be seen in game-theory-based models, since every action of an agent significantly depends on other agents' actions, and the feasible solution is achieved after exploring all possible matching scenarios. Therefore, the most appropriate design for the real-time P2P market is auction-based designs. However, considering the physical constraints of power networks as well as allocating extra costs like power loss, congestion, voltage regulation are the limitations of previous studies. Furthermore, due to the violations of network constraints, many transactions are rejected because of voltage issues or high loss costs among peers. Therefore, forming zones based on the DLMP signals in the distribution network (with at least one prosumer and one consumer per zone) can improve the success rate of transaction approval and reduce the extra costs of each transaction for both prosumers and consumers. Moreover, how to encourage and motivate small-scale prosumers to participate in the P2P market and make the design more reliable are another limitations that need to be addressed.

To address the aforementioned challenges, a multi-round double auction with an average price mechanism (MRDA-APM) integrated with DLMP components is proposed for P2P energy sharing in active distribution networks. The major contributions of the proposed P2P framework are:

- The proposed multi-round double auction provides the flexibility of matchings in bottom-up order (nodal, zonal, and distribution network layer), and encourages prosumers to first negotiate with consumers in nodal, zonal levels, and then seek for possible matchings in the distribution-level auction. The proposed hierarchical auction increases the benefit of agents by reducing additional costs through three rounds of auction. Additionally, the computational time is less compared to the existing iterative-based P2P designs.
- The proposed MRDA-APM algorithm is strongly budget balanced. Therefore, the auctioneer

(DSO) never benefit directly from running the auction. Additionally, the proposed MRDA preserves the rights of agents and increases the motivation of P2P market participants, especially small-scale prosumers, to benefit from P2P market which improves the market efficiency.

- Unlike previous auction-based P2P energy trading mechanisms, the proposed auction-based framework integrates the DLMP to model the additional costs, using components of power loss, congestion, and voltage regulation associated with each transaction; and also integrates these costs into the payments of both prosumers and consumers with equal cost splitting, which enables both prosumers and consumers to share the costs equally for energy trading.

Proposed Peer-to-Peer Energy Trading Framework

The proposed P2P energy trading framework is shown in Fig. 3.1, consisting of three main steps as following.

Extracting Hidden Information of Agents

The first step is to collect the information from all agents who are willing to participate in the P2P market. DSO extracts the information from the participating consumers and prosumers, such as ask and bid prices, amount of power to be traded, by sending two price signals to agents. First, DSO sends a feed-in tariff (FIT) price signal to all prosumers. If prosumers with surplus energy are willing to participate in the P2P market, they should respond to this signal by sharing the information of ask price and the amount of power to be traded with DSO; otherwise, prosumers cannot participate in the market for trading time interval. It is worth mentioning that the FIT price signal is defined as power purchase agreements between utilities and prosumers. In this chapter,

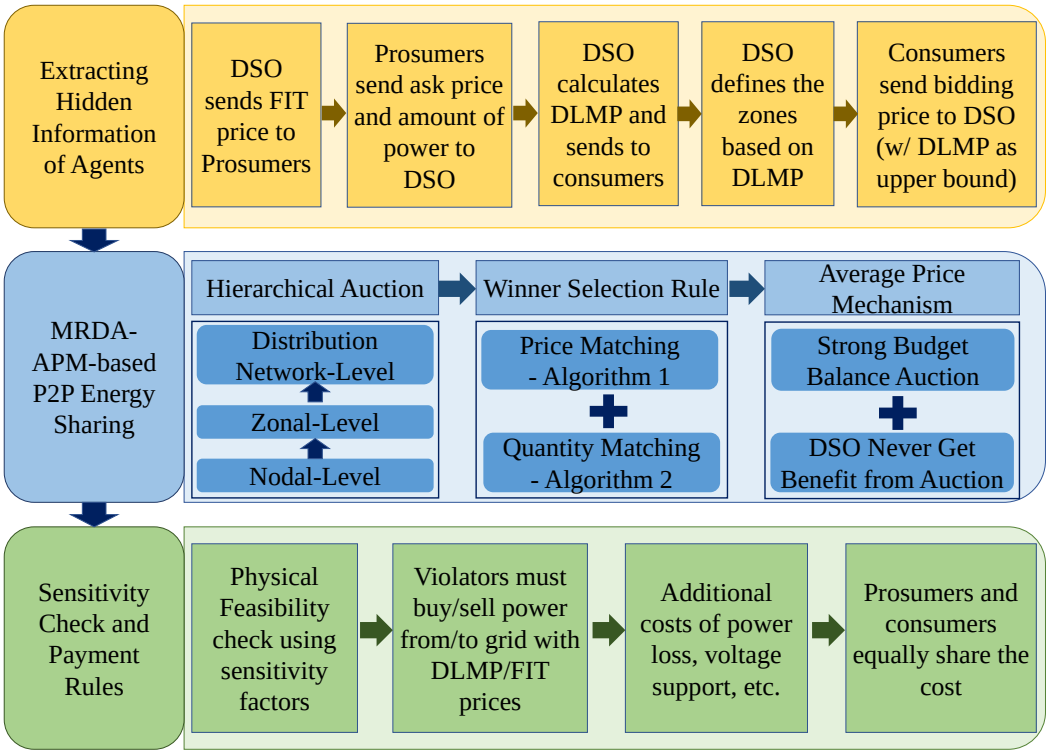

Figure 3.1. Proposed P2P energy sharing framework in distribution network.

the FIT price signal is considered in a way to incentivize prosumers to trade their energy with the grid even if they lose all rounds of the auction in P2P market. Next, after gathering the information of price and amount of power from participating prosumers, DSO calculates DLMP and sends this price signal to consumers. It is worth noting that this price signal is calculated based on the forecast of consumers' consumption level and the generation output of utility-operated distributed generators (DGs), as well as prosumers ask price and amount of power. Then consumers use this price signal as the upper bound to decide and send the bidding price back to DSO. Finally, DSO obtains all required information for running the auction.

MRDA-APM-based P2P Energy Sharing

After gathering all information from prosumers and consumers, including ask/bid prices, amount of surplus power, and requested demand, DSO starts the P2P energy trading with a hierarchical auction (MRDA). The hierarchical auction first starts from the nodal auction to balance the total demand of prosumers and consumers located in the same node. Next, prosumers and consumers trade in the zonal auction, and finally in distribution network (DN)-level auction. It should be noted that the zones are defined based on the criteria of similar DLMP values, including at least one prosumer, and the location in one neighborhood. Each agent is assigned with an identification (ID) number based on the node, zone, and DN number (e.g. N12Z3D1 denotes an agent located in node 12, zone 3 of first DN). The advantage of the MRDA design is to achieve more benefits by sharing energy with closest neighbors, save additional costs, and reduce the possibility of transaction rejection due to power loss, congestion, or voltage regulation. If agents fail to match in nodal, zonal, or DN-level auction, prosumers sell surplus power with the FIT price to the grid, and consumers purchase electricity from the grid with the DLMP price at their locations. Moreover, due to a large number of agents, the proposed MRDA-APM algorithm has other advantages of preserving the right of each market participant to benefit from the P2P market, through providing opportunities for all agents to participate in P2P market and keeping agents motivated to participate in next P2P market. More details and explanations will be explained in Section IV. It should also be mentioned that three auction rounds are needed to complete the MRDA-based P2P market.

In this chapter, the cleared price of matched peers is the average of prosumer and consumer offering prices based on the APM. The preeminent advantage of the APM mechanism over traditional market-clearing prices is to enable the strong budget balance auction, in which all benefits from traded energy are equally dispersed among matched peers. Additionally, the MRDA-APM design satisfies other economic criteria such as individual rationality and truthfulness. It is worth noting

that the framework doesn't involve the bidding strategy design for P2P market participants or consider more options from storage systems and demand response.

Sensitivity Check and Payment Rules

DSO is responsible for checking the security of transactions to determine whether the energy tradings between matched peers violate any network constraints or not, using sensitivity factors to block high-risk transactions. Once transactions satisfy the physical check, additional network costs, such as voltage regulation cost, power loss cost, etc., for every matched transaction, will be integrated into payments of both prosumers and consumers. These cost items can be calculated by the decomposition of DLMP components. Upon the final approval by DSO, prosumers and consumers split the additional cost, which the ratio could be adjusted by the market operator. In this chapter, the simplest ratio is considered and assumed to be 50%.

Problem Formulation

The radial distribution network is represented as a graph (N, E), where N and E are the set of nodes and edges, respectively. The root node is numbered as 0, and the set of all other nodes is defined as $N^+ = N - \{0\}$. The set of nodes connected with DERs as prosumers is denoted as $S = \{1, 2, ..., N_s\}$, and all other nodes with demand are considered as consumers, with the set defined as $B = \{1, 2, ..., N_b\}$; and accordingly, $(S \cup B) = N^+$. Finally, it is assumed that DSO is responsible for determining the number and component of zones.

Entities in Multi-Round Double Auction

Entities in double auctions include sellers (prosumers), buyers (consumers), and the auctioneer (DSO). The indexes of n and m are denoted as prosumers and consumers, respectively.

Prosumers (Sellers)

The ask price and amount of power to be traded in P2P market are denoted by Sp and Sq, respectively. The payoff of prosumer n from auction without considering additional costs, SW_n, is defined as:

$$SW_n = \begin{cases} \sum_{m=1}^{N_b} (\gamma_{nm} - Sp_n) \times Sq_{nm}, & if\ prosumer\ n\ wins \\ 0 & otherwise. \end{cases} \tag{3.1}$$

where γ_{nm} is the auction cleared price of the successful transaction between prosumer n and consumer m.

Consumers (Buyers)

The bid price and amount of energy to be traded in P2P market are denoted by Bp and Bq, respectively. The payoff of consumer m from auction without considering additional costs, BW_m, is defined as:

$$BW_m = \begin{cases} \sum_{n=1}^{N_s} (Bp_m - \gamma_{mn}) \times Bq_{mn}, & if\ consumer\ m\ wins \\ 0 & otherwise. \end{cases} \tag{3.2}$$

Auctioneer (DSO)

Total social welfare of all peers, TW, is defined as the sum of payoffs of both prosumers and consumers in the auction, presented as below:

$$TW = \sum_{n=1}^{N_s} SW_n \ + \sum_{m=1}^{N_b} BW_m \tag{3.3}$$

DLMP Formulation

For DSO, the market-clearing is formulated as a SOCP-based optimization problem with convex relaxation. The DLMP price signal is used as a tool based on existing literature such as [14,77], for extracting hidden and private information of agents and calculating additional transaction costs.

Objective Function

The objective is to minimize the generation cost of utility-operated DGs, and the cost of purchasing power from the grid, which is shown as the first and second terms in (3.4), respectively. It is assumed that PV units are the only generation units controlled by prosumers.

$$min \sum_{t=1}^{T} \left[\sum_{i=1}^{N} (C_{i,t}^{g} \times P_{i,t}^{g}) + (C_{0,t}^{g} \times P_{0,t}^{g}) \right] \tag{3.4}$$

where $C_{i,t}^{g}$ and $C_{0,t}^{g}$ are the marginal cost of DGs and buying power from wholesale or retail markets, respectively. $P_{i,t}^{g}$ and $P_{0,t}^{g}$ are defined as the power related with two cost terms. The objective function is subjected to technical constraints such as voltage limits, line flow limits, generation limits, power balance, etc. The convex relaxation of constraints can be referred in [14]. Based on

KKT conditions and duality analysis [14], nodal prices can be represented as following:

$$\pi_i = \omega_1.\pi_{A_i} + \omega_2.\mu_i + \omega_3.\mu_{A_i} + \omega_4.\eta_i + \omega_5.\eta_{A_i} \tag{3.5}$$

where π_i, μ_i, η_i are active power price, reactive power price, and contribution of complex power at node i. Index A_i refers to the ancestor node of i. More details about the calculation of dual variables ω_i, and the decomposition of DLMP can be referred to [14]. In this chapter, DLMP price signals have two major impacts, 1) serving as the upper bound of consumers' bids; if violated, consumers may lose the auction and have to purchase power from the grid with DLMP price; and 2) including valuable price information about the power transition, such as power loss, voltage regulation, etc. In order to calculate the additional costs associated with every transaction, DLMP differences between seller and buyer nodes are considered.

P2P Energy Sharing Mechanism

There are major challenges of directly applying the literature research of prosumers/consumers in wholesale/retail markets [78] into distribution networks, which have been explained thoroughly in Section I. In this chapter, a hierarchical auction with three rounds of nodal, zonal, and DN-level auction (defined as MRDA) is proposed to address the challenges. The APM mechanism is also integrated into MRDA to enable a strong budget balance, in which the auctioneer (DSO) cannot benefit from running the auction and all the benefits are equally divided among prosumers and consumers. In this chapter, the 15-minute time interval is considered for P2P energy exchanges. It should be mentioned that the design of time intervals depends on the size of system, the number of agents participating in the P2P market, and the auction design. The following subsections will elaborate the details regarding the auction winner selections in price and quantity matching, sensitivity check, and payments of agents considering extra network usage costs.

Winner Selection Based on Price and Quantity

Considering the wholesale market as a reference, after collecting all data from agents, DSO arranges the requests from prosumers and consumers in ascending and descending orders, respectively, as expressed below.

$$Sp_1 < Sp_2 < ... < Sp_n, \quad \forall n \in S \tag{3.6}$$

$$Bp_1 > Bp_2 > ... > Bp_m, \quad \forall m \in B \tag{3.7}$$

After this arrangement, DSO calculates the average price of all agents participating in the P2P market and selects the winners of auction. The MRDA-APM improves the process by introducing the mean price λ, which makes all market players equal in terms of their chances to win auction. A prosumer wins the auction if and only if $Sp_n < \lambda$; and from the consumer point of view, $Bp_m > \lambda$ should be satisfied.

$$\lambda = \frac{\sum_{n=1}^{N_s} Sp_n + \sum_{m=1}^{N_b} Bp_m}{N_s + N_b} \tag{3.8}$$

The MRDA-APM enables agents to first negotiate with their neighbors (at nodal level) based on their IDs, containing information of node, zone, and DN. It should be noted that the cleared transactions in nodal level only need to provide a very small amount of additional cost, comparing to the zonal and DN-level transactions which will procure larger additional cost. If there is no successful matching with any consumer, prosumer n fails in the nodal auction and will participate again in the zonal auction. If prosumer n fails again in the zonal auction, it will participate in DN-level auction (zone crossing condition). If prosumer n fails in all three auctions, it can sell surplus energy to the grid. This three-layer auction process preserves the rights for all agents to participate in the market

so that no agents can sell or buy energy multiple times continuously within one-time interval.

Fig. 3.2 shows an example of how the proposed auction works. To compare with other auction mechanisms in literature, let us first assume prosumers sell surplus energy one by one in Fig. 3.2(a). In this scenario, prosumers sell surplus energy until their energy is sold out. For instance, prosumer 1 has sufficient surplus energy and asks for a lower price, which satisfies more than the need of the first customer. Then prosumer 2 cannot sell its energy until prosumer 1 completely sells all its energy. As a result, other prosumers must wait in line for their turn to sell energy and will be reluctant to participate in future P2P markets, since they may not benefit from P2P market in different time intervals. To fill this gap, the proposed peer matching mechanism preserves the rights of all agents to participate in the P2P market.

Algorithm 1: MRDA-APM Price Match Algorithm

Input: Submitted ask and bid prices of agents, agents ID, DLMP and FIT prices for every time slot t

Output: Winners and Losers of price matching

Initialization;
Define set of pros. S_i (Sp_i, Sq_i, ID_i, $\quad i = n \in N_s$)
Define set of cons. B_j (Bp_j, Bq_j, ID_j, $\quad j = m \in N_b$)
Calculate λ based on (3.8)
Stage 1:
if $Sp_i \leq \lambda$ **then**
| $S_i \rightarrow$ Winner and do quantity match
else
| $S_i \rightarrow$ Considered as Loser and should sell power
| with FIT price to the grid
end
if $Bp_j \geq \lambda$ **then**
| $B_j \rightarrow$ Winner and do quantity match
else
| $B_j \rightarrow$ Considered as Loser and should buy power with DLMP price from the grid
end

As shown in Fig. 3.2(b), prosumer 1 can only sell partial of its surplus energy (based on the demand from consumer 1), and its remaining energy is transferred to the end of the prosumers list, waiting

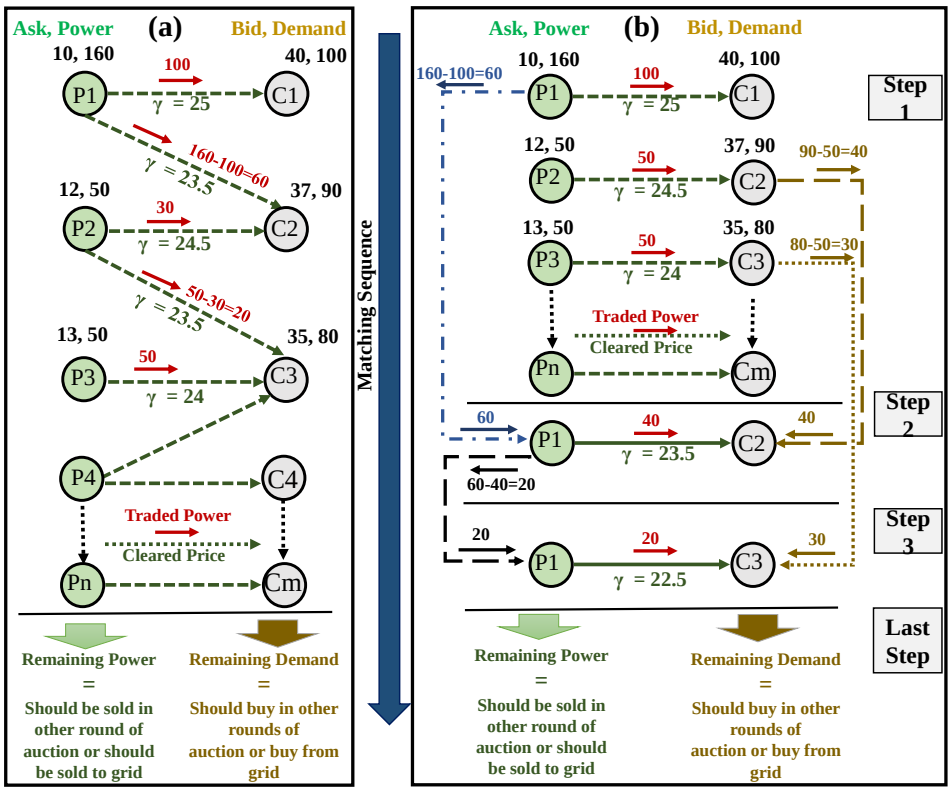

Figure 3.2. The matching sequence example of MRDA at one time interval.

for new consumers. When first transaction is completed, prosumer 2 sells energy to consumer 2. This process continues until no consumers or prosumers on the list. The details of MRDA-APM price and quantity matching mechanism are shown in Algorithm 1, Algorithm 2 and Fig. 3.3, respectively. The benefit of matching in Fig. 3.2(b) is that prosumers and consumers cannot bid strategically to sell/buy all surplus/needed energy. Moreover, MRDA increases the participation level of prosumers and consumers, as all agents have the chance to get benefit from P2P market.

For better elaborating the quantity matching sequence presented in Fig. 3.2, let us assume that there are 2 prosumers and 3 consumers in the P2P market, assuming that DSO has completed the price matching based on Algorithm 1. The surplus power of prosumers 1 and 2 are assumed to

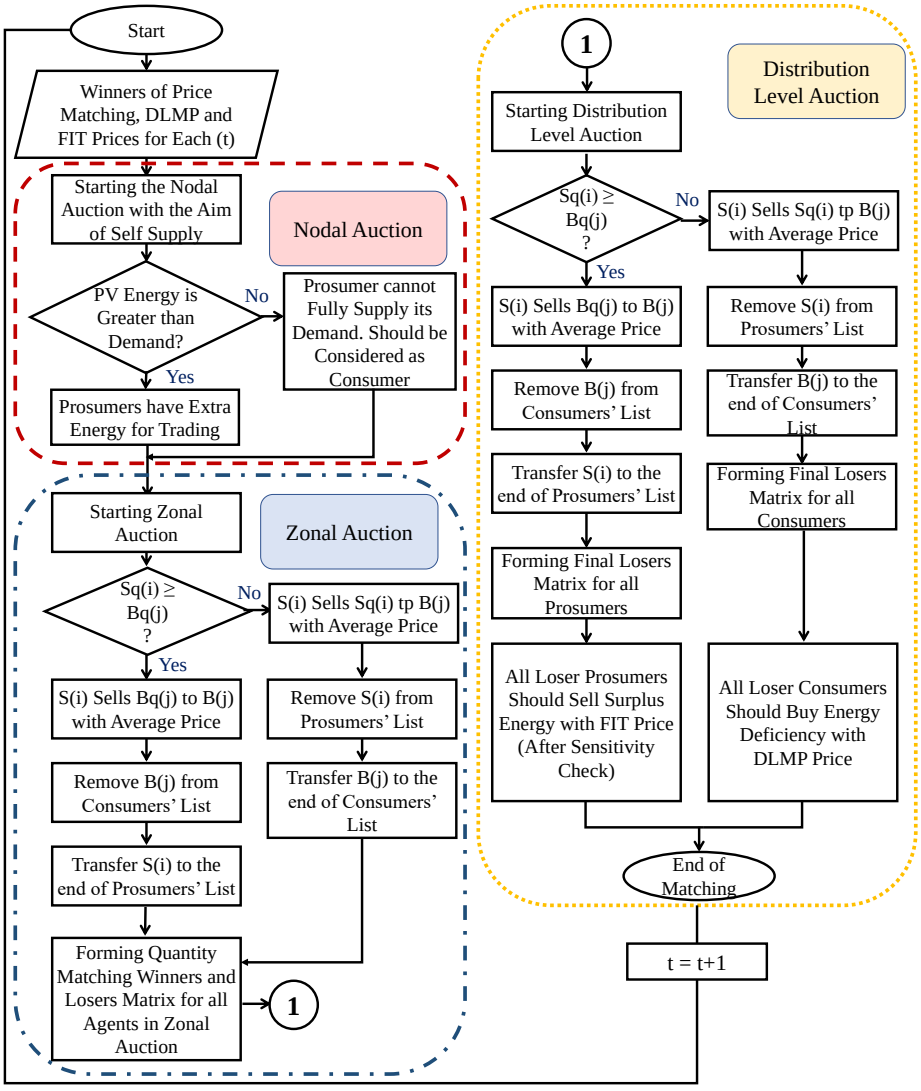

Figure 3.3. The matching sequence flow chart for hierarchical quantity match.

be 100 and 50 kw, respectively; and the demand of consumers 1, 2, and 3 are 25, 25, 50 kw, respectively. The first quantity matching happens between prosumer 1 and consumer 1 with 25 kw traded power. If traditional auctions in Fig. 3.2(a) are considered, the next matching order will be prosumer 1 with consumer 2 with 25 kw traded power, and prosumer 1 with consumer 3 with 50 kw traded power. As a result, during one trading time interval, prosumer 2 never receives benefits

Algorithm 2: MRDA-APM Quantity Match Algorithm in Each Round of Auction

Input: Winners of price matching (Algorithm 1), agents ID, DLMP and FIT prices for every time slot t

Output: Winners and Losers of quantity matching in every round of auction

Stage 2:

for *Each node, zone, and whole DN* **do**

  while *set* $\{S_i\} = \phi$ *or set*$\{B_j\} = \phi$ **do**

    if $Sq_i \geq Bq_j$ **then**

      1. S_i sells Bq_j to B_j with average price
      2. Transfer B_j to pre-matching list and remove B_j from consumers list
      3. Transfer S_i with power of $Sq_i - Bq_j$ to the end of prosumers list

    else

      1. S_i sells Sq_i to B_j with average price
      2. Transfer S_i to pre-matching list and remove S_i from prosumers list
      3. Transfer B_j with demand of $Bq_j - Sq_i$ to the end of consumers list

    end

  end

  Form losers matrix for prosumers and consumers

  $R \leftarrow$ remaining consumers and prosumers list

end

Stage 3:

Do Step 2 for R until no prosumers or consumers remaining on the list

from P2P market. If this happens for more P2P time intervals, the motivation of prosumer 2 will be decreased, and as a result, there is possibilities that this prosumer will not participate in the upcoming P2P markets; and in the long term, prosumer 1 can increase the asking price and be the dominant winner for the upcoming P2P markets. However, considering the matching sequence in Fig. 3.2(b), the matching order is, prosumer 1 with consumer 1 with 25 kw traded power, prosumer 2 with consumer 2 with 25 kw traded power, and prosumer 1 with consumer 3 with 50 kw traded power. As it can be seen, this matching sequence motivates small-scale prosumers to participate more since they can benefit from the market. It should be noted that this mechanism also depends on the number of prosumers and consumers in the network.

Additionally, this matching sequence, as shown in detail in Fig. 3.3 (with assumption that there is either one prosumer or one consumer located at each node), prevents agents, like prosumer 1, from

bidding intentionally lower to sell all their power. The proposed mechanism also enhances the cyber-resilience by not depending on the limited number of prosumers. For instance, if prosumer 1 is an attacker and intentionally reports 100 kw surplus power (but in reality it only has 5 kw surplus power, or is even a consumer), with traditional auctions the DSO must supply the load by purchasing power from the grid for the 90 kw deficiency. However, with the proposed matching sequence more prosumers are involved in P2P energy sharing markets and the system resiliency can be improved (by reducing the risk of cyber attacks), and DSO does not have to purchase more power from the upper grid or operate DGs to supply the load.

Apart from quantity matching, at each stage, the clearing price of matched peers is the average of prosumer and consumer bidding prices, defined as APM. The main advantage of the APM mechanism over traditional market clearing-prices is to enable strong budget balanced auctions, in which all benefits from traded energy in the P2P market are equally dispersed among matched peers, not the auctioneer or the central entity who runs the auction. However, DSO can indirectly benefit from P2P market by bringing small-scale prosumers into the market and keep them motivated to participate in all time periods when they have excess energy. Therefore, DSO can supply some of the load with prosumers' surplus energy (who are considered as final losers of the auction) and purchase less energy from the upper-level network with LMP price to minimize the operational cost. In the end, if the auction completes with no consumers, all prosumers should sell their remaining energy to the grid with FIT price; otherwise, if the auction completes with no prosumers, all consumers should purchase their remaining energy from the grid with DLMP price.

Sensitivity Check

After the completion of the auction, there will be a large number of transactions successfully matched in different rounds of auction. Next, DSO will check the physical feasibility of these

transactions, preventing the power injections that may violate network constraints. In this chapter, sensitivity factors are used to check the violation of physical network constraints.

$$Pf^p = M \times \Delta P_{inj}; \quad Pf^q = M \times \Delta Q_{inj} \tag{3.9}$$

$$\Delta V = R \times Pf^p + X \times Pf^q \tag{3.10}$$

$$SF_v = \frac{\partial \Delta V}{\partial \Delta P_{inj}} = R \times M \tag{3.11}$$

$$SF_{lp} = \frac{\partial Pf^p}{\partial \Delta P_{inj}} = M; \quad SF_{lq} = \frac{\partial Pf^q}{\partial \Delta Q_{inj}} = M \tag{3.12}$$

$$Pf_i^p = \sum_{i=1}^{N} SF_{lp,i} \times \Delta P_{inj,i} \tag{3.13}$$

$$PTDF_{ij}^E = Pf_i^p - Pf_j^p \tag{3.14}$$

$$P_{loss} = \sum_{i=1}^{N} R_l \times I_l^2 \approx \sum_{i=1}^{N} R_l \times Fl_l^2 \tag{3.15}$$

$$LF_i^p = \frac{\partial P_{loss}}{\partial \Delta P_{inj}} = \sum_{i=1}^{N} 2 \times Fl_i^p \times R_l \times \sum_{i=1}^{N} SF_{lp,i} \tag{3.16}$$

where M is the injection shift factor (ISF) that represents the sensitivity between nodal active (reactive) power injection ΔP_{inj} (ΔQ_{inj}) and active (reactive) line flow Pf^p (Pf^q), as shown in (3.9). In distribution network, voltage difference ΔV can be approximated using line flow and line resistant R and reactance X, as shown in (3.10). In (3.11), SF_v represents the sensitivity factor

between voltage difference and nodal active power injection by DERs; and the second equation can be achieved by substituting (3.9) and (3.10) into (3.11). In (3.12), SF_lp and SF_lq represent the sensitivity factor between line flow and nodal active/reactive power injection; and the second equation can be achieved by substituting (3.9) into (3.12). (3.13) represents the active power flow equals to the summation of all nodal active power injection multiplied by sensitivity factor. Then power transfer distribution factor (PTDF), $PTDF_{ij}^{E}$, can be obtained, which provides the sensitivity of active power flow in branch E with respect to one active power injection at bus i and the other active power withdrawn at bus j, as shown in (3.14). In (3.15), linear approximation of active power loss, P_{loss}, can be presented using active power flow in branches. Loss sensitivity factor, LF_i^p, represents the sensitivity between power loss and injected power at bus i, as shown in (3.16) [79]. After DSO's final approval of transactions, network costs will be added to the payment of all matched transactions. It should be noted that this chapter only considers the active power cost.

Payments and Allocation of Extra Costs

The MRDA-APM cleared prices can be integrated into nodal pricing schemes, which are based on marginal costs. For example, in PJM market, nodal price (NP) consists of system marginal energy price (SMP), e.g. locational marginal price (LMP), congestion price (CP) and loss price (LP) [80, 81].

$$NP = SMP + CP + LP \tag{3.17}$$

To integrate the proposed auction clearing price to distribution nodal pricing, SMP should be replaced with γ which indicates the cleared price of matched peers. Therefore, NP can be reformulated as below:

$$NP = \gamma + CP + LP \tag{3.18}$$

Additionally, matched peers should pay for power loss, voltage support, etc. The additional costs can be accessed by DLMP components from power injection by prosumers and power absorption by matched consumers. The payment of matched transactions confirmed by DSO can be presented as below:

$$SR_n = \sum_{m=1}^{N_b} SW_n \; - \; \sum_{m=1}^{N_b} \left(\frac{|DLMP_i \; - \; DLMP_j|}{2} \right) Sq_{nm} \tag{3.19}$$

$$BP_m = \sum_{n=1}^{N_s} BW_m \; + \; \sum_{n=1}^{N_s} \left(\frac{|DLMP_j \; - \; DLMP_i|}{2} \right) Bq_{mn} \tag{3.20}$$

where SR_n and BP_m denote to prosumers final revenue and consumers final payment, respectively. The first term of (3.19) and (3.20) denotes the traded energy benefit from P2P market. The second term of both equations is related to additional costs, which are equally split among matched peers.

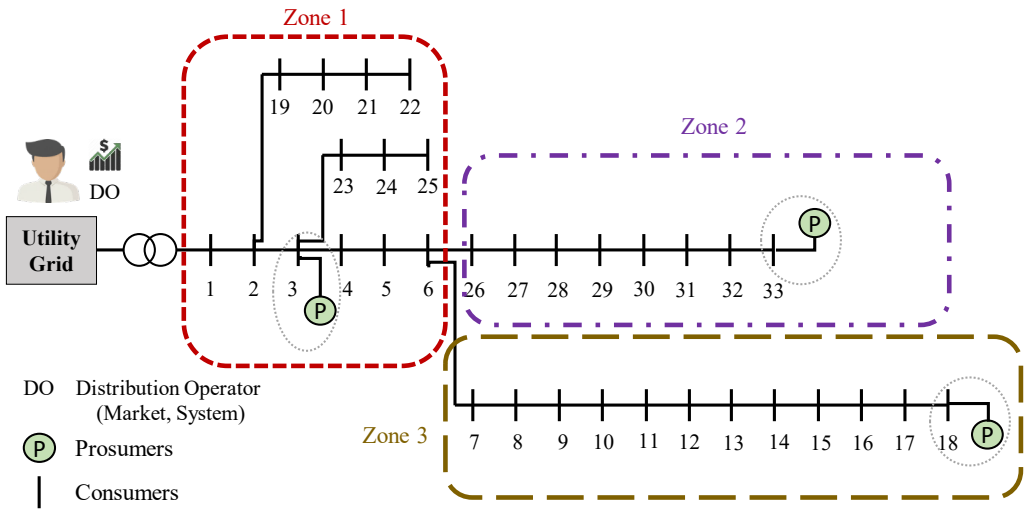

Figure 3.4. 33-node distribution test system.

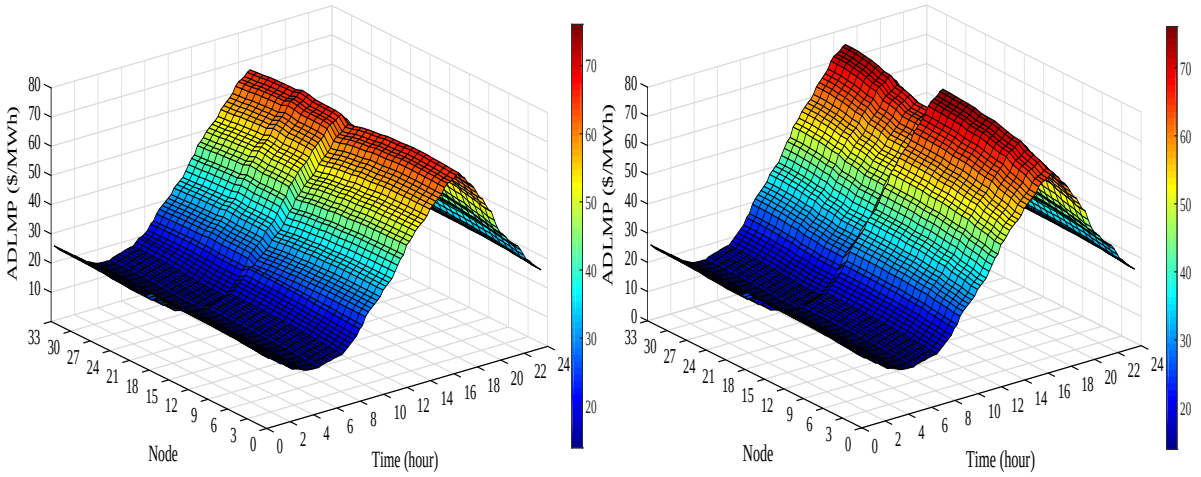

(a) DLMP w/ considering prosumers role

(b) DLMP w/o considering prosumers role

Figure 3.5. 33-node DLMP signals before and after P2P energy exchange.

Numerical Results

The proposed P2P framework is first validated on the modified 33-node distribution test system [82] with pre-defined zones, as shown in Fig. 7.2. This test system has been used as a standard test system in various studies such as [79], [81], and [82]. Three 1,000 kW PVs are installed at nodes 3, 18, and 33, which represent three prosumers [79]. The nodes with load are considered as consumers. The network is clustered into 3 different zones, following the modification from [20]. All asks and bids are randomly generated and received by DSO. The hourly load data are obtained from [79], and PVs data are from CAISO for the first day of July 2019. Moreover, the hourly LMPs are from PJM, which can be referred to [79]. The time steps between each P2P market are set as Δt = 15 minutes for a whole day. Next, the framework is further tested in 141-node distribution system [83, 84] for scalability analysis and better explaining the benefits of defining the zones. Simulations are carried out on a PC with Intel Core i7-7700, 3.6 GHz CPU, and 16 GB RAM, with interfacing MATLAB and GAMS softwares.

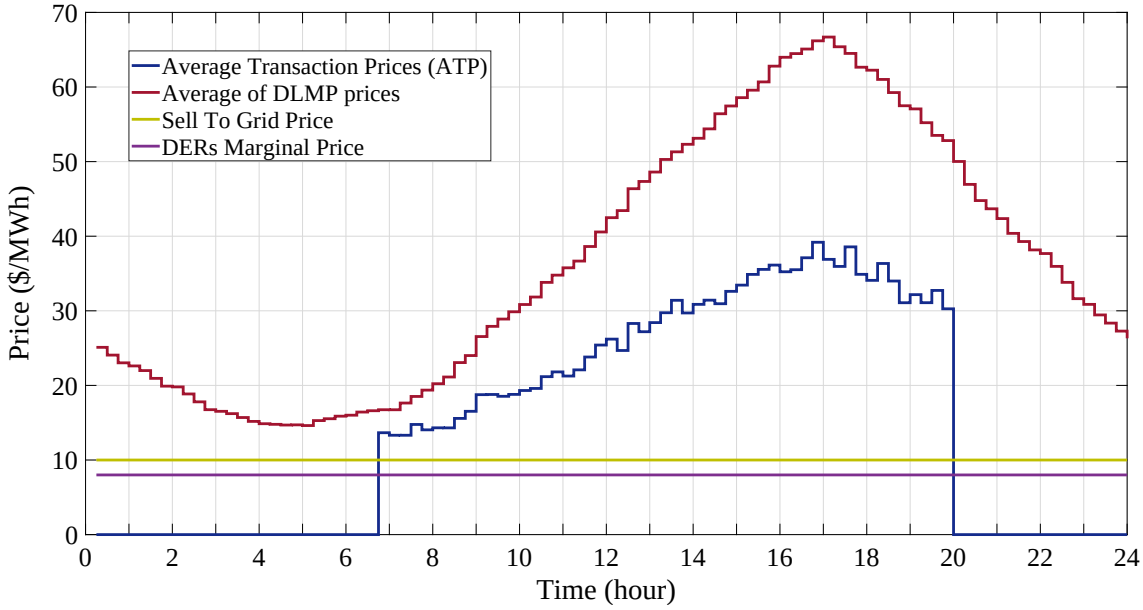

Figure 3.6. Comparison of hourly prices w/o and w/ P2P market.

DLMP Results

Based on the hourly forecasting data and LMP data from the wholesale market, DSO performs the DLMP calculation. Nodal prices of active power for all nodes with and without the participation of prosumers for 24 hours are shown in Fig. 3.5a and Fig. 3.5b, respectively. Considering Fig. 3.5b, the nodal prices vary between \$15/MWh and \$75/MWh, with the peak in the afternoon around 5 pm due to the peak demand. It should be mentioned that by prosumers participation in the P2P market, the DLMP prices decrease because of surplus energy injection to the grid and neighbors (maximum DLMP price based on Fig. 3.5a is \$66/MWh). Additionally, every 15 minutes, DSO sends these price signals to all consumers, and receives Bp_j, and Bq_j, which help determine the number of agents to participate in P2P market, and the amount of load to be supplied at these time slots.

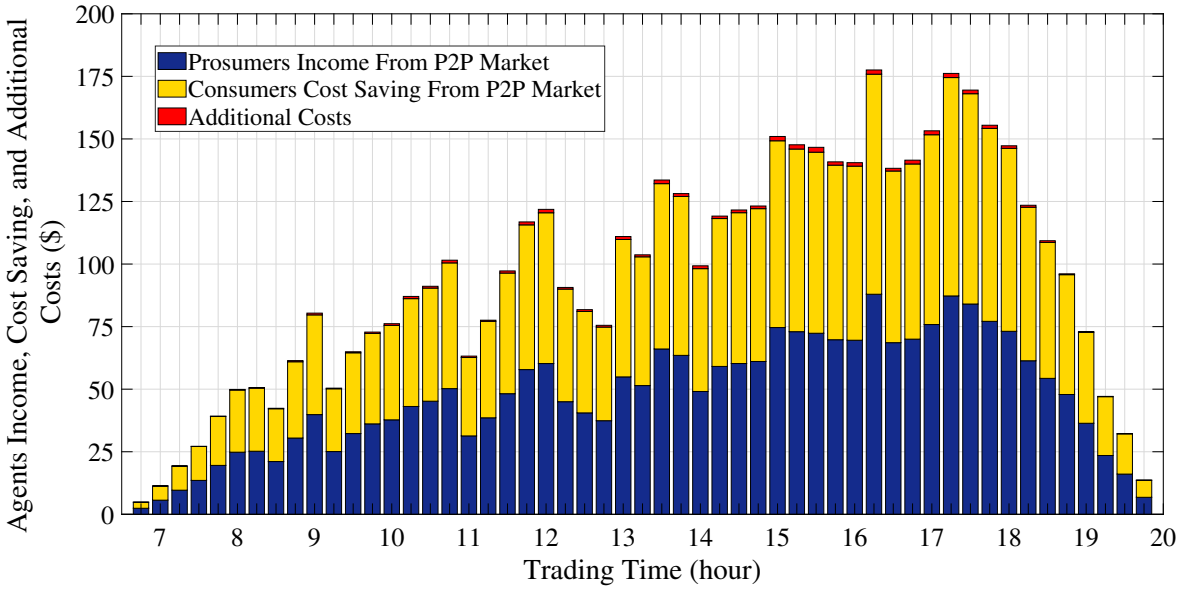

Figure 3.7. Prosumers income, consumers cost saving, additional transaction costs in P2P market.

P2P Transaction Prices vs. Traditional DLMP

The average P2P transaction prices for every time slot is shown in Fig. 3.6. The upper and lower bounds of asks and bids are the average DLMP price and FIT price, respectively, which varies from \$14.6/MWh to \$66.7/MWh. Moreover, in first 7 hours and last 4 hours, the average transaction prices for P2P energy trading is zero, due to zero surplus energy for prosumers to participate in P2P market.

Financial Benefits of Participating in P2P Market

To demonstrate how the proposed P2P market benefits both prosumers and consumers, different load and generation scenarios are considered for trading, as shown in Fig. 3.7. Three bars with different colors show prosumers' income and consumers' cost saving from the P2P market and additional costs associated with each peer for using the DN to trade energy. As MRDA-APM

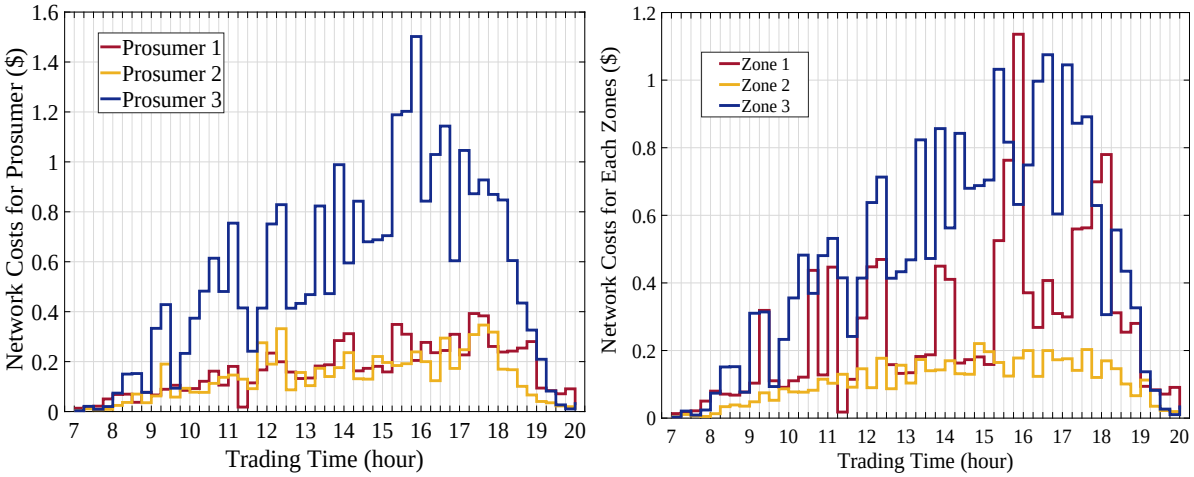

(a) Extra network costs of prosumers

(b) Extra network costs of consumers

Figure 3.8. Comparison of extra network costs.

is strongly budget balanced, all traded energy and resulted income and cost saving at each time interval should be equal for both prosumers and consumers, as shown in Fig. 3.7. Take 1:30-1:45 pm as an example, total power traded at this time interval is 2.793 MW, and the income and cost saving for total prosumers and total consumers are the same of $66.065, which validates the proposed double auction.

To reveal more details on network costs associated with transactions, Fig. 3.8a and Fig. 3.8b are depicted to present total network costs for each prosumer and all consumers in each zone at different trading hours, respectively. Considering 1:30-1:45 pm in Fig. 3.8a, the total network cost is $1.45 for all prosumers. Based on the formulation, network costs can be calculated based on DLMP differences between two nodes with DSO's final approval of energy transition. Based on Fig. 3.8a, prosumer 3 has the highest network cost, due to the cleared prices between prosumer 3 and consumers in zone 3. In some hours, if prosumers 3 asks for higher prices, it can affect DLMP in that zone. As a consequence, DLMP differences become larger, and accordingly network costs increase.

Table 3.1. Revenue of Sellers w/o vs. w/ P2P Market

Sellers	Benefit without P2P ($)	Benefit with P2P ($)		Benefit Improvement (%)
		w/o Utility and Extra Costs	w/ Utility and Extra Costs	
Pros. 1	378.9	1017.9	550.8	45.36
Pros. 2	393.1	702.4	507.7	29.15
Pros. 3	378.9	795.7	484.4	27.84

According to the proposed methodology, both consumers and prosumers benefit from participating in the P2P market. Table 3.1 and Table 3.2 show the benefit improvement with and without participating in P2P market. Table 3.1 shows the P2P market benefits for each prosumer. If prosumers only sell surplus energy to the grid with the FIT price, the revenue for each prosumer will be $378.9, $393.1, and $378.9, respectively. However, by participating in P2P market, prosumers can get more benefits. Furthermore, columns 3 and 4 of Table 3.1 show the benefit of participating in market without and with considering utility and additional costs. The benefit enhancements for prosumers 1, 2, and 3 with participating in the P2P market and considering additional network costs and utility, are 45.36%, 29.15%, and 27.84%, respectively.

Different from prosumers, if consumers cannot get successfully matched with any prosumer in the auction, they have to purchase power from the grid with DLMP price. Table 3.2 shows different scenarios for consumers. For simplicity, the results of consumers cost are demonstrated by comparing aggregated consumers in each zone. If consumers in zones 1, 2, and 3 do not participate in the P2P market, their total cost of paying to receive power from DSO in that time period is $1783.5, $1841.4, and $1772.2, for each zone respectively. However, their cost will be reduced by participating in P2P market. Considering additional costs in consumers' payment, the total cost for zones 1, 2, and 3 is $615.82, $320.12, and $390.74, respectively; and with the cost saving improvement of 65.47%, 82.61%, and 77.59%, respectively.

Table 3.2. Cost Saving of Buyers w/o vs. w/ P2P Market

Buyers	Cost without P2P ($)	Cost with P2P and Extra Network Costs ($)	Cost Saving Improvement (%)
Zone 1 Cons.	1783.5	615.82	65.47
Zone 2 Cons.	1841.4	320.12	82.61
Zone 3 Cons.	1772.2	390.74	77.95

Voltage Comparison w/ and w/o P2P Energy Trading

To capture the voltage issues, two scenarios with and without P2P energy trading are considered to show voltage problems, as shown in Fig. 7.4a and Fig. 7.4b for the 33-node distribution system, and in Fig. 3.10a and Fig. 3.10b for 141-node distribution system, respectively. Comparing results in Fig. 7.4b and Fig. 7.4a, the voltage variation without P2P trading as a benchmark is from 0.915 p.u. to 1 p.u., which is increased to the range of 0.95 p.u. and 1.04 p.u. with P2P trading. The reason is that when prosumers have surplus energy during certain times of a day, they participate in the P2P market; depending on whether they are successful in P2P matching or not, prosumers inject power to either supply consumers or sell to the grid, which causes voltages to increase. Additionally, for the 141-node test system, hour 12:30 pm is selected for better analysis of voltage values during the trading period.

Simulation Results for 141-Node Distribution System

For scalability analysis and demonstrating how the zones can benefit both prosumers and consumers, 141-node real distribution system is considered for additional simulations. To validate how the proposed P2P framework works, 12 PV units representing prosumers, and 2 utility-operated DGs (each with the maximum capacity limit of 2 MW) are added to the 141-node system, as

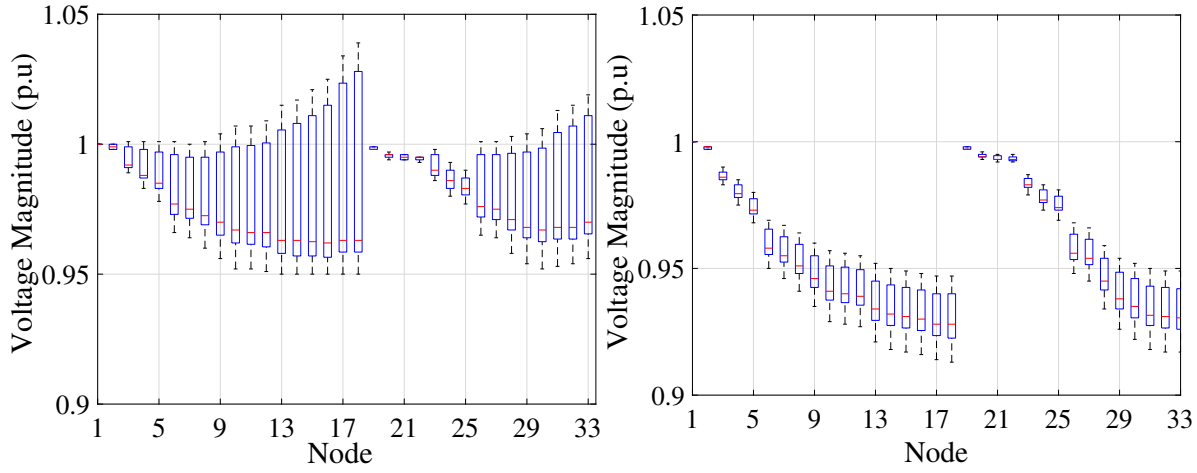

(a) Voltage values w/ P2P market

(b) Voltage values w/o P2P market

Figure 3.9. 33-node voltage magnitude before and after P2P energy exchange.

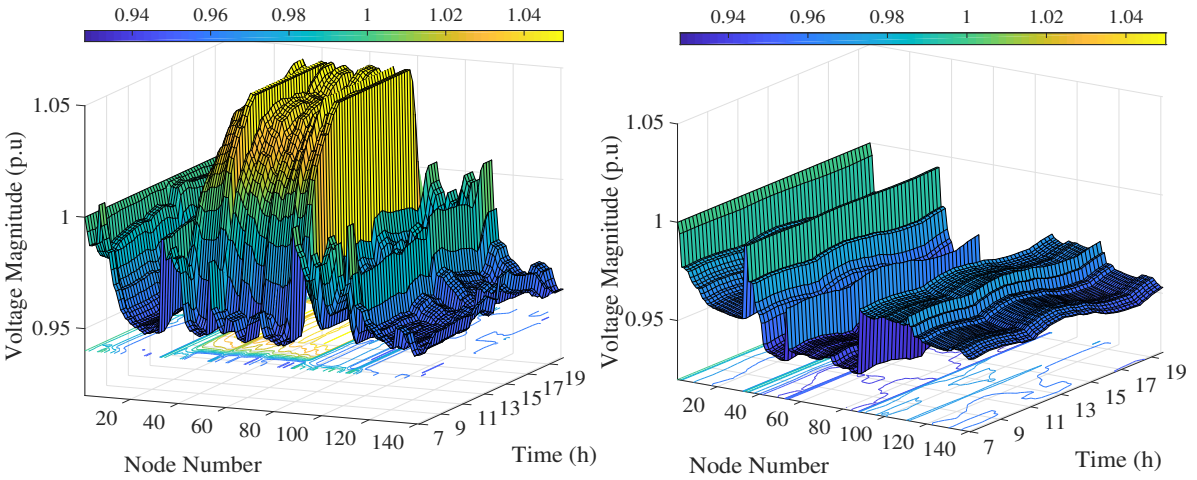

(a) Voltages with P2P

(b) Voltages without P2P

Figure 3.10. Voltage values w/o P2P energy sharing for 141-node distribution network during trading time.

Table 3.3. Prosumers Location and Maximum Capacity

Prosumers Location	5	26	30	40,50 60,80	70,95 101,125	138
Capacity (MW)	0.2	0.5	0.75	1.5	1	0.75

shown in Fig. 3.11. The location of prosumers and DGs and their maximum capacity limits are presented in Table 3.3. The entire distribution system is divided into 5 zones with the criteria of similar DLMP signals and location of agents. For better analysis, hour 12:30 pm is selected, and the DLMP signals, as well as voltage values, are presented in Fig. 3.12 and Fig. 3.13, respectively. Based on Fig. 3.12, it can be seen that when utility supplies the consumers' demand by purchasing power from upper grid or DGs, the DLMP signals are above \$52/MWh. However, if the prosumers participate in the P2P market, then DLMP is reduced due to the cheaper energy supply by prosumers. In addition, the variations of DLMP for different zones depend on the density of prosumers in the zones, the number of prosumers participating in P2P market, the total demand of zones, and the auction design.

To elaborate how defining zones can benefit both prosumers and consumers, different scenarios are designed based on hour 12:30 pm results. The goal is to compare which option is more beneficial for prosumers, to negotiate either with a consumer with a lower bid price within the zone or another consumer with a higher bid price outside the zone. For instance, zone 1 and zone 4 are selected with average DLMP prices of \$20/MWh and \$53/MWh, respectively. Moreover, the operational cost for prosumers is \$10/MWh. Two scenarios are proposed to perform the economic analysis for energy trading within and outside the zone. The first scenario can be considered as our proposed model, and the second scenario can be considered as the traditional auction as stated in [24].

In the first scenario, both agents within zone 1 are negotiating with offering prices of \$15/MWh (prosumer) and \$18/MWh (consumer). Based on the average price mechanism, agents' cleared

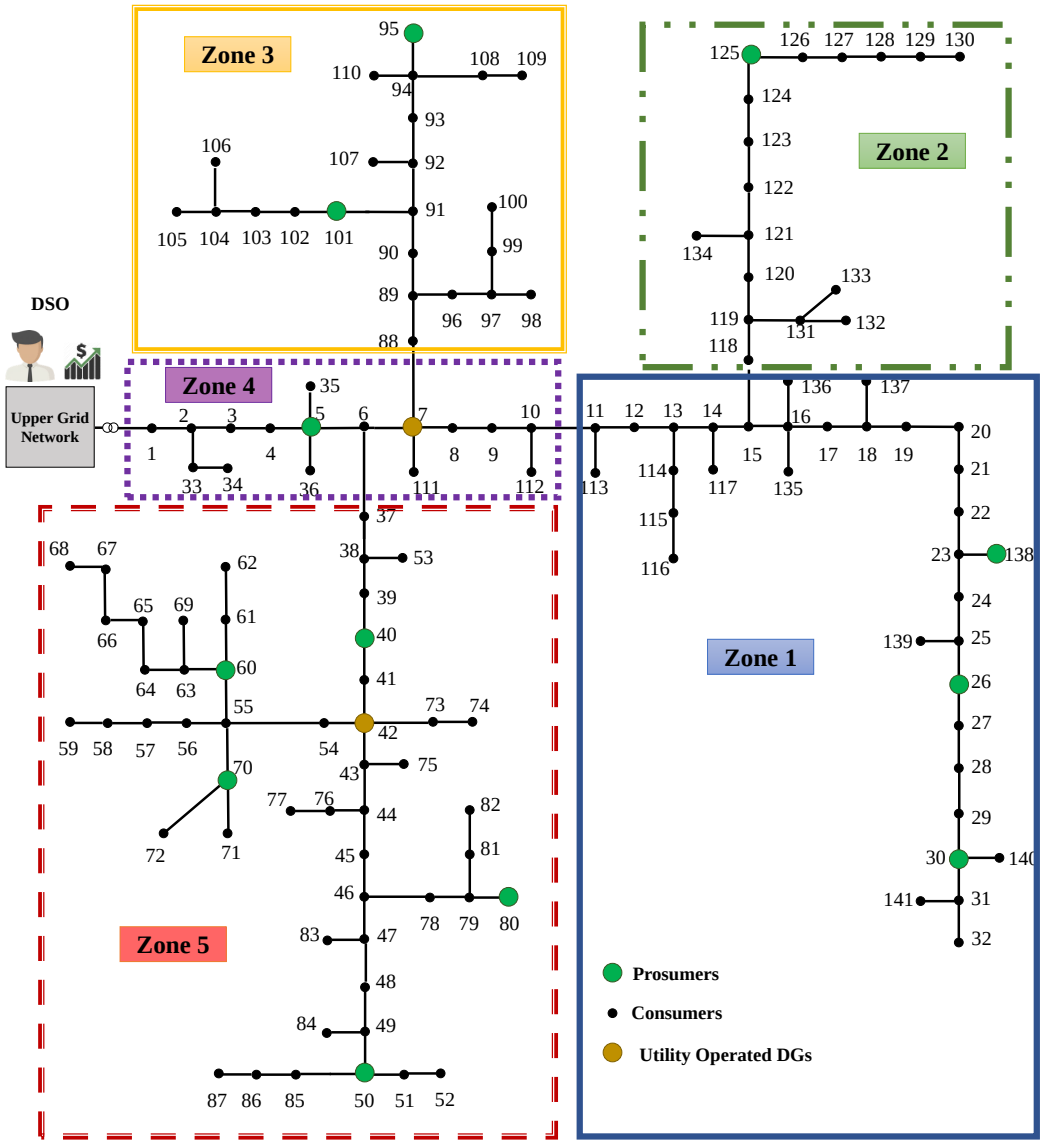

Figure 3.11. 141-node distribution test system.

price is \$16.5/MWh. The extra cost for this transaction is calculated based on DLMP differences, which is \$0.23/MWh. For simplicity, assuming there is 1 MWh energy flow, and DLMP at prosumer and consumer node is \$20.04/MWh and \$20.5/MWh, respectively. Total net revenue of prosumer in zone 1 = 16.5 – 10 – 0.23 = \$6.27; and total cost saving for consumer in zone 1 = 20 – 16.5 + 0.23 = \$3.73. In the second scenario, agents are negotiating outside their zone (DN-level

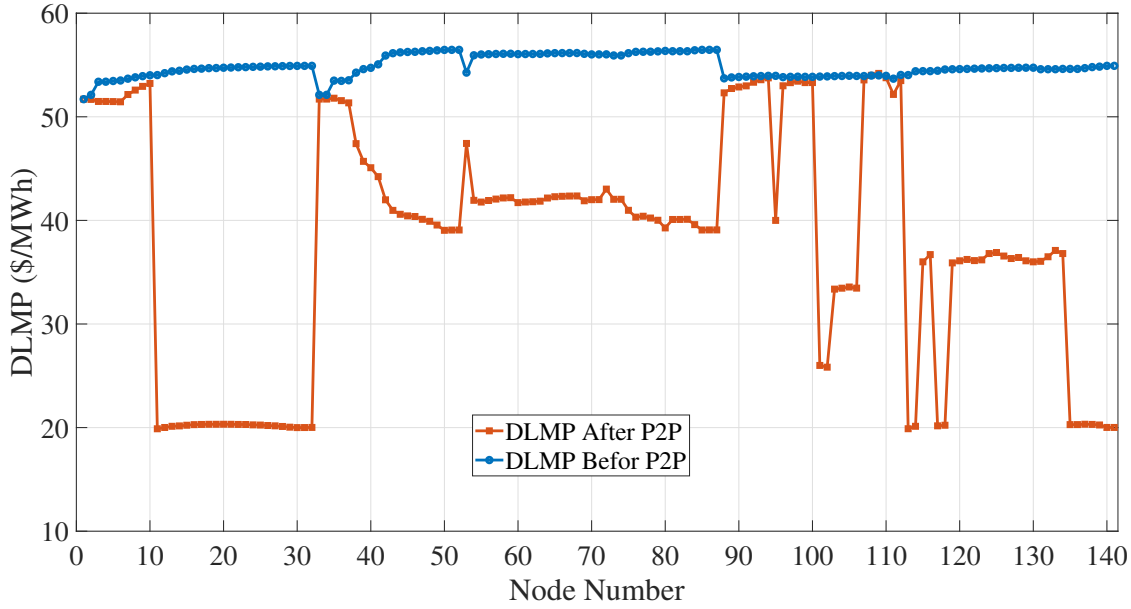

Figure 3.12. DLMP price signals in hour 12:30 pm.

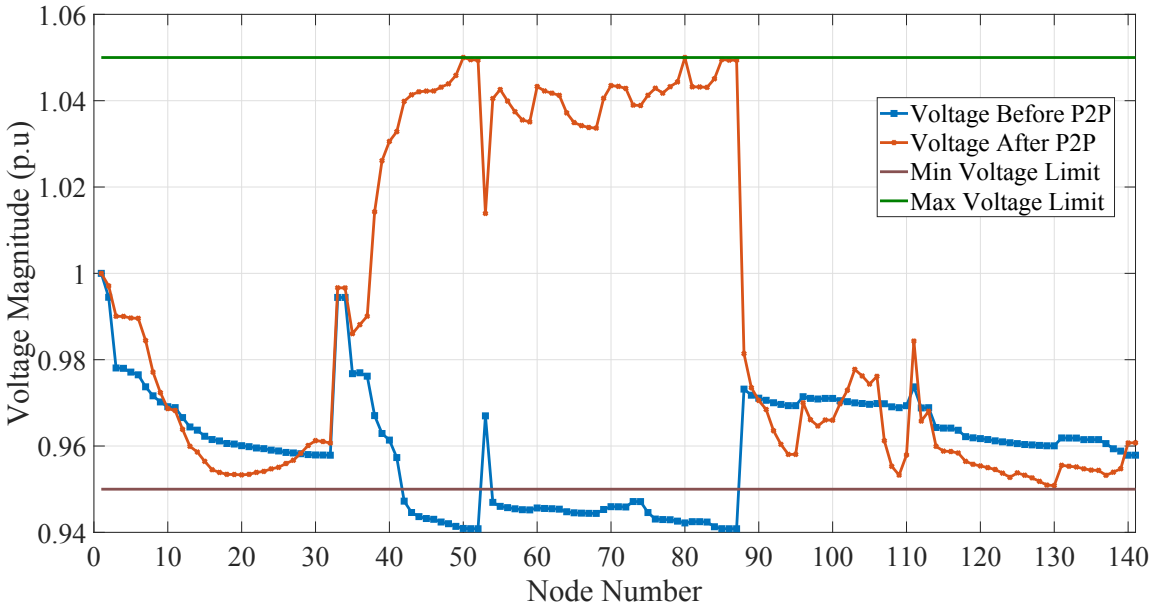

Figure 3.13. Voltage magnitudes in hour 12:30 pm.

auction) with offering prices of \$15/MWh (prosumer) and \$45/MWh (consumer). Based on the average price mechanism, agents' cleared price is \$30/MWh, and extra cost for this transaction is \$16.5/MWh. Total net revenue of prosumer in zone 1 = 30 – 10 – 16.5 = \$3.5; and total cost saving for consumer in zone 4 = 53 – 30 + 16.5 = \$39.5. Based on the results from scenarios 1 and 2, it can be seen that if prosumers negotiate within zones, then the net revenue is higher, compared to the scenario that prosumers trade energy with consumers outside the zone even with higher bid prices. This analysis clearly demonstrates the effectiveness of the proposed model in this chapter over the matching presented by [24].

Besides the presented scenarios, trading outside the zones might be beneficial in some specific scenarios, which mainly depends on the bid prices of agents. For instance, prosumers bid close to the operational cost and consumers bid close to the DLMP signal. However, this scenario is not beneficial (from economic perspective) for agents, since prosumers prefer to maximize their welfare by bidding reasonably high compared to operational cost, and consumers prefer to bid lower for welfare maximization and more cost savings. It is worth mentioning here that if prosumers still have surplus energy after zonal auctions (completely supplying the loads in zonal level), they can negotiate with consumers outside the zones since both peers can benefit from P2P market. But again, this scenario depends on agents behaviour and their power/demand amount.

The computational time of the proposed P2P framework depends on calculating the DLMP and P2P matchings in the hierarchical nodal, zonal, and DN-level auction. It should be mentioned that the total computational time for calculating the DLMP and P2P matching of the 141-node test system is 1.6 and 0.25 minutes, respectively, which is more efficient compared to the iterative-based P2P mechanisms. It should also be mentioned that the simulation time depends on the participation level of prosumers, DSO calculating DLMP, and trading time intervals.

Conclusion

This chapter proposes a framework for P2P energy exchange in the active distribution network. The framework utilizes the multi-round double auction with an average pricing mechanism, which preserves the rights of agents for negotiation, and gives the priority to neighboring nodes for energy exchange during the multi-round auction. The proposed MRDA-APM also satisfies the auction criteria from economic perspective. Moreover, this chapter integrates additional network costs for each transaction, such as power loss cost, voltage regulation cost, etc., into the payments of all prosumers and consumers, through DLMP component decomposition. Simulation results demonstrate the advantage and benefits for not only prosumers and consumers but also DSO (reliable operation and reduce peak hour generation) from the proposed P2P market.

The proposed framework is based on assumptions to provide an alternative with advantages in certain areas, rather than totally replacing other market mechanisms. The possible future research directions include, 1) considering the impact of P2P energy sharing on integrated transmission and distribution network and considering realistic assumptions such as polynomial bid prices for agents; 2) extension of the proposed model by considering the uncertainty of renewable generation and its impact on DLMP and real-time auction models; 3) inclusion of energy storage to address renewable energy curtailment issues, comparing the performance of different energy storage systems, e.g. hydrogen and battery, and analyzing the local markets with considering P2P and hydrogen market; and 4) considering fully distributed P2P market with distributed DLMP and distributed auction with the aim of privacy-preserving of agents.

CHAPTER 4: RISK-AVERSE COOPERATIVE OPERATION OF PV AND HYDROGEN SYSTEMS IN ACTIVE DISTRIBUTION NETWORKS [1]

Introduction

Environmental emissions and decreasing costs of renewable energy sources (i.e. photovoltaic (PV), wind, hydrogen (H2), etc.) are prompting a sharp increase in renewable energy penetration into the grid. Among various energy sources, H2 energy with its promising technical, economic, and environmental merits has demonstrated great potential for large deployment in distribution systems. This chapter proposes a multi-objective network-constrained framework for the day-ahead scheduling of hydrogen systems (HS), including hydrogen production from water electrolysis by electrolyzers, hydrogen storage, stationary fuel cells, and fueling of fuel cell electric vehicles (FCEVs). This framework includes various physical constraints to ensure reliable operation and considers integrated demand response and conservation voltage reduction, and reactive power support from HSs for realistic day-ahead scheduling. It also incorporates the cooperative operation of PV units and HSs to supply power for water electrolysis from stationary HSs equipped with onsite PVs. Moreover, Conditional Value-at-Risk (CVaR) is applied to address the risk of PV output, FCEVs' H2 demand, loads, and market price. The proposed model is formulated as a mixed-integer linear programming problem and validated by testing on a 33-node distribution test feeder.

From previous research efforts, there are remaining gaps in the techno-economic analysis of hydrogen storage and hydrogen fuel station scheduling in the day-ahead electricity market. For instance,

[1] This chapter is prepared based on the paper presented at [62]:
Hamed Haggi, Wei Sun, James M. Fenton, and Paul Brooker "Risk-Averse Cooperative Operation of PV and Hydrogen Systems in Active Distribution Networks ", *IEEE Systems Journal*, 2021. [Link]

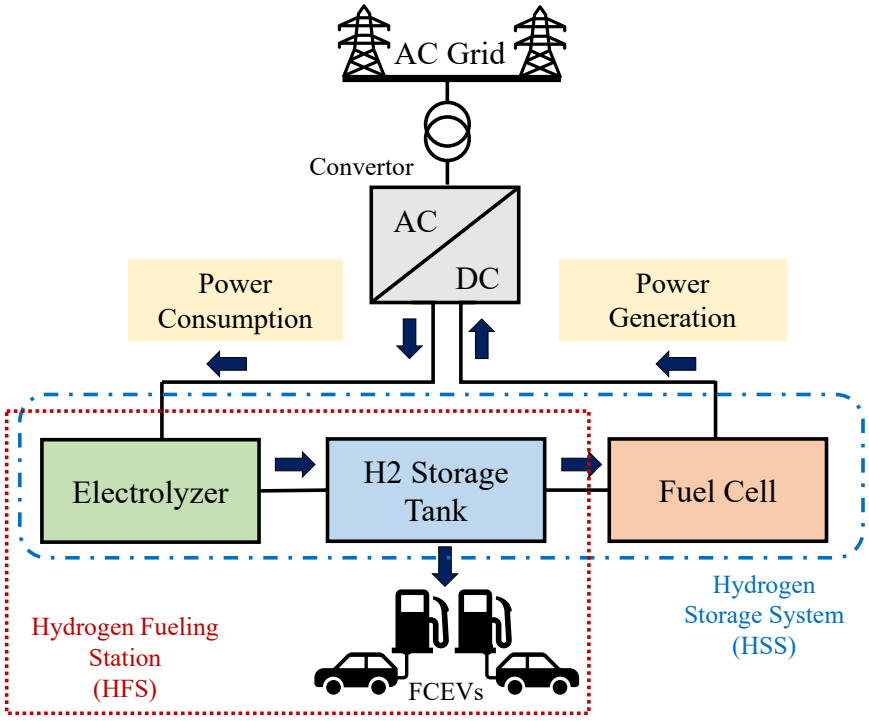

Figure 4.1. Hydrogen System (HS) interface with distribution power grid.

power quality issues (i.e. voltage deviation) can happen in the case of imposing a huge amount of H2 demand from FCEVs; and as a consequence, reactive power support by PV and HS inverters and other voltage control methods should be considered in the practical operation of power systems, which is largely missing from previous studies. Additionally, [51]– [60] did not address the risks and uncertainty of renewable energy output, wholesale market price, power grid load, and H2 demand, or [58]– [67] neglected network constraints of power systems, which are critical for the reliable operation of these assets. Additionally, previous studies failed to consider the cooperative scheduling of hydrogen systems with their onsite PV assets to produce cheap H2 energy. Therefore, this chapter develops a new model for optimal scheduling of distributed HS in power distribution networks considering the H2 demand from FCEVs in the transportation sector. The major contributions of this chapter include:

- A multi-objective network-constrained framework is proposed for day-ahead scheduling of hydrogen systems (Fig. 4.1) including HSS for power grid balancing and HFS for supplying the H2 demand from transportation sector. Since H2 demand from transportation sector can impose a huge load on nodes with HSs, reliable operation with power quality concerns is considered.

- Risk management is incorporated into the stochastic model using Conditional Value-at-Risk (CVaR) to address the risk of uncertainties from PV output power, nodal demand, wholesale market price, and H2 demand from FCEVs.

- The framework considers the cooperative operation of onsite HS equipped with PV units to support the H2 demand of HFS with both self-supply and power from the grid which results in lower H2 production costs.

- Framework also considers the practical operation by, 1) developing linear integrated DR with conservation voltage reduction (CVR) model for active/reactive power shifting preserving the load power factor and lowering cost; and 2) reactive power support from HS, PV and distributed generators (DG) to improve voltage profiles.

The following indices are used for defining parameters and variables throughout this chapter. **Sets and Indices**

- $\mathcal{S}$ Set of scenarios, indexed by s.
- $\mathcal{N}$ Set of nodes, indexed by i.
- $\mathcal{T}$ Set of scheduling time interval, indexed by t.
- $\mathcal{N}_{\mathcal{PV}}$ Set of nodes with PVs, indexed by p.
- $\mathcal{N}_{\mathcal{HS}}$ Set of nodes with HSs, indexed by h.

- $\mathcal{N}_{\mathcal{DG}}$ Set of nodes with DGs, indexed by d.
- $\mathcal{N}_{\mathcal{UG}}$ Set of upper grid nodes, indexed by sub.
- $\mathcal{L}$ Set of network lines, indexed by $(i,j) \subset \mathcal{N} \times \mathcal{N}$.

Parameters

- λ^{Grid} Upper grid electricity price ($/MWh).
- λ^{PV} Operational cost of PV units ($/MWh).
- λ^{DG} Operational cost of DG units ($/MWh).
- ρ_s Probability of each scenario.
- ρ_{PV} Probability of each PV scenario.
- ρ_{HDE} Probability of each hydrogen demand scenario.
- ρ_{load} Probability of each load scenario.
- ρ_{price} Probability of each wholesale market price scenario.
- ζ Linear load flow constant.
- HDE H2 demand from aggregated FCEVs (Kg/h).
- BF Beta function of solar data.
- ω_i Coefficient indicating priority of nodes.
- G^l / B^l Conductance / susceptance of line.
- PL^{base} Active power consumption (MW).
- QL^{base} Reactive power consumption (MVar).
- ι_i Percentage of shiftable load (%).
- S^{shift} Amount of shiftable apparent power (MVA).
- PL^{shift} Amount of shiftable active power (MW).

- QL^{shift} Amount of shiftable reactive power (Mvar).
- LPF Load power factor.
- K^{PZ}/K^{QZ} Constant active/reactive impedance coefficient.
- K^{PI}/K^{QI} Constant active/reactive current coefficient.
- K^{PP}/K^{QP} Constant active/reactive power coefficient.
- π_t / ϖ_t Beta function parameters.
- μ_t / σ_t Mean and variance of solar data.
- P_{ST} Rated power st standard test condition.
- T_j Cell temperature (°C).
- $NOCT$ Nominal operating cell temperature (°C).
- n_{PV_s} / n_{PV_p} Number of PV modules in series or in parallel.
- γ Power temperature coefficient.
- T_{amb} Ambient temperature (°C).
- $S^{PV,inv}$ PV inverter size (MVA).
- $S^{DG,inv}$ Maximum apparent power for DGs (MVA).
- $S^{HS,inv}$ HS inverter size (MVA).
- S^{UG} Maximum apparent power for purchasing power from upper grid (MVA).
- η^{EL} / η^{FC} Efficiency of electrolyzer / Fuel Cell (%).
- $P2H^{EL}$ Electrolyzer power to hydrogen conversion factor (Kg/MWh).
- $H2P^{FC}$ Fuel cell hydrogen to power conversion factor (MWh/Kg).
- $SOH^{H2,init}$ Initial Mass of hydrogen in tank (Kg).
- $SOH^{H2,min}$ Minimum limit of H2 mass in tank (Kg).
- $SOH^{H2,max}$ Maximum H2 storage tank capacity (Kg).
- V^{max} / V^{min} Max. and min. voltage magnitude (pu).

- $M1$ A big number for linearization.
- β Level of risk aversion.
- α Confidence level in risk management.
- $PL^{DR,max}$ Upper bound of PL^{DR} (MW).
- $PL^{DR,min}$ Lower bound of PL^{DR} (MW).
- λ^{Dsp} Dissipation rate of HS .
- $P^{EL,min}$ minimum electrolyzer capacity (MW).
- $P^{EL,max}$ maximum electrolyzer capacity (MW).
- $P^{FC,min}$ minimum stationary FC unit capacity (MW).
- $P^{FC,max}$ maximum stationary FC unit capacity (MW).
- ϕ^{init} Initial percentage of H2 in the tank.

Variables

- PQI Power quality index.
- P^{FC} Fuel cell output power (MW).
- P^{EL} Electrolyzer import power (MW).
- $P^{EL,jo}$ Imported power by electrolyzer in cooperative mode (MW).
- $N^{FC,H2}$ Inflow of H2 in fuel cell (Kg/h).
- $N^{EL,H2}$ Outflow of H2 from electrolyzer (Kg/h).
- P^{PV} / Q^{PV} PV output active/reactive power (MW/Mvar).
- P^{DG} / Q^{DG} DG output active/reactive power (MW/Mvar).
- P^{UG} / Q^{UG} Active/reactive power from upper grid (MW/Mvar).
- P^{CVR} Active load value after DR and CVR (MW).

- Q^{CVR} Reactive load value after DR and CVR (Mvar).
- FL^P/FL^Q Net injected active/reactive power to node (MW/Mvar).
- V Voltage magnitude of nodes (pu).
- θ Voltage angle of nodes (pu).
- PL^{DR}/QL^{DR} Active/reactive power after DR (MW/Mvar).
- G_t Solar radiation variable (W/m^2).
- SOH^{H2} State of hydrogen in tank (Kg).
- Q^{HS} Reactive power support by HS inverter (Mvar).
- ψ Binary variable for HS.
- PL / QL Active/reactive power flow in line l (MW/Mvar).
- SL Apparent power flow in line l (MVA).
- φ_s Auxiliary variable for risk management.
- W Auxiliary variable of bilinear optimization.
- δV^+ / δV^- Positive/negative voltage deviation.
- δV Voltage deviation.
- VaR Value at risk.
- χ Binary variable for linearization.

Problem Formulation

Objective Functions

The multi-objective functions consist of both economic and technical objectives. In the following formulation, the index s, representing scenarios of variables and parameters, is removed to simplify equations due to space limitations.

Total Operating Cost (OC) Minimization

The first objective function is to minimize the total system operating cost, as modeled in (4.1). The first term of (4.1) relates to the purchasing power from the upper grid, and the other three terms are the operating cost of utility-operated DGs, PVs, and HSs.

$$OC_t = \sum_{t=1}^{T}[(P_{t,sub}^{UG} \times \lambda_t^{Grid}) + (P_{t,d}^{DG} \times \lambda_t^{DG}) + (P_{t,p}^{PV} \times \lambda_t^{PV}) + ((P_{t,h}^{EL} - P_{t,h}^{FC}) \times \lambda_t^{Grid})] \quad (4.1)$$

Power Quality Improvement (PQI)

The second objective function is to minimize the voltage deviation of nodes with higher priorities as shown in (4.2). It is assumed that nodes with HSs have higher priority due to the H2 demand of the transportation sector which must be supplied. Due to the efficiency of electrolyzers (which is assumed to be 60% in this chapter) and accordingly H2 demand pattern, more power should be consumed to produce 1 kg of H2. This results in higher loading of the node and consequently significant voltage issues in the nodes with HSs. To that end, in order to provide a reliable and safe operation of these assets, more reactive power support is needed to keep the voltages near to 1 per unit (p.u.). Equation (4.2) minimizes the voltage deviation compared to 1 p.u. Better voltage profiles can be obtained by increasing the value of ω_i in equation (4.2).

$$PQI_{t,i} = \sum_{t=1}^{T}\sum_{i=1}^{N} \omega_i \ \left|V_{t,i} - V_{t,i}^{*}\right| \quad (4.2)$$

where $V_{t,i}^{*}$ is the nominal voltage assumed to be 1 (p.u.).

Solar Radiation and PV Generation Modeling

Solar radiation is one of the preeminent factors that affects the output power of PV generators. The literature shows that solar radiation roughly follows the beta distribution function as expressed in (4.3)-(4.7).

$$BF(G_t) = \frac{\Gamma(\pi_t + \varpi_t)}{\Gamma(\pi_t)\,\Gamma(\varpi_t)} \times (1 - G_t)^{\varpi_t - 1} \times (G_t)^{\pi_t - 1} \tag{4.3}$$

$$\pi_t = \frac{\mu_t \times \varpi_t}{1 - \mu_t}, \quad \varpi_t = (1 - \mu_t) \times (\frac{\mu_t \times (1 + \mu_t)}{\sigma_t^2} - 1) \tag{4.4}$$

$$P_{PV} = \left[P_{ST} \times \frac{G_t}{1000} \times (1 - \gamma \times (T_j - 25)) \right] \times n_{PV_s} \times n_{PV_p} \tag{4.5}$$

$$T_j = T_{amb} + \frac{G_t}{800} \times (\mathbf{NOCT} - 20) \tag{4.6}$$

$$(P_{t,p}^{PV})^2 + (Q_{t,p}^{PV})^2 \leq (S_{t,p}^{inv,PV})^2 \tag{4.7}$$

where π_t and ϖ_t are parameters of PV output power and cell temperature as defined in (4.4), (4.5) and (4.6) respectively [85] [86] [87]. The PV units are equipped with inverters to provide both active and reactive power, as limited by (4.7).

Hydrogen System Modeling

Operating constraints of HSs, including electrolyzer, FC, hydrogen storage tank, and HFS are listed in (4.8)-(5.18).

$$N_{t,h}^{EL,H2} = \eta^{EL} \times (P_{t,h}^{EL,jo}) \times P2H^{EL} \tag{4.8}$$

$$P_{t,h}^{EL,jo} = P_{t,h}^{EL} + P_{t,p}^{PV} \qquad ,\forall\ h = p \tag{4.9}$$

$$P_{h}^{EL,min} \times \psi_{t,h}^{HS} \ \leq P_{t,h}^{EL,jo} \ \leq P_{h}^{EL,Max} \times \psi_{t,h}^{HS} \tag{4.10}$$

$$0 \leq N_{t,h}^{EL,H2} \leq \ N_{max}^{EL,H2} \times \psi_{t,h}^{HS} \tag{4.11}$$

$$N_{t,h}^{FC,H2} = \frac{P_{t,h}^{FC}}{\eta^{FC}\ H2P^{FC}} \tag{4.12}$$

$$P_{h}^{FC,min} \times (1 - \psi_{t,h}^{HS}) \ \leq P_{t,h}^{FC} \ \leq P_{h}^{FC,Max} \times (1 - \psi_{t,h}^{HS}) \tag{4.13}$$

$$0 \leq N_{t,h}^{FC,H2} \leq \ N_{max}^{FC,H2} \times (1 - \psi_{t,h}^{HS}) \tag{4.14}$$

$$\begin{aligned} SOH_{t,h}^{H2} \ = SOH_{t-1,h}^{H2} \ - \lambda^{Dsp} \times SOH_{t,h}^{H2} \ + (N_{t,h}^{EL,H2} \\ - HDE_{t,h} - N_{t,h}^{FC,H2})\ \Delta t \end{aligned} \tag{4.15}$$

$$SOH_{t,h}^{H2,min} \leq SOH_{t,h}^{H2} \leq SOH_{t,h}^{H2,Max} \tag{4.16}$$

$$SOH_{t,h}^{H2,init} \geq \phi_{t,h}^{init} \times SOH_{h}^{H2,Max}, \quad \forall\, t = 1 \tag{4.17}$$

$$(P_{t,h}^{EL} - P_{t,h}^{FC})^2 + (Q_{t,h}^{HS})^2 \leq (S_{t,h}^{inv,HS})^2 \tag{4.18}$$

where equation (4.8) represents the amount of H2 produced by the PEM electrolyzer. The cooperative operation of PV and power from the upper grid for electrolyzer usage is modeled in (4.9). If the HS is equipped with PV, both PV output power and power from the grid can be used by the electrolyzer for H2 production; otherwise, the only source of power for water electrolysis is the purchased electricity from the grid, then $P_{t,p}^{PV}$ will be zero in (4.9). Electrolyzer power capacity limits and the generated H2 from operating the electrolyzer are presented in (4.10) and (4.11), respectively. Equation (4.12) models the H2 consumption by stationary FC to generate electricity. FC power limits and H2 consumption levels for generating power are shown in (4.13) and (4.14), respectively. To prevent simultaneous H2 production and consumption, a binary variable, $\psi_{t,h}^{HS}$, is defined. If $\psi_{t,h}^{HS}$ gets the value of 1, electrolyzers consume power, and stationary FC units could not consume H2 for injecting power into the grid (in this scenario the FC units are remaining off). On the other hand, if this variable gets the value of 0, FC units consume H2 and convert it into the power, and electrolyzers are remaining off. H2 mass at each hour, H2 storage tank minimum and maximum mass capacity limits, and initial mass of H2 of the tank are defined in (4.15), (4.16) and (4.17), respectively. The inverter of HS poses limits on the power transfer from HS, as shown in (5.18). Conversion factors of $P2H^{EL}$ and $H2P^{FC}$ are determined based on [54].

Demand Response and CVR Modeling

Appropriate load modeling is needed to provide a realistic power consumption profile. DR enables customers to reduce their consumption level during peak hours and shift some portion of their

load to off-peak hours to reduce their bills. This chapter considers both active and reactive power shifting while preserving the power factor of each load. Defining the active base load as $PL_{t,i}^{base}$, (4.19)-(4.24) show the DR formulation.

$$QL_{t,i}^{base} = PL_{t,i}^{base} \ (tan(arccos\ LPF_i)) \tag{4.19}$$

$$\left| S_{t,i}^{shift} \right| \leq \iota_i \sqrt{(PL_{t,i}^{base})^2 + (QL_{t,i}^{base})^2} \tag{4.20}$$

$$PL_{t,i}^{shift} = S_{t,i}^{shift} \times LPF_i \tag{4.21}$$

$$QL_{t,i}^{shift} = PL_{t,i}^{shift} \times \ (tan(arccos\ LPF_i)) \tag{4.22}$$

$$\sum_{t=1}^{T} PL_{t,i}^{shift} = 0, \quad \sum_{t=1}^{T} QL_{t,i}^{shift} = 0 \tag{4.23}$$

$$PL_{t,i}^{DR} = PL_{t,i}^{base} + PL_{t,i}^{shift}\ ,\ QL_{t,i}^{DR} = QL_{t,i}^{base} + QL_{t,i}^{shift} \tag{4.24}$$

Where reactive power consumption and shiftable apparent power are shown in (4.19) and (4.20), respectively. Shiftable active and reactive power can be calculated in (4.21) and (4.22). Constraint (4.23) ensures that the reduced and increased amount of active and reactive load should be equal during total operation hours. The reason for considering reactive power shifting is to keep the load power factor constant. Finally, (4.24) express active and reactive power consumption after load shifting.

To address the dependency of loads to voltage magnitude at different time horizons, the polynomial ZIP load model is utilized for the deployment of CVR. CVR can also be deployed by utilities to further reduce the load and bills of customers, which the non-linear model was investigated in [88].The mathematical formulation of CVR can be represented as below.

$$P_{t,i}^{CVR} = PL_{t,i}^{DR} \ (K_{t,i}^{PZ}(\frac{V_{t,i}}{V_{t,i}^{*}})^2 + K_{t,i}^{PI}(\frac{V_{t,i}}{V_{t,i}^{*}}) + K_{t,i}^{PP}) \tag{4.25}$$

$$Q_{t,i}^{CVR} = QL_{t,i}^{DR} \ (K_{t,i}^{QZ}(\frac{V_{t,i}}{V_{t,i}^{*}})^2 + K_{t,i}^{QI}(\frac{V_{t,i}}{V_{t,i}^{*}}) + K_{t,i}^{QP}) \tag{4.26}$$

Network Constraints

Network-related constraints are expressed in (4.27)-(4.34) to address physical limits of power grids. Active and reactive power balance are presented in (4.27) and (4.28), respectively. It should be noted that $P_{t,i,s}^{CVR}$ could be replaced with PL^{DR} or $PL_{t,i}^{base}$ for considering scenarios that only address load with DR or base load of system. The general form of AC power flow constraints are shown in (4.29) and (4.30). (4.31) presents active and reactive line flow limits based on the line capacity. Accordingly, (4.32) and (4.33) are active and reactive power capacity limits for DGs and purchasing power from the upper grid. Finally, (4.34) keeps the voltage magnitude within the specified limit (i.e., $\pm 5\%$ of nominal voltage in p.u.) [89].

$$\sum_{j=1}^{N} FL_{t,(i,j)}^{P} = P_{t,sub}^{UG} + P_{t,d}^{DG} + P_{t,p}^{PV} + P_{t,h}^{FC} - P_{t,i}^{CVR} - P_{t,h}^{EL,jo} \tag{4.27}$$

$$\sum_{j=1}^{N} FL^{Q}_{t,(i,j)} = Q^{UG}_{t,sub} + Q^{DG}_{t,d} + Q^{PV}_{t,p} - Q^{CVR}_{t,i} - Q^{HS}_{t,h} \tag{4.28}$$

$$FL^{P}_{t,(i,j)} = \ G_{i,j}(V^{2}_{t,i} - V_{t,i}\ V_{t,j}\ \cos(\theta_{t,i} - \theta_{t,j})) - B_{i,j}(V_{t,i}\ V_{t,j}\ \sin(\theta_{t,i} - \theta_{t,j})) \tag{4.29}$$

$$FL^{Q}_{t,(i,j)} = -B_{i,j}(V^{2}_{t,i,s} - V_{t,i}\ V_{t,j}\ \cos(\theta_{t,i} - \theta_{t,j})) - G_{i,j}(V_{t,i}\ V_{t,j}\ \sin(\theta_{t,i} - \theta_{t,j})) \tag{4.30}$$

$$(FL^{P}_{t,(i,j)})^{2} + (FL^{Q}_{t,(i,j)})^{2} \leq (SL_{t,(i,j)})^{2} \tag{4.31}$$

$$(P^{DG}_{t,d})^{2} + (Q^{DG}_{t,d})^{2} \leq (S^{DG}_{t,d})^{2} \tag{4.32}$$

$$(P^{UG}_{t,sub})^{2} + (Q^{UG}_{t,sub})^{2} \leq (S^{UG}_{t,sub})^{2} \tag{4.33}$$

$$V^{min} \leq V_{t,i} \leq V^{Max} \tag{4.34}$$

Linearization Procedure

Nonlinearity in constraints (4.2), (4.7), (5.18), (4.25)-(4.26) and (4.29)-(4.33) are linearized to build the MILP model.

Second Objective Function Linearization

Linearization of second objective function PQI can be found in (4.35)-(4.39), which replaces (4.2) as the second objective function.

$$Min.\ PQI = \sum_{t=1}^{T} \sum_{i=1}^{N} \omega_i \ \left(\delta V_{t,i}^{+} + \delta V_{t,i}^{-}\right) \tag{4.35}$$

$$\delta V_{t,i} = V_{t,i} - V_{t,i}^{*} \tag{4.36}$$

$$\delta V_{t,i} = \delta V_{t,i}^{+} - \delta V_{t,i}^{-} \tag{4.37}$$

$$0 \leq \delta V_{t,i}^{+} \leq M1(1 - \chi_{t,i}) \tag{4.38}$$

$$0 \leq \delta V_{t,i}^{-} \leq M1\ \chi_{t,i} \tag{4.39}$$

Second-order Constraints Linearization

A minimum power factor is required for PV integration in power grids. The linearization of (4.7) can be defined as follows [90]:

$$\frac{P}{\sqrt{P^2\ + Q^2}} \geq K \tag{4.40}$$

$$-\frac{P\sqrt{1-K^2}}{K} \leq Q \leq \frac{P\sqrt{1-K^2}}{K} \tag{4.41}$$

where K is a constant value related to the power factor of PV units. Additionally, the general form of second order constraints (4.31)-(4.33) is presented in (4.42), which can be linearized based on equations (4.43)-(4.45). As an example, considering equation (4.33), x, y, and z can be replaced by $P^{UG}_{t,sub}$, $Q^{UG}_{t,sub}$, and $S^{UG}_{t,sub}$, respectively.

$$x^2 + y^2 \leq z^2 \tag{4.42}$$

$$-\sqrt{3}\,(x+z) \leq y \leq -\sqrt{3}\,(x-z) \tag{4.43}$$

$$-\frac{\sqrt{3}}{2}\,z \leq y \leq \frac{\sqrt{3}}{2} \tag{4.44}$$

$$\sqrt{3}\,(x-z) \leq y \leq \sqrt{3}\,(x+z) \tag{4.45}$$

It should be noted that hexagon approximation is used in this chapter for the best compromise between error and size of the optimization problem [91].

DR and CVR Constraints Linearization

Nonlinearity of (4.25)-(4.26) can be linearized in two steps. First, considering the standard voltage range of [0.95-1.05] (p.u.), the second-order term of voltage $(\frac{V_{t,i}}{V^*_{t,i}})^2$ can be linearized as follows.

$$P^{CVR}_{t,i} = PL^{DR}_{t,i}\ (K^{PZ}_{t,i}(1 + 2(V_{t,i} - V^*_{t,i})) + K^{PI}_{t,i}(\frac{V_{t,i}}{V^*_{t,i}}) + K^{PP}_{t,i}) \tag{4.46}$$

$$Q^{CVR}_{t,i} = QL^{DR}_{t,i}\ (K^{QZ}_{t,i}(1 + 2(V_{t,i} - V^*_{t,i})) + K^{QI}_{t,i}(\frac{V_{t,i}}{V^*_{t,i}}) + K^{QP}_{t,i}) \tag{4.47}$$

Second, the McCormick method [92] is applied to replace the bilinear terms of the product of two continuous variables ($PL^{DR}_{t,i}$ and $V_{t,i}$) with a new variable ($W_{t,i}$). Then (4.46) can be reformulated as follows:

$$W_{t,i} = PL^{DR}_{t,i} \times V_{t,i} \tag{4.48}$$

$$P^{CVR}_{t,i} = W_{t,i}\ (2K^{PZ}_{t,i} + K^{PI}_{t,i}) - PL^{DR}_{t,i}K^{PZ}_{t,i} + PL^{DR}_{t,i}K^{PP}_{t,i} \tag{4.49}$$

To reduce the search space, upper and lower bounds of two continuous variables should be set

appropriately.

$$W_{t,i} \geq -PL_{t,i}^{DR,max}\ V_{t,i}^{max} + PL_{t,i}^{DR}\ V_{t,i}^{max} + PL_{t,i}^{DR,max}\ V_{t,i} \tag{4.50}$$

$$W_{t,i} \geq -PL_{t,i}^{DR,min}\ V_{t,i}^{min} + PL_{t,i}^{DR}\ V_{t,i}^{min} + PL_{t,i}^{DR,min}\ V_{t,i} \tag{4.51}$$

$$W_{t,i} \leq -PL_{t,i}^{DR,max}\ V_{t,i}^{min} + PL_{t,i}^{DR}\ V_{t,i}^{min} + PL_{t,i}^{DR,max}\ V_{t,i} \tag{4.52}$$

$$W_{t,i} \leq -PL_{t,i}^{DR,min}\ V_{t,i}^{max} + PL_{t,i}^{DR}\ V_{t,i}^{max} + PL_{t,i}^{DR,min}\ V_{t,i} \tag{4.53}$$

Finally, (4.49)-(4.53) are the linearized form of (4.46). As similar approach was applied to linearize (4.47).

AC Power Flow Constraints Linearization

linearized form of AC power flow equations with consideration of the loss factor is incorporated into the model as used in [93] [94] for radial distribution networks.

$$FL_{t,j}^{P} = \sum_{i=1}^{N}(G_{i,j}(V_{t,i} + V_{t,j} - 1) + B_{i,j}(\theta_{t,i} - \theta_{t,j})) \tag{4.54}$$

$$FL_{t,j}^{Q} = \sum_{i=1}^{N}(-B_{i,j}(V_{t,i} + V_{t,j} - 1) + G_{i,j}(\theta_{t,i} - \theta_{t,j})) \tag{4.55}$$

$$PL_{t,(i,j)} = -G_{i,j}(V_{t,i} + V_{t,j}) + B_{i,j}(\theta_{t,i} - \theta_{t,j}) \tag{4.56}$$

$$QL_{t,(i,j)} = B_{i,j}(V_{t,i} + V_{t,j}) + G_{i,j}(\theta_{t,i} - \theta_{t,j}) \tag{4.57}$$

$$SL_{t,(i,j)} = PL_{t,i,j} + \xi_{t,i,j} \times QL_{t,i,j} \tag{4.58}$$

$$\left|SL_{t,(i,j)}\right| \leq SL_{i,j}^{Max} \tag{4.59}$$

Equations (4.54)-(4.55) refer to linearized AC power flow constraints in which $FL_{t,j}^{p}$ and $FL_{t,j}^{q}$ refer to the net injected active and reactive power into the node j at hour t. Additionally, (4.56)-(4.59) express the active, reactive, and apparent power flow in line l, which connects node i to node j, respectively. More details regarding the linearized formulation can be found in [94].

Risk-Aversion

CVaR is applied to address the risk of uncertain parameters in day-ahead scheduling. For a given confidence level $\alpha \in [0, 1]$, CVaR can be defined as the expected cost of $(1-\alpha) \times 100$ of the worst-case scenarios [94, 95]. The CVaR and risk constraints can be integrated into the optimization problem as presented in (4.60)-(4.63).

$$min\ \{(1-\beta)\sum_{s=1}^{S}\rho_s \times OC_{t,s}\ + \beta\ (VaR + \frac{1}{1-\alpha}\sum_{s=1}^{S}\rho_s \times \varphi_s)\} \tag{4.60}$$

$$OC_{t,s} - VaR - \varphi_s \leq 0 \tag{4.61}$$

$$\varphi_s \geq 0 \tag{4.62}$$

$$\rho_s = \rho_{PV} \times \rho_{HDE} \times \rho_{load} \times \rho_{Price} \tag{4.63}$$

where $\beta \in [0, 1]$ is a tuning parameter for managing the level of risk aversion with 0 meaning risk neutral and 1 meaning fully risk averse.This chapter considers the simultaneous risk of grid load, wholesale market price, H2 demand, and PV generation as defined in (4.63).

ε-constrained Method

To solve both objective functions simultaneously in the multi-objective MILP problem, a proper and fair compromise should be considered. The weighted sum technique is one of the common methods, but the determination of proper weights of each objective function is a major challenge. In this chapter, ε-constrained method [96, 97] is used for solving the multi-objective problem. In the first step, this technique considers one objective as the major objective function, and the other objectives are considered as constraints. The formulation is presented in (4.64)-(4.65).

$$minimize \quad OC_t \tag{4.64}$$

$$s.t \quad \begin{cases} -\infty \ \leq \ PQI_t \ \leq \ +\infty \\ \text{All linear constraints} \end{cases} \tag{4.65}$$

The second step starts with considering a reasonable deviation (Υ^{OC}) for the first objective function, as follows.

$$minimize \quad PQI_t \tag{4.66}$$

$$s.t \quad \begin{cases} OC_t \leq OC_t^{Optimal} \times (1 + \Upsilon^{OC}) \\ \text{All linear constraints} \end{cases} \tag{4.67}$$

where (Υ^{OC}) can be considered as a parameter for achieving the compromise between two objective functions. For instance, (Υ^{OC} = 10 %) explains that the voltage deviation is minimized with the cost of 10% deviation from its optimal value.

Simulation Results and Analysis

Description of Test System and Assumptions

The proposed multi-objective risk-based model is validated on the 33-node distribution test system [82] [98] as depicted in Fig. 6.2 with an hourly time step. There are two distributed HSs, three PV units with the maximum capacity of 0.5MW each, and three utility-operated DGs with a maximum and minimum capacity of 3MW and 0.21MW each, respectively [72]. The DGs and PVs are assumed to supply the loads with the operational cost of $50/MWh and $10/MWh. These costs are selected to incentivize the use of cheaper generation assets [99]. PEM Electrolyzer, reservoir tank, and PEM FC units data are from [54], and H2 demand pattern is obtained from [56]. H2 demand from FCEVs at HS1 and HS2 is 285.3kg and 142.6kg of H2 (which approximately equals to 95 and 47 FCEVs), respectively. FCEVs are 2020 Honda Clarity models [100] considering with the assumption that these cars arrive at HFSs with 45% fuel in their tank (FCEVs fill the tanks

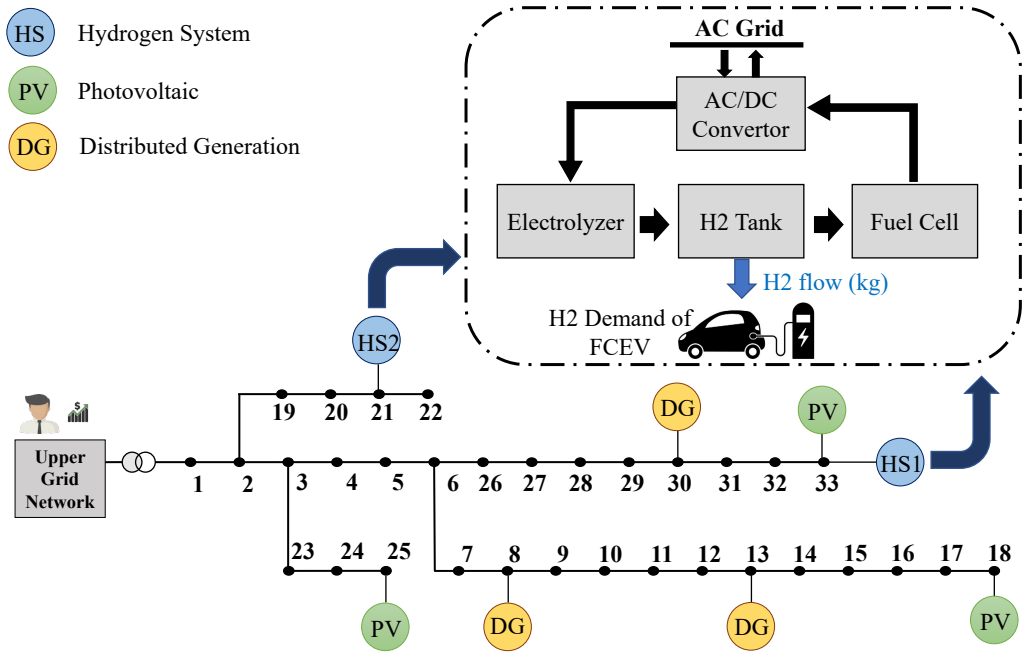

Figure 4.2. Distribution system with RESs and distributed HSs.

for the remaining tank capacity which is 55%). Moreover, the maximum apparent power limits for purchasing/generating power from/to upper grid, PVs, DGs, and HSs are assumed as their maximum generation capacities.

A one-month (July 2019) statistical analysis of the PJM market (for capturing the real mean and variance of actual data) [80] is performed to provide realistic upper-grid market prices and load data. Monte Carlo simulation was applied to generate 1,000 scenarios, which were downsized to 7 scenarios using forward selection probability distance algorithm (Kantrovich distance) [95], as shown in Fig. 4.3. To demonstrate the results effectively, scenario 3 is chosen to present details, as it has the highest probability among all scenarios shown in Table 4.1. Accordingly, Fig. 4.4(a) and Fig. 4.4(b) show Hourly data for load, market price, H2 demand, and output PV power for scenario 3. It should be mentioned that multiplier in Fig. 4.4(b) refers to the normalized coefficient based on the maximum value of data. For instance, the maximum H2 demand from FCEVs at hour 7 AM

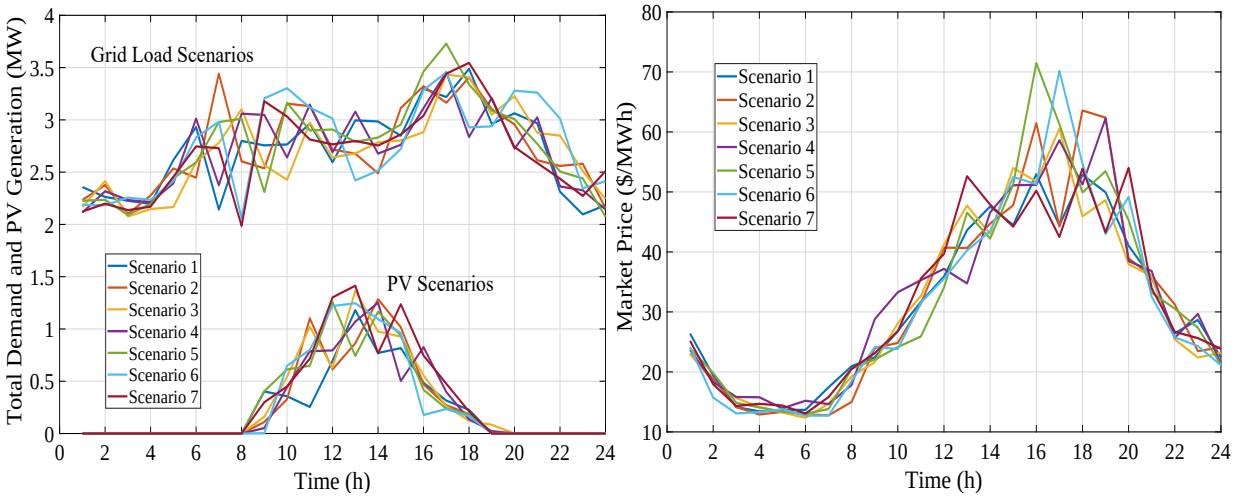

(a) PV and grid load scenarios

(b) Wholesale market price scenarios

Figure 4.3. PV, demand, and wholesale market price scenarios.

is approximately 41 kg, and multiplier 1 shows the 41 kg of H2 demand. Since the H2 demand of HFS 2 is 20.5 kg (the maximum H2 demand for HFS 2), the maximum multiplier for HFS 2 is 0.5.

The power factor is considered as 0.9, and voltage-dependent load coefficients are calculated based on the method presented in [101]. However, deep learning methods can also be used for these coefficients as peresented in [102]. Moreover, the boundary for load shifting is assumed to be 15% of apparent power, which is calculated based on active/reactive load power factor. Additionally, H2 demand scenarios are generated based on [56] with the standard deviation of 0.1. The confidence level for risk-averse analysis is assumed to be 0.95.

The simulations are carried out on a PC with an Intel Core-i7 CPU of 1.8 GHz and 16 GB RAM. Additionally, the proposed MILP framework was solved using IBM ILOG CPLEX 12.6 and GAMS IDE with a gap of 0%.

Table 4.1. Probability of Each Scenario

Scenario #	Probability (%)	Scenario #	Probability (%)
Scenario 1	16.4	Scenario 5	12.6
Scenario 2	9.8	Scenario 6	3.6
Scenario 3	23.6	Scenario 7	14.6
Scenario 4	19.4		

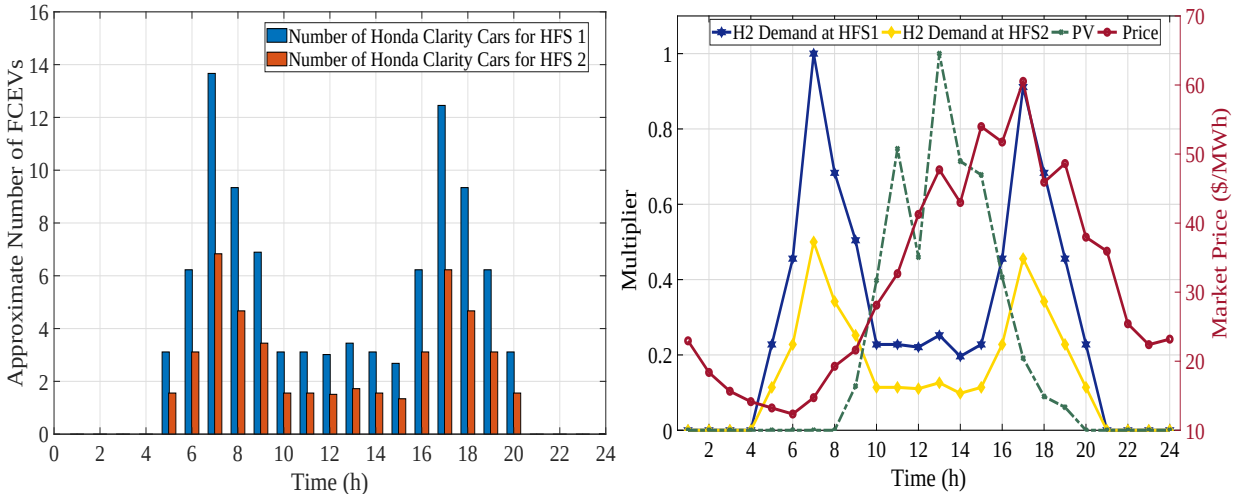

(a) Hourly Number of FCEVs

(b) HFS1, HFS2, and PV multipliers

Figure 4.4. Hourly data for load, wholesale market price, H2 demand, and output PV power for scenario 3.

The Impact of DR and CVR on Load Profile

Fig. 4.5 shows the impact of DR and CVR on the load curve in three scenarios. Based on the 15% DR, a portion of total demand at every hour is shifted from hours when the wholesale market price is high to hours when the market price is low. Due to the voltage-dependent loads, after deploying CVR from the utility side, total demand at each hour is reduced as shown in green curve. Therefore, this reduction in voltage values results in decreasing the load and accordingly the electricity bill

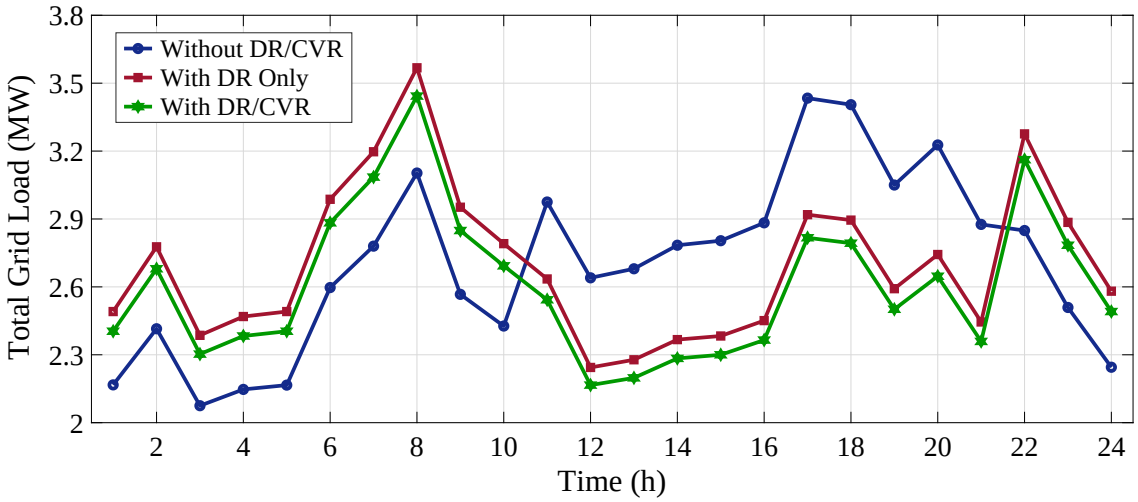

Figure 4.5. Total grid load w/ and w/o DR/CVR.

of customers due to the voltage dependent loads. Consequently, both utilities and customers can save money. More details regarding the impact of risk levels on operating cost will be presented in section 4.

The Impact of Power Quality Enhancement

To analyze the impact of power quality enhancement, the model is solved without and with considering PQI, which is the second objective function that pushes the voltage towards the nominal voltage. Fig. 4.6a and Fig. 4.6b demonstrate the voltage values for all nodes before and after considering the PQI. The range of voltage magnitude is reduced after considering PQI, which can provide more reliable operation of the entire distribution system.

In this chapter, nodes with HS must supply hydrogen to FCEVs, and they are considered as high-priority nodes. The comparison of before and after considering PQI at nodes 21 and 33 are shown in Fig. 4.7 and Fig. 4.8, respectively. Voltage values deviate less from nominal voltage with PQI

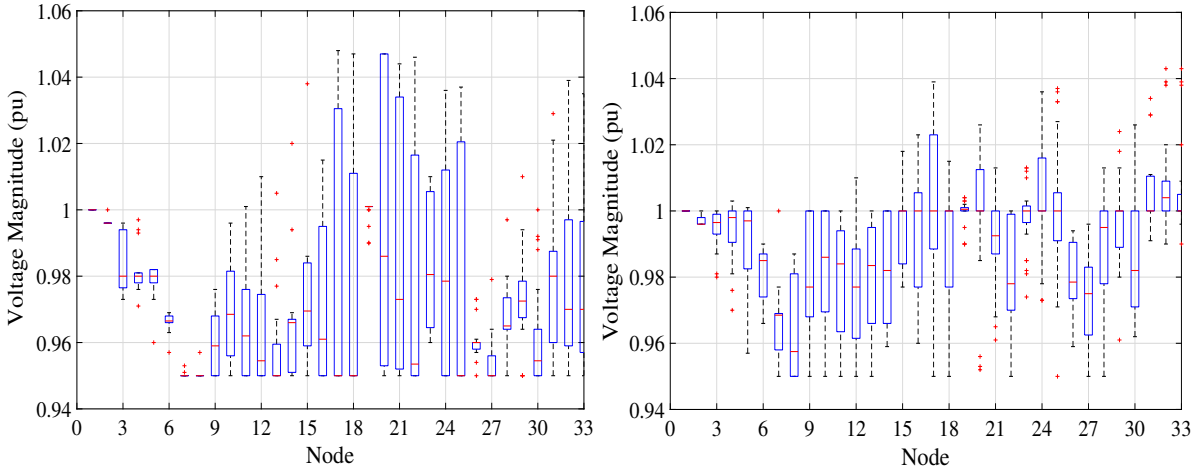

(a) Voltages before considering PQI

(b) Voltages after considering PQI

Figure 4.6. Voltage profile w/o and w/ considering PQI

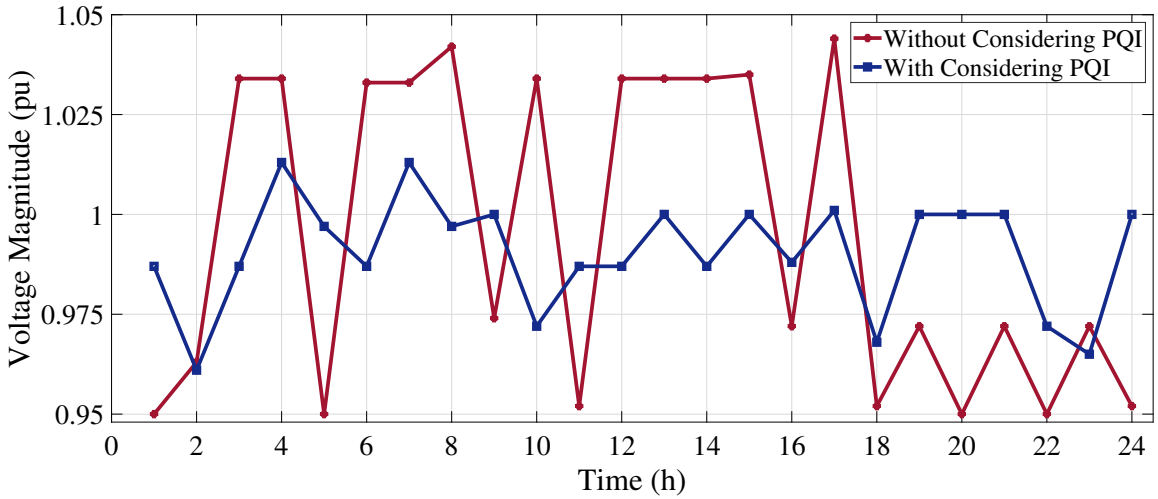

Figure 4.7. Voltage of node 21 before and after considering PQI

compared to the case without PQI, which shows the reliable operation of these nodes.

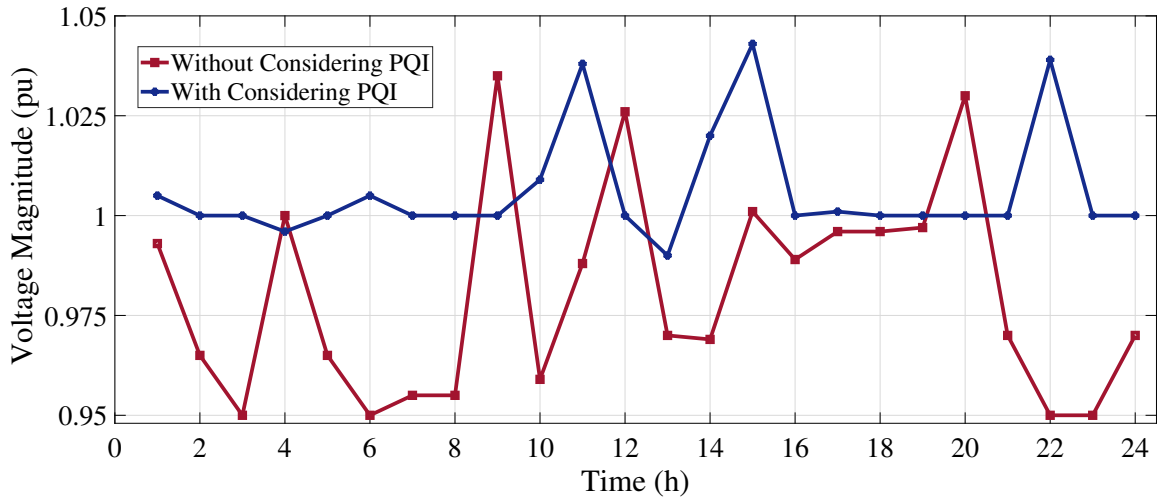

Figure 4.8. Voltage of node 33 before and after considering PQI.

HS Operation w/ and w/o Cooperative Operation with PV

The bidding of HSs significantly depends on market price, H2 demand from FCEVs, and PV output (for the cooperative operation of HS and PV). Two cases are considered in this study; 1) without considering the cooperative (joint) operation, 2) with considering a cooperative operation. In the first case, HS purchases power from the grid at market price for electrolyzer operation and supplying the H2 demand. For example, HS1 must purchase power from grid even though a PV is installed at node 33, as the owners of HS and PV units are assumed to be different. The second case is when both the PV and HS belong to the same owner, who can also receive power from upper grid. The second case study is only considered for HS1.

The bidding strategy of HS2 is the same for both case studies since there is no PV to be cooperatively operated at node 21. Fig. 4.9a demonstrates the bidding strategy for minimizing the operating cost of HS2 besides supplying the H2 demand of FCEVs. It shows that HS purchases power for electrolyzer operation (H2 production) from grid when the market price is lower (1 am to 8 am); and when the market price is higher (at 1 pm and 3-7 pm), extra H2 is converted to power

by the FC and injected to grid. The mass of hydrogen at each hour is also depicted in Fig. 4.9b.

The bidding strategy of HS1 and the mass of hydrogen in the tank are shown in Fig. 4.10 for both case studies. In the first case, same as HS2, electrolyzer consumes power to produce H2 in the early hours due to cheaper electricity price. As it can be seen from Fig. 4.10(a), in this case (without joint operation) the exported power from FC units into the grid is zero MW since it is not cost-effective to generate power. It is because the PV energy is used to supply the grid load, rather than enabling electrolyzers to produce H2 for FC consumption. For this reason, the yellow bars did not appear in the Fig. 4.10(a). However, considering the case of cooperative (joint) operation with PV, there is potential to import power directly from PV from 9 am till 6 pm, assuming that HS directly uses PV power. Therefore, there is no need for the electrolyzer to be fully operated in the early hours. Instead, some portion of H2 demand can be supplied from PV in the next hours, as shown in Fig. 4.10a. For instance, total power consumed by electrolyzer at 9 am is 1.287MW, in which 1.233MW is purchased from grid and 0.054MW is from PV generation. Another example at 1 pm (maximum PV output), total 8.07Kg H2 (based on 0.455MW PV output) is produced and stored at H2 tank. Additionally, in cooperative mode, FC injects 0.5 MW power into the grid at 5 pm, since market price reaches the maximum based on Fig. 4.4b.

Additional analysis is that if an HS only purchases power from the grid with market price, it should produce hydrogen in the early hours of the day, which forces HS to have larger hydrogen tanks to store H2. However, the capacity of the tank can be reduced by cooperative operation of PV, as shown in Fig. 4.10b. Moreover, it can be recognized that in the cooperative operation mode, there is potential for FC to transform excess H2 energy to power and inject it into the grid for more benefits.

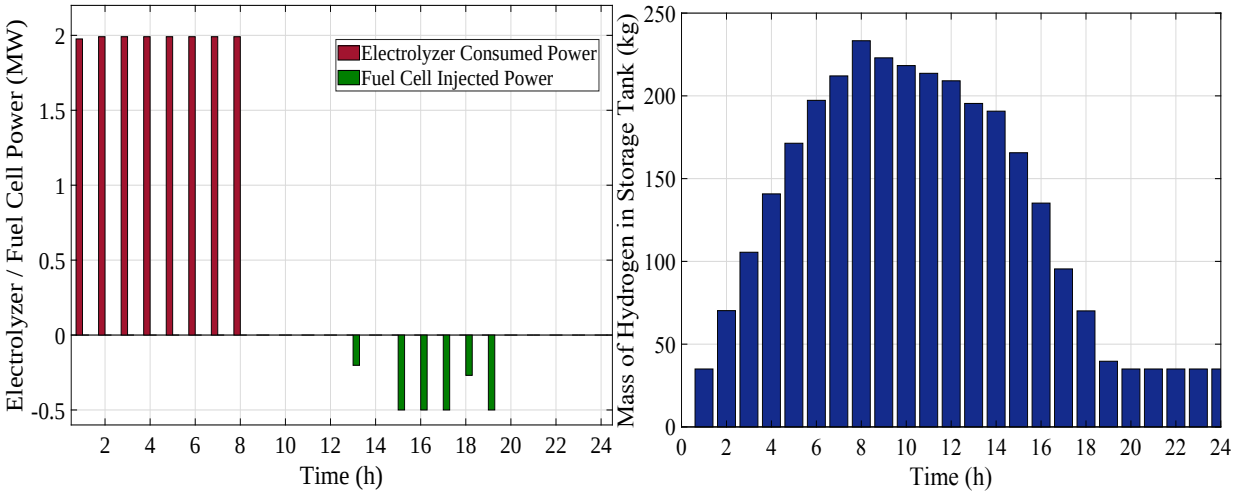

(a) Electrolyzer/FC consumed/injected power (b) Mass of hydrogen in tank

Figure 4.9. Results of hydrogen system (HS2) located at node 21

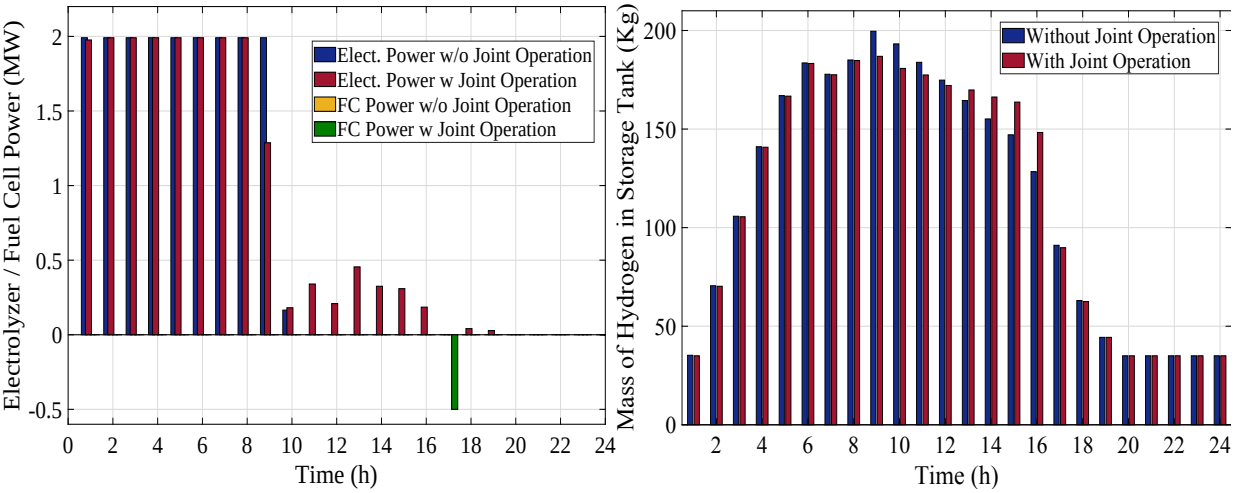

(a) Electrolyzer/FC consumed/injected power (b) Mass of hydrogen in tank

Figure 4.10. Results of hydrogen system (HS1) located at node 33

Impact of Risk Level on Operating Cost

The impact of risk level on system operating cost in different scenarios is presented in Fig. 4.11. First, in the risk-neutral case ($\beta = 0$), the total operating cost for the techno-economic model without considering DR, CVR, or cooperative operation is \$3109.432. Through the participation of DR and CVR, the total operating cost is reduced by \$174.841 (which equals to the total cost of \$2934.59) compared to the base case. Furthermore, if DR, CVR, and cooperative operation of PV and HS are all considered, the total operating cost is reduced by \$91.8 compared to the second scenario. It should be noted that since there is only one PV with maximum capacity of 0.5 MW cooperatively operated with HS1, the amount of cost reduction seems limited. However, if all HSs are operated with onsite PVs with larger capacities, the total cost saving will be more than the demonstrated value in case studies. Additionally, as the risk level increases, total operating cost increases. Because, in risk-neutral case, there is no risk for operator from uncertain parameters. However, as β reaches 1, which means fully risk-averse condition, the expected risk cost is added to the operating cost. For instance, with considering DR, CVR, cooperative operation, and the risk level of 100%, the total operating cost considering PQI is \$2985.5.

Conclusion

This chapter proposed a multi-objective risk-based model for day-ahead scheduling of HSs, considering the uncertainty of H2 demand, load, PV generation, and market price. Power quality enhancement was also incorporated in the model to improve the voltage profiles for nodes with higher priority such as nodes with HS. Additionally, linear model for DR and CVR were developed and deployed to present realistic results. Moreover, day-ahead scheduling of HS in the case of normal and cooperative operation with PV was presented. Simulation results indicate that the cooperative operation of HS with PV lowers the total cost of operation. The future work will in-

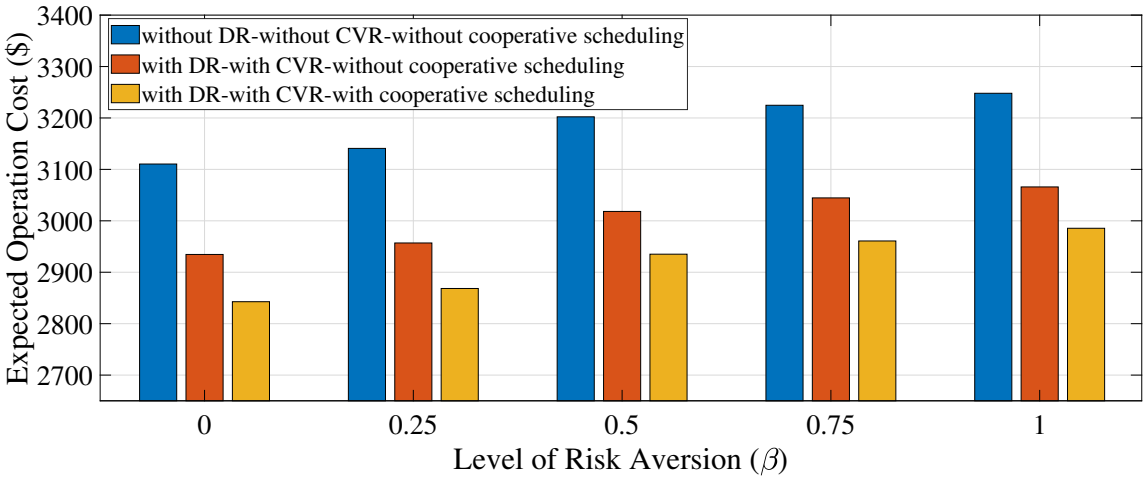

Figure 4.11. The impact of β on CVaR-based case studies.

clude the operation of detailed models of HS, FCEVs and their travel behavior in integrated power and transportation networks. Additionally, since the scope of this chapter was on the day-ahead operation and risk management, scalability was not the focus. However, in the case of considering intra-day and real-time markets, distributed optimization techniques can be applied to address the scalability issue for larger test systems.

CHAPTER 5: PROACTIVE ROLLING-HORIZON BASED SCHEDULING OF HYDROGEN SYSTEMS FOR RESILIENT POWER GRIDS [1]

Deploying DERs and other smart grid technologies have increased the complexity of power grids and made them more vulnerable to natural disasters and cyber-physical-human (CPH) threats. To deal with these extreme events, proactive plans are required by utilities to minimize the damages caused by CPH threats. This chapter proposes a proactive rolling-horizon-based scheme for resilience-oriented operation of hydrogen (H2) systems in integrated distribution and transmission networks. The proposed framework is a bi-level model in which the upper-level is focused on distribution system operation in both normal and emergency operation modes, and the lower-level problem accounts for the transmission network operation. Two preeminent aspects of H2 systems are considered in this chapter, 1) to show the flexibility of H2 systems, capacity-based demand response signals are considered for electrolyzers, stationary fuel cell (FC) units, and H2 storage tanks are considered in both normal and emergency operation modes; 2) unlike the batteries which can only charge and discharge energy based on maximum duration times and power ratings, H2 systems can be considered as the flexible long-term energy storage by storing H2 for days and supplying power to FC in the case of *N-m* outages lasting for more than 10 hours. Moreover, H2 production cost based on water electrolysis and storage costs is calculated. Simulation results demonstrate that utilities can improve the system-level resilience using H2 systems as long-term backup power resources.

Considering the aforementioned discussion, research efforts are mainly focused on normal opera-

[1] This chapter is prepared based on the paper presented at [103]:
Hamed Haggi, Wei Sun, James M. Fenton, and Paul Brooker, "Proactive Rolling Horizon based Scheduling of Hydrogen Systems for Resilient Power Grids", *IEEE Transactions on Industry Applications*, vol. 58, no. 2, pp. 1737-1746, 2022. [Link]

tion scheduling of H2 systems [52]- [67], and the techno-economic merit of H2 systems in enhancing the grid resilience has not been investigated yet. However, unlike the battery energy storages which can only store, charge, and discharge energy based on their maximum energy rating (maximum duration time), H2 systems can be considered as long-term energy storages to produce H2 by electrolyzers, store it in the tank, then convert it to power with FC units and inject power into the grid with the maximum FC capacity for longer period of time (e.g. days, months, etc.). In addition, the coordinated operation scheduling of distribution and transmission networks has been only focused on normal operation and planning context [104]- [105]. However, proactive scheduling of DERs in integrated transmission and distribution systems with the aim of resilience enhancement has not been investigated. Additionally, previous proactive scheduling frameworks only addressed the distribution network operation without considering the benefits of selling or purchasing power from transmission networks [71]- [75]. Therefore, this chapter extends authors' previous work presented in [7] by developing a bi-level framework for resilient scheduling of H2 systems in integrated distribution and transmission networks. The major contributions of this chapter compared to [7] are:

- A bi-level resilience-oriented framework considering the coordinated operation of distribution and transmission networks with the focus on scheduling the H2 systems (including both H2 refueling station and long-term energy storage system), in both normal and emergency operation mode is proposed. The upper-level and lower-level problems are focused on distribution network managed by distribution system operator (DSO) and transmission network managed by transmission system operator (TSO), respectively. To efficiently solve the bi-level problem, duality theory is deployed to recast it as a single-level equivalent problem.
- Capacity-based demand response (CBDR) signals are considered in pre-event operation. In normal operation, H2 systems can follow the signals imposed by DSO and assist the grid by acting as load (operating the electrolyzers) or generation unit (operating FC units). For the

emergency operation preparation, as soon as having the access to extreme event time based on the forecast, DSO sends signals to H2 systems to fill their storage tanks and be prepared for long-duration outages.

- Rolling horizon approach is deployed to limit the access of DSO to the perfect forecast of extreme event time (by providing only the next-day forecast), CBDR signals, and other information of renewables. Additionally, rolling-based operation can show the capability of H2 systems as fast-response DERs which provides more realistic results.

- Water electrolysis and storage costs are calculated for defining the selling price of H2 to FCEVs and providing a realistic revenue for DSO. It should be mentioned that H2 production cost is calculated based on real capacity factor (CF) of electrolyzers, distributional locational marginal price (DLMP), etc., which is more realistic due to the consideration of integrated operation of distribution and transmission networks energy price, congestion, power loss, and voltage regulation costs.

The rest of the chapter is organized as follows. Section 5 introduces the framework of this chapter. Section 5 presents the problem formulation. Section 7 presents numerical results and analysis, and finally Section 7 concludes the chapter and presents future work directions. More details on the linearization of the problem formulation is presented in Appendix.

Sets and Indices

- $\mathcal{N}$ Set of nodes, indexed by i.
- $\mathcal{T}$ Set of scheduling time interval, indexed by t.
- $\mathcal{N}_{\text{PV}}$ Set of nodes with photovoltaic units.
- $\mathcal{N}_{\text{W}}$ Set of nodes with wind units.

- $\mathcal{N}_{\text{HS}}$ Set of nodes with hydrogen system units.
- $\mathcal{N}_{\text{DG}}$ Set of nodes with generation units.
- $\mathcal{L}$ Set of network lines, indexed by $(i,j) \subset \mathcal{N} \times \mathcal{N}$.

Parameters

- β Sold electricity price to wholesale market ($/MWh).
- b/k No load cost ($) and ramping cost of DGs ($/MWh).
- $P/Q^{DG,min}$ Minimum active/reactive power output of DGs (MW).
- $P/Q^{DG,max}$ Maximum active/reactive power output of DGs (MW).
- S^{DG} Apparent power limit of DGs (MVA).
- ρ^{SU}/ρ^{SD} Startup and shutdown costs ($).
- S^{PV} Inverter capacity of PV units (MVA).
- $P^{PV,max}$ Maximum output power of PVs (MW).
- η^{EL}/η^{FC} Electrolyzer and Fuel Cell Efficiency (%).
- π^{EL} Power to H2 and H2 to power conversion factors (kg/MWh).
- π^{FC} H2 to power conversion factors (MWh/kg).
- $QH^{EL/FC,min}$ Minimum H2 production/consumption limit (kg).
- $QH^{EL/FC,max}$ Maximum H2 production/consumption limit (kg).
- π^{Dsp} Dissipation rate of H2 in tank (%/h).
- QH^{dem} H2 demand from transportation sector (kg/h).
- S^{HS} Inverter capacity of HS units (MW).
- $MOH^{min/max}$ Mass of hydrogen limits (kg).
- PDR^{Sgl} Capacity based demand response signal by DSO (MW).

- κ Emergency operation reserve percentage imposed by DSO (%).
- R/X Resistant and reactance of lines (pu).
- V^{max}/V^{min} Maximum and minimum voltage limits (pu).
- P^{load}/Q^{load} Active/reactive power demand (MW).
- S^{line} Distribution system lines' capacity (MVA).
- $VOLL$ Value of loss of load (\$/MWh).
- C^{g} Operation cost of generators (\$/MWh).
- $Pg^{min/max}$ Minimum and maximum output power of generators (MW).
- $TFl^{min/max}$ Minimum and maximum limits of transmission lines (MVA).
- Pw^{max} Maximum wind power output (MW).
- $P^{UG,max}$ Maximum limit for exchanged power between DSO and TSO (MW).
- TD Transmission system power demand (MW).

Variables

- P^{EXb} Purchased power from wholesale market (MW).
- P^{EXs} Sold power to wholesale market (MW).
- C^{DG} Operation cost of DGs (\$/MWh).
- C^{PV} Operation cost of PVs (\$/MWh).
- C^{SU}/C^{SD} Startup and shutdown costs of DGs (\$).
- $C^{Load,shd}$ Grid load curtailment cost (\$).
- x^{DG} Binary variable for status of DG (1 if unit is on and 0 if unit is off.)
- P^{DG}/Q^{DG} Active/Reactive power output of DGs (MW/MVAr).
- P^{PV}/Q^{PV} Active/Reactive power output of PVs (MW/MVAr).

- QH^{EL} Outflow of H2 from Electrolyzer (kg/h).
- P^{EL} Power consumed by Electrolyzer (MW).
- QH^{FC} Inflow of H2 into Fuel Cell (kg/h).
- P^{FC} Power generated by Fuel Cell (MW).
- Q^{HS} Output reactive power of H2 systems (MVAr).
- ψ^{HS} Binary variable for avoiding simultaneous H2 production and consumption.
- MOH^{H2} Mass of H2 in the storage tank (kg).
- CF^{EL} Capacity factor of Electrolyzer (%).
- $P^{EL,Shd}$ Electrolyzer demand curtailment (MWh).
- $P^{load,Shd}$ Active/reactive power demand curtailment (MW/MVAr).
- V Squared voltage magnitude of distribution nodes.
- $f^{p/q}$ Active/reactive power flow in distribution lines (MW/MVAr).
- a Squared current magnitude of distribution system nodes.
- Pg Active power of generators (MW).
- Pw Output power of wind farms (MW).
- Tfl Active power flow of transmission lines (MW).
- U Binary variable for preventing of simultaneous purchasing and selling power.
- λ Locational marginal price (Dual variable of power balance) ($/MWh).
- $\underline{\alpha}$ / $\overline{\alpha}$ Dual variable of min/max output of generators.
- $\underline{\psi}$ / $\overline{\psi}$ Dual variable of exchanged power with DSO.
- $\underline{\delta}$ / $\overline{\delta}$ Dual variable of min/max capacity limit of transmission lines.
- γ Dual variable of maximum output wind power.
- ζ Dual variable of transmission line power flow.
- θ Voltage phase angle of nodes in transmission network.

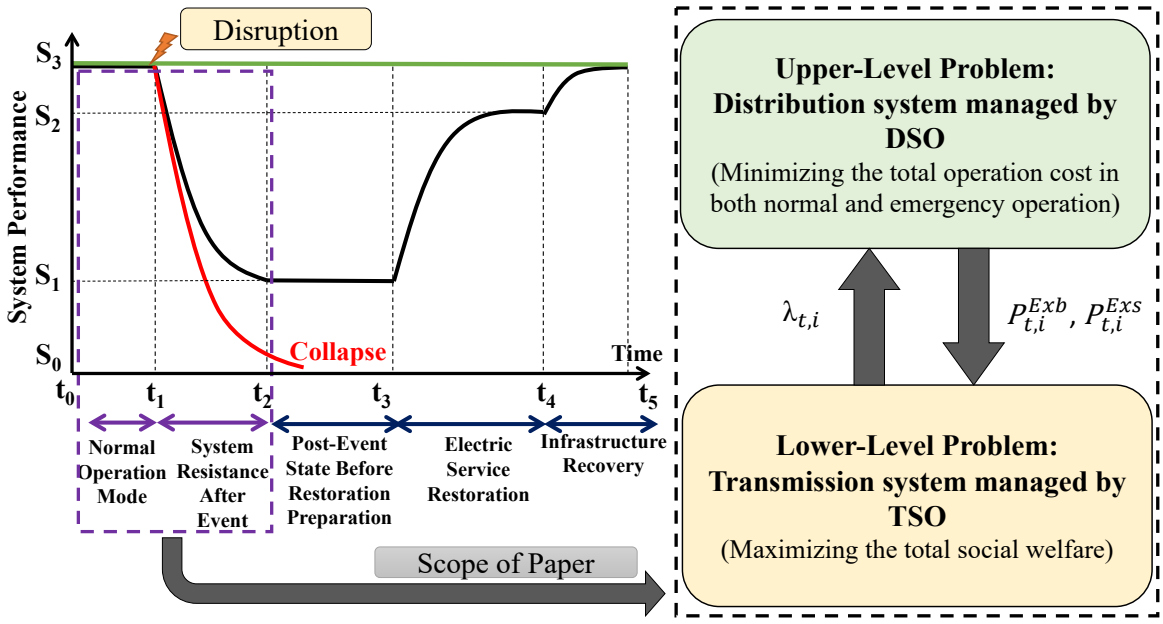

Figure 5.1. The proposed bi-level resilience-oriented framework for integrated transmission and distribution networks.

Proposed Framework

The proposed bi-level resilience-oriented framework with the focus on proactive scheduling of integrated transmission and distribution networks is presented in Fig. 5.1. It shows that the scope of this chapter is proactive scheduling and survivability analysis for the normal and emergency operation, respectively. The upper-level (UL) problem minimizes the total operation cost of all assets in both normal and emergency operation modes from DSO's perspective. On the other hand, the lower-level (LL) problem maximizes the total social welfare of the wholesale market managed by TSO. In this framework, distribution network (DN) is connected to transmission network (TN) via single root bus. It should be mentioned that, DSO participates in wholesale market by submitting the offers $P_{t,i}^{Exs}$ and bids $P_{t,i}^{Exb}$ for selling and purchasing power, respectively. On the other hand, TSO defines the locational marginal price (LMPs) which is defined as $\lambda_{t,i}$.

In this resilience-oriented framework, a vertically integrated DN is considered in a way that DSO operates utility-operated photovoltaic (PV) units and natural gas power plants. DSO must supply the power to H2 systems, including electrolyzers, storage tanks, and stationary fuel cell (FC) units. In the normal operation, distributed H2 systems are scheduled to exploit renewable energy resources and minimize the total operation cost and energy not supplied (based on load priority). The H2 production cost, consisting of water electrolysis cost and storage cost, is calculated based on the distributional locational marginal prices (DLMPs) considering the LMP prices of transmission network. Additionally, CBDR signals are incorporated into the optimization problem to demonstrate the flexibility of H2 systems. Prior to an emergency operation mode, DSO sends emergency CBDR signals to H2 systems in order to fill their storage tank and be prepared for post-event times. This results in maximizing the survivability by using the stored H2 for stationary FC consumption and consequently the resilience improvement. Moreover, the rolling horizon approach is applied to the bi-level framework, in order to address the challenge from the unavailable perfect forecasts for system operators. With this model, DSO does not know the exact time of disruption, output power of renewable energy resources, transportation sector demand, and CBDR signals for scheduling; However, DSO only has the access to next 24-hour forecasts (total rolling horizon period is 48 hours). At each time period, the final status of DGs, mass of H2 in the tank state, etc., will be fixed as initial condition for the next rolling horizon-based scheduling as depicted in Fig. 5.2. This results in more realistic results in the case of major disruption. In this chapter, the optimization horizon is the same for both DSO and TSO.

Problem Formulation

The problem formulation of the proposed bi-level resilience-constrained problem (RCP) is presented in this section. The proposed RCP model is formulated as a mixed integer quadratic constrained program (MIQCP). Given a network, $(\mathcal{N}, \mathcal{L})$, where $\mathcal{N}$ and $\mathcal{L}$ are the set of nodes and

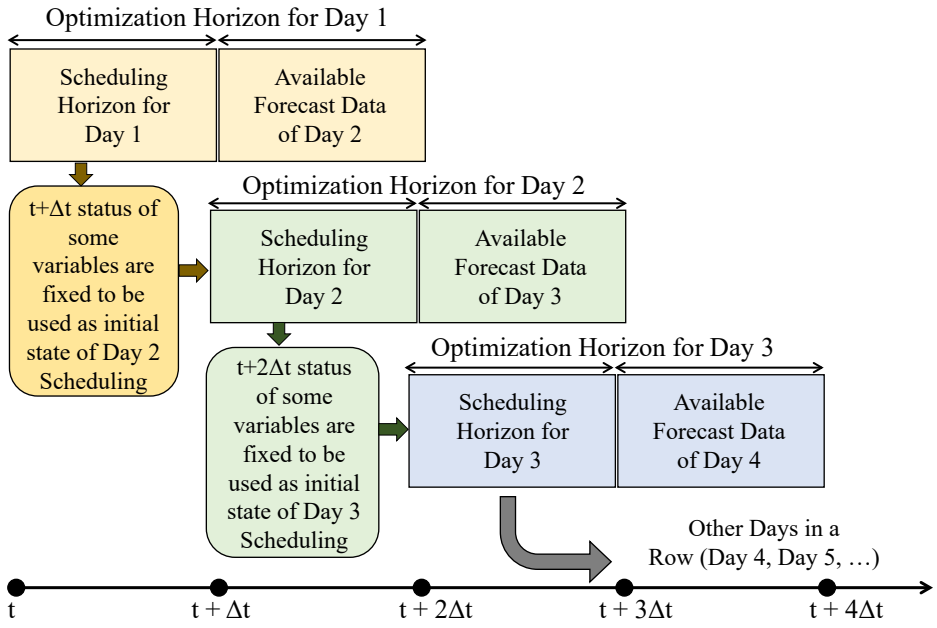

Figure 5.2. Rolling-horizon based approach for resilient day-ahead scheduling.

lines indexed by i and l. For DN and transmission network, the sets of nodes and lines are $\mathcal{N}_{\mathcal{D}}$ and $\mathcal{L}_{\mathcal{D}}$, $\mathcal{N}_{\mathcal{T}}$ and $\mathcal{L}_{\mathcal{T}}$, respectively. The root node of DN is connected to the bus two of TN. $\mathcal{T}$ represents the set of time steps indexed by t.

Upper-Level Problem Formulation: DSO Perspective

Objective Function of UL Problem

The objective function of the UL is to minimize the total operation cost in both normal and emergency conditions. For the sake of brevity, the problem formulation is not divided into normal and emergency operation modes. However, prior to the major disruption, all equations are valid except

for load shedding terms, which should be removed or considered as zero in the equations.

$$\min. \sum_{t=1}^{T} \Big\{ \lambda_{t,i} \,.\, P_{t,i}^{Exb} - \beta_{t,i} \,.\, P_{t,i}^{Exs} + \sum_{i=1}^{N_G} C_{t,i}^{DG} + \sum_{i=1}^{N_G} C_{t,i}^{SU} + \sum_{i=1}^{N_G} C_{t,i}^{SD} + \sum_{i=1}^{N_{PV}} C_{t,i}^{PV} + \sum_{i=1}^{N} C_{t,i}^{Load,Shd} \Big\} \tag{5.1}$$

In (5.1), the first term refers to the purchasing power from the wholesale market. The second term refers to selling power from the distribution network to the wholesale market. The third, forth, and fifth terms refer to operating cost, startup, and shutdown cost of DGs, respectively. The next two terms refer to operational cost of utility operated PV units and cost of energy not supplied based on the load priority (e.g. critical, moderately-critical, and non-critical grid load). It should be noted that the costs associated with H2 systems are not taken into account and DSO only schedules its system demand. In this chapter, both DSO and H2 system owners perform the cost benefit analysis separately, and exchange energy with power purchase agreement price. Moreover, the cost of FCEVs demand curtailment is not considered in the objective function since the value of loss of EV load is negligible compared to loss of grid load.

Operational Constraints of DG Units

The operational constraints for utility-operated DGs are shown in (5.2)-(5.8). Equations (5.2)-(5.4) show the operational cost and active/reactive power output limits of DGs, respectively. Equation (5.5) expresses the reactive power support limit based on active power flow. Moreover, equations (5.6) and (5.7) show the startup and shutdown cost of DGs, respectively. Finally, equation (5.8) presents the ramping up and down limits of DGs.

$$C_{t,i}^{DG} = x_{t,i}^{DG}.\, b^{DG} + k^{DG}.\, P_{t,i}^{DG} \tag{5.2}$$

$$P_i^{DG,min}.\ x_{t,i}^{DG} \leq P_{t,i}^{DG} \leq P_i^{DG,max}.\ x_{t,i}^{DG} \tag{5.3}$$

$$Q_i^{DG,min}.\ x_{t,i}^{DG} \leq Q_{t,i}^{DG} \leq Q_i^{DG,max}.\ x_{t,i}^{DG} \tag{5.4}$$

$$(P_{t,i}^{DG})^2 + (Q_{t,i}^{DG})^2 \leq (S^{DG})^2 \tag{5.5}$$

$$C_{t,i}^{SU} \geq (x_{t,i}^{DG} - x_{t-1,i}^{DG}).\ \rho^{SU}, \quad \text{if} \quad x_{t,i}^{DG} \ \geq \ x_{t-1,i}^{DG} \tag{5.6}$$

$$C_{t,i}^{SD} \geq (x_{t-1,i}^{DG} - x_{t,i}^{DG}).\ \rho^{SD}, \quad \text{if} \quad x_{t-1,i}^{DG} \ \geq \ x_{t,i}^{DG} \tag{5.7}$$

$$-R_i^D \leq P_{t,i}^{DG} - P_{t-1,i}^{DG} \leq R_i^U \tag{5.8}$$

Operational Constraints of PV Units

The operational costs of utility-operated PV units, minimum and maximum limit of output power, and inverter capacity constraints are presented in equations (5.9)-(5.11), respectively.

$$C_{t,i}^{PV} = c^{PV}.\ P_{t,i}^{PV} \tag{5.9}$$

$$0 \leq P_{t,i}^{PV} \leq P^{PV,max} \tag{5.10}$$

$$(P_{t,i}^{PV})^2 + (Q_{t,i}^{PV})^2 \leq (S^{PV})^2 \tag{5.11}$$

Operational Constraints of H2 Systems

The operational constraints of H2 systems are presented in (5.12)-(5.18). Equations (5.12)-(5.15) refer to the H2 production/consumption level of electrolyzer/stationary FC units based on efficiencies and converting factors. Additionally, these constraints prevent the simultaneous operation of electrolyzer and FC units by considering a binary variable $\psi_{t,i}^{HS}$. For instance if $\psi_{t,i}^{HS} = 1$, the electrolyzer consumes power and the FC cannot inject power into the grid; and if $\psi_{t,i}^{HS} = 0$, it means that the FC is operated and the electrolyzer cannot consume power. H2 mass balance equation including transportation demand from FCEVs and dissipation rate is expressed in (5.16). The storage tank capacity limits and H2 systems' inverter for reactive power support are presented in equations (5.17) and (5.18), respectively. Finally, electrolyzer capacity factor during the optimization horizon and limits on electrolyzer load curtailment can be calculated based on equations (5.19) and (5.20), respectively.

$$QH_{t,i}^{EL} = \pi^{EL}.\ P_{t,i}^{EL}.\ \eta^{EL} \tag{5.12}$$

$$P_{t,i}^{FC} = \pi^{FC}.\ QH_{t,i}^{FC}.\ \eta^{FC} \tag{5.13}$$

$$QH_i^{EL,min}.\ \psi_{t,i}^{HS} \leq QH_{t,i}^{EL} \leq QH_i^{EL,max}.\ \psi_{t,i}^{HS} \tag{5.14}$$

$$QH_i^{FC,min}.\ (1 - \psi_{t,i}^{HS}) \leq QH_{t,i}^{FC} \leq QH_i^{FC,max}.\ (1 - \psi_{t,i}^{HS}) \tag{5.15}$$

$$MOH_{t,i}^{H2} = MOH_{t-1,i}^{H2} - \pi^{Dsp}.\ MOH_{t,i}^{H2} + (QH_{t,i}^{EL} - QH_{t,i}^{dem} - QH_{t,i}^{FC}).\ \Delta t \tag{5.16}$$

$$MOH_{i}^{H2,min} \leq MOH_{t,i}^{H2} \leq MOH_{i}^{H2,max} \tag{5.17}$$

$$(P_{i,t}^{EL} - P_{i,t}^{FC})^2 + (Q_{i,t}^{HS})^2 \leq (S^{HS})^2 \tag{5.18}$$

$$CF_{i}^{EL} = \frac{\sum_{t=1}^{T} P_{t,i}^{EL}}{\sum_{t=1}^{T} P_{i}^{EL,max}} \tag{5.19}$$

$$0 \leq P_{t,i}^{EL,Shd} \leq \frac{QH_{t,i}^{dem}}{\pi^{EL}.\ \eta^{EL}} \tag{5.20}$$

To show the flexibility of H2 systems during the normal and emergency operations, three CB-DRS are considered. In (5.21) and (5.22), CBDR signals, shown as PDR^{Sgl}, are expressed for electrolyzers and FC units. In the case of any external signal from DSO, based on their available capacity (electrolyzer, storage tank, and FC units), H2 systems follow the signal and act as load or generation asset based on equations (5.21) and (5.22). Accordingly, in the case of $N-m$ contingencies, H2 systems can act as long-term energy storage with long-duration times compared to batteries. To that end, constraint (5.23) expresses the demand response (DR) signal, in which κ_t denotes the percentage of H2 required from DSO regarding the H2 mass in the tank, as a reserve before emergency operation. Prior to any forecasted disruption ($t < t_{event}$), DSO asks H2 system owners to fill their tank completely as a backup generation unit for supplying the load in the post-event time ($t \geq t_{event}$). This will help DSO to minimize the total cost and total load curtailment

during $N - m$ contingencies.

$$Sgn(PDR^{Sgl}) \; . \; PDR^{Sgl} \leq \sum_{i=1}^{N_H} P_{t,i}^{EL} \leq \sum_{i=1}^{N_H} P^{EL,max}, \;\; if \; PDR^{Sgl} \geq 0. \tag{5.21}$$

$$Sgn(PDR^{Sgl}) \; . \; PDR^{Sgl} \leq \sum_{i=1}^{N_H} P_{t,i}^{FC} \leq \sum_{i=1}^{N_H} P^{FC,max}, \;\; if \; PDR^{Sgl} \leq 0. \tag{5.22}$$

$$\sum_{i=1}^{N_H} MOH_{t,i}^{H2} \geq \kappa_t \; . \; \sum_{i=1}^{N_H} MOH^{H2,max} \tag{5.23}$$

SOCP-based Distribution Network AC Power Flow Model

The AC power flow constraints (addressing both normal and emergency operation) based on branch flow model are presented in (7.7)-(7.22). The voltage constraints are shown in (7.7) and (7.18). The active and reactive power balance equations are shown in (7.12) and (7.13), respectively. Line flows are limited by equations (5.28) and (7.14), and SOCP-based constraints are presented in (5.30). More details regarding the exact conic relaxation can be found in [106]. Finally, equations (7.20)-(7.22) express the constraints for emergency operation which may result in load curtailment. It should be noted that load curtailment is penalized by the value of loss of load ($VOLL$) , based on the load importance. For instance, this value is \$10,000/MWh for critical loads , \$5,000/MWh for moderately-critical loads, and \$1,000/MWh for non-critical loads.

$$V_{t,i} = V_{t,j} - 2(R_{ji} \; . \; f_{i,t}^{p} - X_{ji} \; . \; f_{t,i}^{q}) + (R_{ji}^2 + X_{ji}^2) \; . \; a_{t,l} \tag{5.24}$$

$$(V^{min})^2 \leq V_{t,i} \leq (V^{max})^2 \tag{5.25}$$

$$\begin{aligned} f^p_{t,i} =& P^{Load}_{t,i} + \sum_{j \to i} f^p_{t,j} + R_{ji}.a_{t,l} + P^{EL}_{t,i} + P^{Exb}_{t,i} - P^{Exs}_{t,i} - P^{FC}_{t,i} - P^{PV}_{t,i} - P^{DG}_{t,i} \\ & - P^{EL,Shd}_{t,i} - P^{Load,Shd}_{t,i} \end{aligned} \tag{5.26}$$

$$\begin{aligned} f^q_{t,i} =& Q^{Load}_{t,i} + \sum_{j \to i} f^q_{t,j} + X_{ji}.a_{t,l} + Q^{EL}_{t,i} - Q^{FC}_{t,i} - Q^{PV}_{t,i} - Q^{DG}_{t,i} - Q^{Load,Shd}_{t,i} \\ & + Q^{HS}_{t,i} \end{aligned} \tag{5.27}$$

$$(f^p_{t,i})^2 + (f^q_{t,i})^2 \leq (S^{line})^2 \tag{5.28}$$

$$(f^p_{t,i} - R_{ji} \,.\, a_{t,l})^2 + (f^q_{t,i} - X_{ji} \,.\, a_{t,l})^2 \leq (S^{line})^2 \tag{5.29}$$

$$[(f^p_{t,i})^2 + (f^q_{t,i})^2] \,.\, \frac{1}{a_{t,l}} \leq V_{t,i} \tag{5.30}$$

$$C^{Load,Shd}_{t,i} = VOLL(i).\ P^{Load,Shd}_{t,i} \tag{5.31}$$

$$0 \leq P^{Load,Shd}_{t,i} \leq P^{Load}_{t,i} \tag{5.32}$$

$$Q^{Load,Shd}_{t,i} = P^{Load,Shd}_{t,i} \,.\, \frac{Q^{Load}_{t,i}}{P^{Load}_{t,i}} \tag{5.33}$$

Lower-Level Primal Problem: TSO Perspective

The objective function and constraints of LL primal problem are presented in (5.34)-(5.41). The objective of TSO is to maximize the social welfare, or equivalently minimizing the total operation cost. In (5.34), the first term relates to the operation cost of large-scale generators. The second and third terms are denoting the exchanged power cost with DSO, and finally the last term refers to the operation cost of wind farms. It should be mentioned that, in order to integrate the dual of LL primal problem into UL problem, dual variables are assigned to all equations (5.36)-(5.41). Equations (5.35) and (5.36) show the generator minimum and maximum generation limits, and power balance for transmission network, respectively. Additionally, (5.37) and (5.38) model the line flow and its thermal limits based on DC power flow, in which δ denote the voltage phase angle. Moreover, wind power constraint is presented in (5.39). Finally, the active power exchange between DN and TN are constrained by (5.40) and (5.41). Please note that, more detailed formulation including generators minimum uptime, minimum downtime, etc. can be found in [107].

$$\text{min.} \sum_{t=1}^{T} \Big\{ \sum_{i=1}^{N_G} C_i^g Pg_{t,i} - \rho_t^b \; P_{t,i}^{Exb} + \rho_t^s \; P_{t,i}^{Exs} + \sum_{i=1}^{N_W} C_i^w \; Pw_{t,i} \Big\} \tag{5.34}$$

$$Pg_i^{min} \leq Pg_{t,i} \leq Pg_i^{max} \quad : (\underline{\alpha}_{t,i}, \overline{\alpha}_{t,i}) \tag{5.35}$$

$$\sum_{i=1}^{NG} Pg_{t,i} + \sum_{i \to j} Tfl_{t,i}^{p} - \sum_{j \to i} Tfl_{j,t}^{p} - P_{t,i}^{Exb} + P_{t,i}^{Exs} + Pw_{t,i} = TD_{t,i} \quad : (\lambda_{t,i}) \tag{5.36}$$

$$Tfl_{t,i} = \frac{1}{X_l}(\delta_i - \delta_j) \quad : (\zeta_{t,i}) \tag{5.37}$$

$$TFl_l^{min} \leq Tf l_{t,l} \leq TFl_l^{max} \quad : (\underline{\delta}_{t,l}, \overline{\delta}_{t,l}) \tag{5.38}$$

$$Pw_{t,i} \leq Pw_{t,i}^{max} \quad : (\gamma_{i,t}) \tag{5.39}$$

$$P_{t,i}^{Exs} \leq P^{UG,max} \,.\, U_{t,i} \quad : (\overline{\psi}_{t,i}) \tag{5.40}$$

$$P_{t,i}^{Exb} \leq P^{UG,max} \,.\, (1 - U_{t,i}) \quad : (\underline{\psi}_{t,i}) \tag{5.41}$$

Lower-Level Dual Problem: TSO Perspective

The duality-based technique [108] is used to solve the aforementioned bi-level problem, by integrating the dual of LL problem into UL problem and achieving a single-level equivalent problem. The following equations are the dual problem of equations (5.34)-(5.41).

$$\begin{aligned} \text{max.} \sum_{t=1}^{T} \Big\{ & \sum_{i=1}^{N_G} (Pg_i^{min} \underline{\alpha}_{t,i} + Pg_i^{max} \overline{\alpha}_{t,i}) + \sum_{l=1}^{N_l} (TFl_l^{min} \underline{\delta}_{t,l} + TFl_l^{max} \overline{\delta}_{t,l}) \\ & + \sum_{i=1}^{N_i} (P^{UG,max} \,(1 - U_{t,i})\, \underline{\psi}_{t,i} + P^{UG,max} \, U_{t,i} \, \overline{\psi}_{t,i}) \\ & + \sum_{i=1}^{N_i} \lambda_{t,i} TD_{t,i} + \sum_{i=1}^{N_i} \gamma_{i,t} Pw_{t,i} \Big\} \end{aligned} \tag{5.42}$$

$$\overline{\alpha}_{t,i} + \underline{\alpha}_{t,i} + \lambda_{i,t} = C_i^g \tag{5.43}$$

$$\overline{\delta}_{t,l} + \underline{\delta}_{t,l} + \zeta_{t,l} + \lambda_{t,i} - \lambda_{t,j} = 0 \tag{5.44}$$

$$\overline{\psi}_{t,i} + \lambda_{t,i} \leq \rho_t^s \tag{5.45}$$

$$\underline{\psi}_{t,i} - \lambda_{t,i} \leq \rho_t^b \tag{5.46}$$

$$-\sum_{l=ord(i)}^{N_L} \frac{\zeta_{t,l}}{X_l} + \sum_{l=ord(j)}^{N_L} \frac{\zeta_{t,l}}{X_l} = 0 \tag{5.47}$$

$$\gamma_{t,i} + \lambda_{t,i} \leq C_i^w \tag{5.48}$$

Strong Duality for Primal and Dual Problems of TSO

The strong duality theory is applied on primal and dual LL problems to obtain the optimal solution, as expressed in equation (5.49).

$$\begin{aligned}
&\sum_{t=1}^{T} \Big\{ \sum_{i=1}^{N_G} C_i^g Pg_{t,i} - \rho_t^b P_{t,i}^{Exb} + \rho_t^s P_{t,i}^{Exs} + \sum_{i=1}^{N_W} C_i^w \; w_{t,i} \Big\} \\
&= \sum_{t=1}^{T} \Big\{ \sum_{i=1}^{N_G} (Pg^{min} \underline{\alpha}_{t,i} + Pg^{max} \overline{\alpha}_{t,i}) + \sum_{l=1}^{N_l} (TFl^{min} \underline{\delta}_{t,l} \\
&+ TFl^{max} \overline{\delta}_{t,l}) + \sum_{i=1}^{N_i} (P^{UG,max} \; (1 - U_{t,i}) \; \underline{\psi}_{t,i} \\
&+ P^{UG,max} \; U_{t,i} \; \overline{\psi}_{t,i}) + \sum_{i=1}^{N_i} \lambda_{t,i} TD_{t,i} \sum_{i=1}^{N_i} + \gamma_{t,i} Pw_{t,i} \Big\}
\end{aligned} \tag{5.49}$$

Algorithm 3: H2 Production Cost Calculation Based on Water Electrolysis and Storage Tank Cost

Input: H2 system input data, CF, DLMP, etc.
Output: Water electrolysis cost, storage cost, average H2 production cost.

Initialization:
1. Electrolyzer system cost = CAPEX value $\times$ Electrolyzer size.
2. Lifetime output = (Electrolyzer size $\times$ Operational hours $\times$ CF) / (Specific energy).
3. CAPEX cost = (Electrolyzer system cost) / (Lifetime output).
4. Water electrolysis cost = (Specific energy $\times$ DLMP) + CAPEX cost.
5. Storage system cost = CAPEX value $\times$ Tank capacity.
6. Storage cost = (Storage system cost) / (Tank capacity $\times$ Operational hours $\times$ cycles per day)
7. H2 production cost ($/kg) = Water electrolysis cost + Storage cost.

Single-Level Equivalent Optimization

After integrating the dual of LL problem into the UL problem, the single-level equivalent problem is as follows:

$$\begin{aligned} &\text{min. Equation (5.1)} \\ &\text{s.t} \\ &\text{Equations (5.2)-(7.22), (5.35)-(5.41), (5.43)-(5.49)} \end{aligned} \tag{5.50}$$

H2 Production Cost Calculation for Optimization Horizon

Based on the outcome of the aforementioned optimization problem and the solution technique presented in [14], DLMP for each node including power loss, voltage regulation, and congestion costs of DN can be calculated for each node of DN. As a result, H2 production cost including water electrolysis and storage cost can be calculated based on Algorithm 3.

Simulation Results and Analysis

The proposed method is validated by testing on IEEE 24-bus transmission test system [109], and 33-node distribution test feeder [82] with an hourly time step during the week. The transmission network hosts six wind farms located at buses 3, 5, 7, 16, 21, and 23. More information regarding the transmission system and wind farms' capacity can be found in [109]. The distribution network includes three natural gas power plants, six utility-operated PV units with the total capacity same as total grid load (based on scaling factors), and three H2 systems, as shown in Fig. 6.2. The operational costs including capital expenditures (CAPEX) are considered for generation assets based on National Renewable Energy Laboratory's (NREL) advanced technology baseline [6]. The H2 demand requested by FCEVs is calculated based on the method presented in [110]. These FCEVs are considered as Honda Clarity models [100] assuming that these cars arrive at the H2 fueling station with 45% H2 fuel in their tanks. Moreover, the load, solar (without scaling factor), and FCEVs weekly patterns are shown in Fig. 5.4 and Fig. 5.5, respectively. In this , it is assumed that H2 systems' leakage is negligible (compared to the cryogenic and salt dome H2 systems) due to the high pressure of H2 energy. Moreover, in this it is assumed that the electrolyzer and fuel cell efficiencies are 60% and 70%, respectively. Different from other research efforts focused on line outages, in order to show the benefits of H2 systems over batteries, it is assumed that the tie line connecting distribution network to transmission network as well as three natural gas power plants are out of service for almost two days. The rolling optimization horizon is 48 hours, in which the DSO release the day-ahead operation based on the next 24 hours data forecasts. The electrolyzer and FC units sizes are considered as 0.5 MW. Additionally, specific energy, electrolyzer and FC efficiencies are from [7].

The simulations are carried out on a PC with an Intel Core-i7 CPU of 1.8 GHz and 16 GB RAM. The proposed framework is solved using GAMS/Gurobi [111] with a gap of 0.1%.

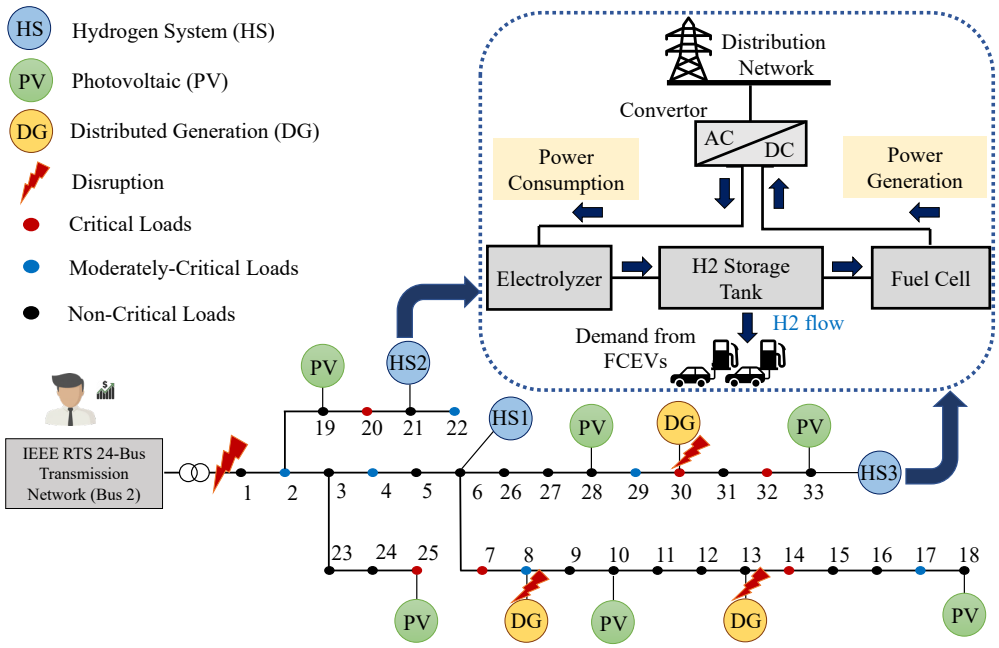

Figure 5.3. 33-node distribution test system which is connected to bus 2 of IEEE RTS 24-bus test system.

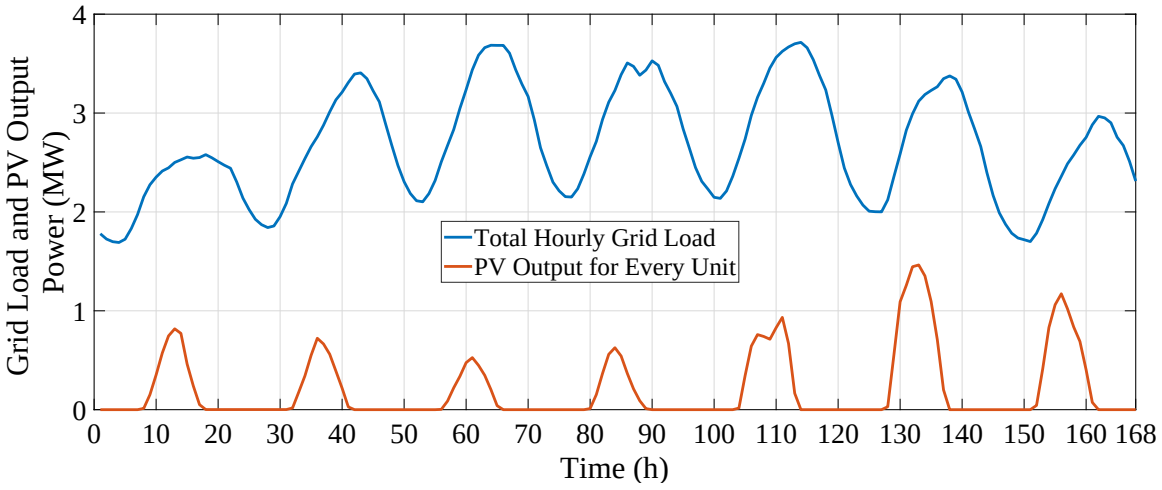

Figure 5.4. Hourly 33-node load pattern and output PV power pattern.

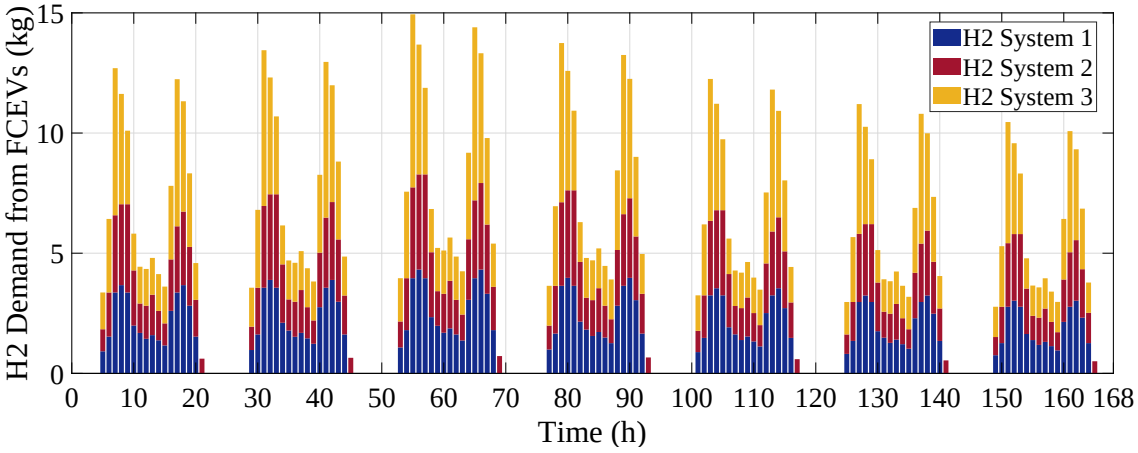

Figure 5.5. Hourly hydrogen demand from transportation sector.

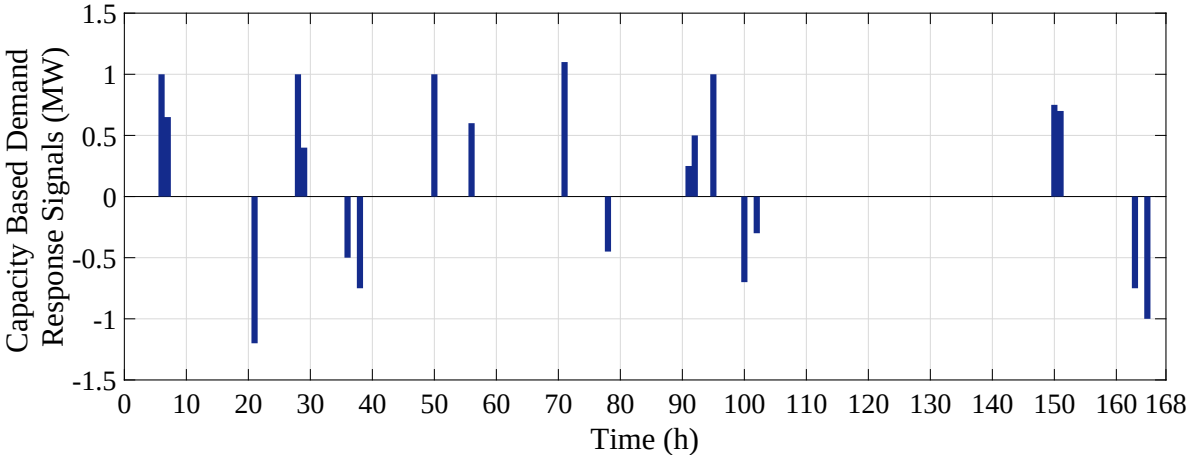

Figure 5.6. Demand response signals imposed to H2 systems by DSO.

Results for Operation of Integrated Distribution and Transmission Networks

Considering the coordinated operation of distribution and transmission systems, Fig. 5.7 shows the hourly LMP prices of bus 2 of transmission systems, which TSO shares with DSO for power exchanges. As it can be seen, due to the different participation levels of generation units located in transmission network, different LMP values are obtained. Additionally, due to the high wind

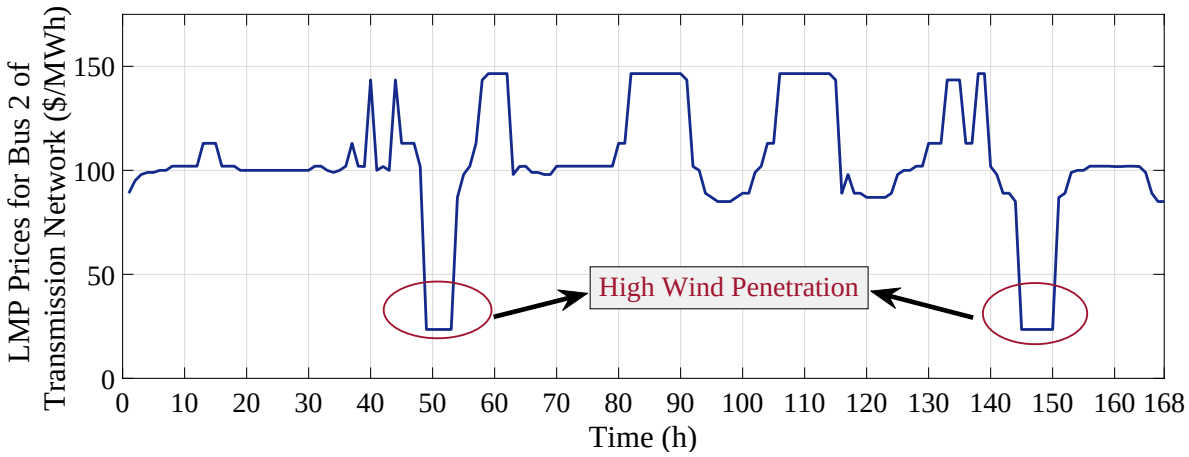

Figure 5.7. LMP prices,λ, from transmission network.

penetration during hours 49 to 53 and 145 to 150, LMP values are \$23.5/MWh. In these hours, TSO sells energy to distribution system since the lowest DG operational cost is \$36/MWh. Moreover, in the case of emergency, DSO must purchase energy from TSO in the case that total DN generation capacity is not sufficient. More details will be presented in the following section.

Results for Proactive Scheduling of H2 Systems with and without Rolling Horizon Approach

The results of proactive management of H2 systems including electrolyzers, storage tanks, and FC units, with and without considering rolling horizon approach are shown in Fig. 5.8 to Fig. 5.10, and Fig. 5.11 to Fig. 5.13, respectively. In the proposed framework, H2 systems should follow the CBDR signals in both normal and proactive mode imposed by DSO, as depicted in Fig. 5.6. It should be mentioned that positive and negative signals are for electrolyzers and FC units, respectively. In both scenarios (with and without rolling horizon), H2 systems respond to these signals. For instance, considering hours 21, 36 and 38, DSO asks the H2 systems to generate power for some purposes. Based on Fig. 5.9 and Fig. 5.12, it can be easily seen that these signals are addressed by H2 systems. It should be noted that the level of participation in CBDR signal

is based on the technical reasons, such as the available capacity of electrolyzer, storage, FC, or economic reasons. On the other hand, DSO also sends signals to H2 systems to produce H2 (act as load in the system) due to the arrival of heavy duty H2 trucks, which requires at least 50kg of H2 for filling the tank [112]. For example, considering DR signal in hours 28 and 29, Fig. 5.8 and Fig. 5.11 clearly show that these signals are addressed.

In the case of disruption, DSO must schedule its resources in advance to minimize the cost and load curtailment. However, sometimes the forecasts are inaccurate and proactive scheduling cannot reduce but even increase the operational cost, due to the increasing amount of reserve capacity. For instance, the hurricane direction is forecasted to hit the location, but changes the direction one or two days later. Fig. 5.10 shows the mass of H2 in the tank without considering rolling horizon. In this scenario, DSO has the access to perfect forecasts regarding the output power of PV units, the exact time of extreme event, etc., and imposes CBDR signals to H2 systems to fill their storage tank and be prepared for post-event times. That's the reason why the H2 mass in the tank gradually increases from hour 1 until hour 115 (when the extreme event happens). This can also be seen from Fig. 5.8, in which from the first day of week, electrolyzers consume power to minimize the cost and address the CBDR signal regarding the extreme event. However, the aforementioned scenario is not applicable in real-world applications due to the reasons that DSO never has access to the perfect forecasts, and the expectations regarding the extreme event may not be true. To this end, Fig. 5.13 shows the mass of H2 in the tank considering rolling horizon approach in which limits the access of DSO to the perfect forecasts regarding the extreme time and input data. As it can be seen, for the first 3 days, DSO normally supplies the grid load and transportation sector demand. However, in the rolling period of fourth day (which starts from hour 73 to 120), DSO sends the CBDR signal to H2 systems to fill their storage tank prior to hour 115 based on the available capacity of H2 system components. Different from the previous scenario, that's the reason why the H2 mass is not gradually increasing in the first 3 days. After the notice of DSO, H2 systems

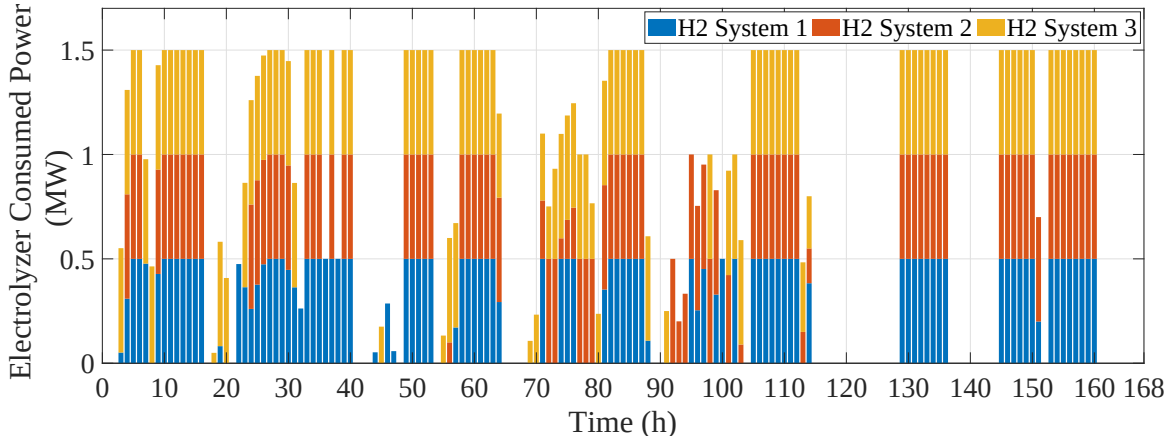

Figure 5.8. Electrolyzer scheduling w/o considering rolling horizon approach.

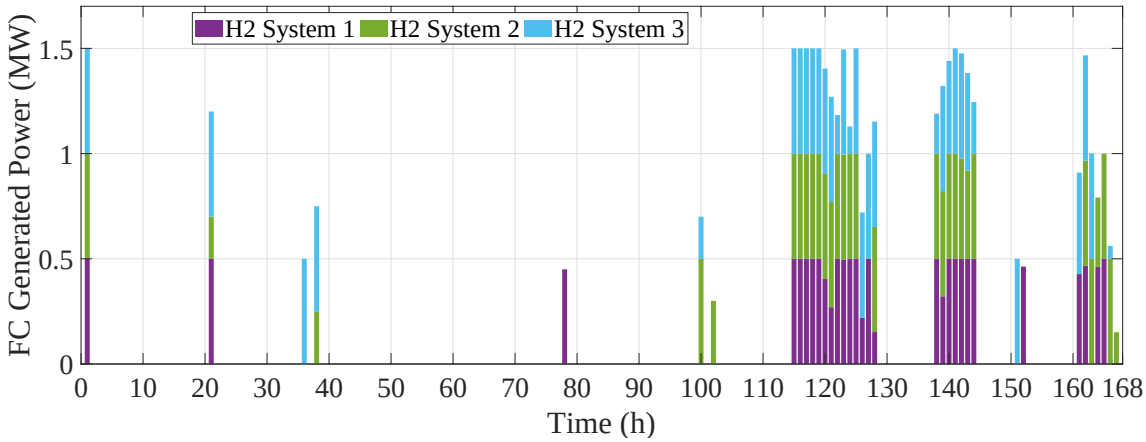

Figure 5.9. FC units scheduling w/o considering rolling horizon approach.

consume power to fill their tank as much as possible. This can also be seen in Fig. 5.11 in which electrolyzers are fully operated from hours 73 to 114. Additionally, based on Fig. 5.12, from hour 115, FC units start injecting power into the grid to supply the critical and moderately-critical loads. More details regarding the energy not supplied and the resilience index of H2 systems will be presented in the following sections.

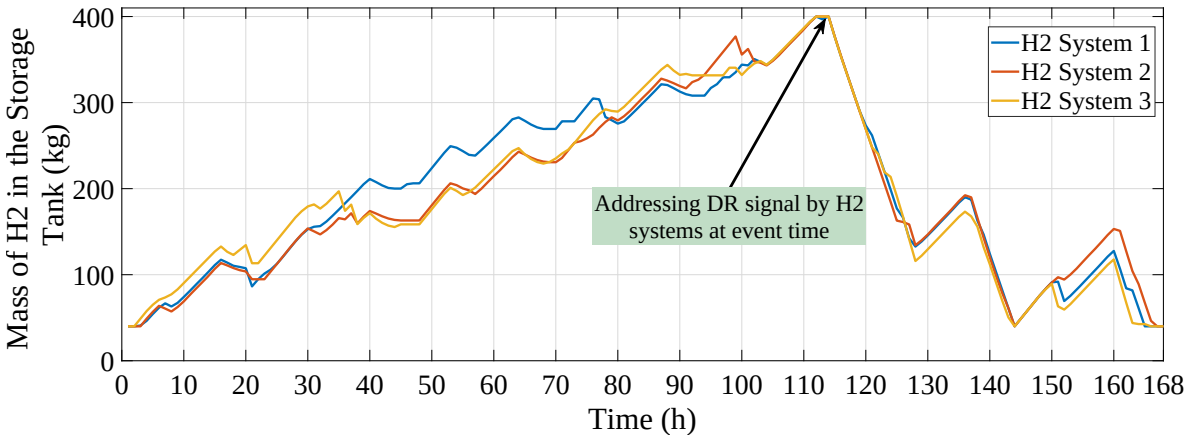

Figure 5.10. Mass of H2 in storage tank w/o considering rolling horizon approach.

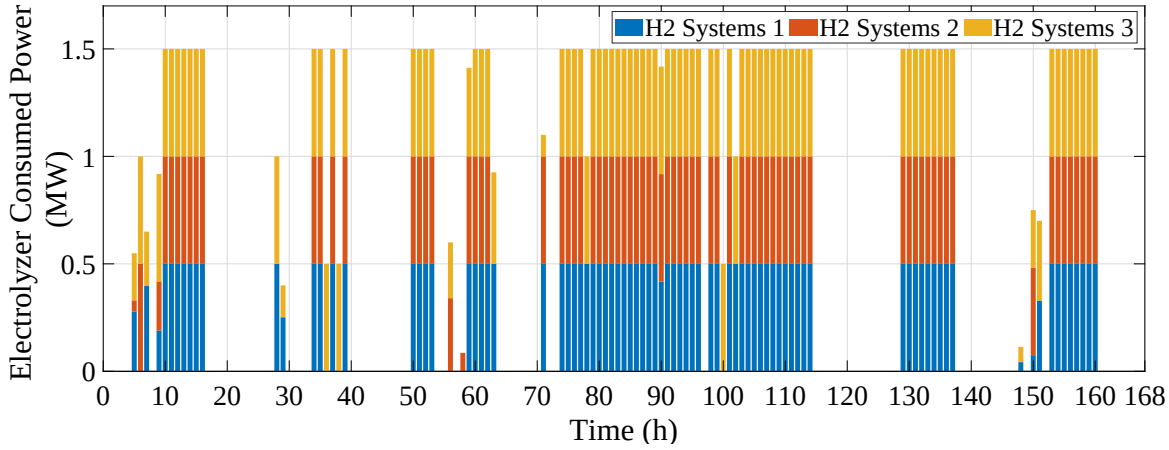

Figure 5.11. Electrolyzer scheduling considering rolling horizon approach.

Resilience Analysis for H2 systems Compared to Batteries with Different Duration Times

To provide a fair comparison of the performance between H2 system and battery energy storage systems with different duration times, it is assumed that the transit sector demand is zero kg, and battery energy storage power ratings are the same as electrolyzers and FC units. Moreover, the battery efficiencies are considered as 90%, and the constraints related to the CBDR signals are ignored. Five case studies are considered for comparing the resilience performance of the H2

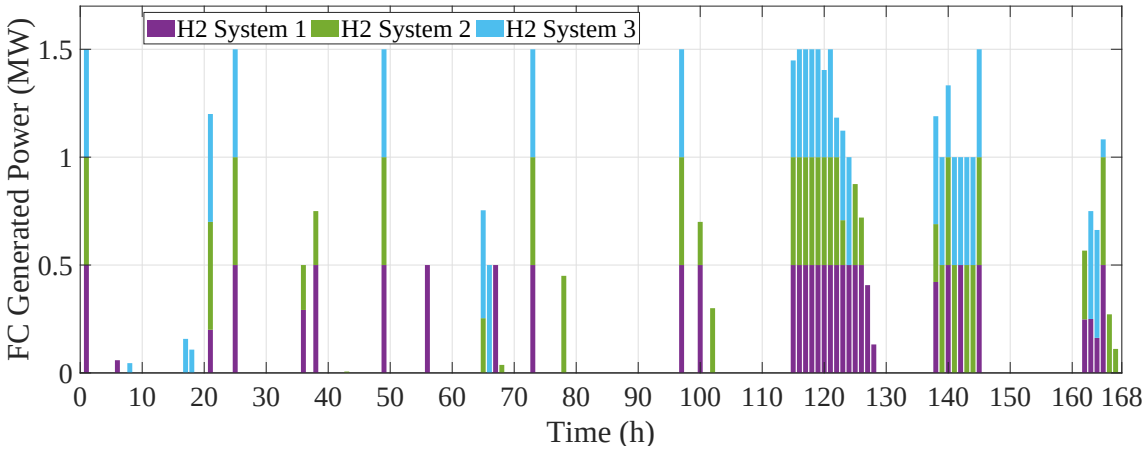

Figure 5.12. FC units scheduling considering rolling horizon approach.

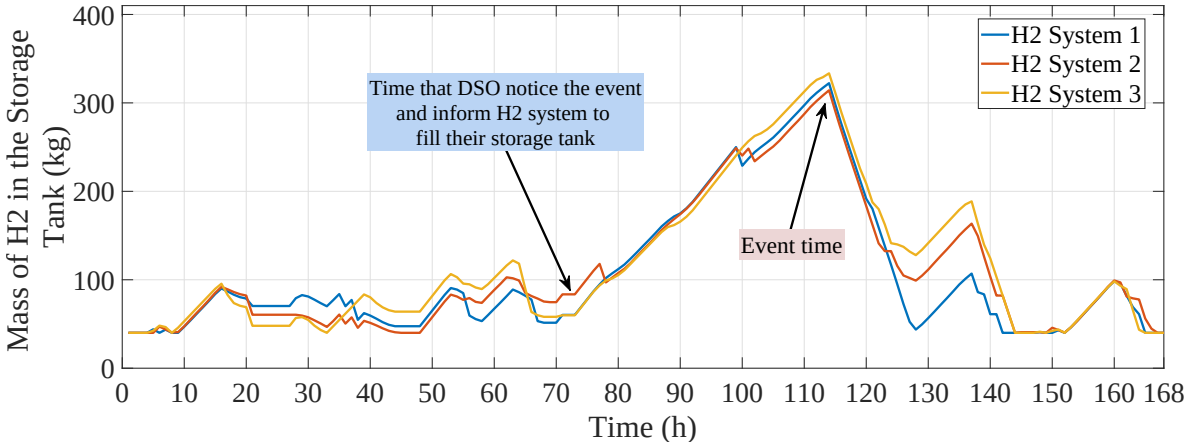

Figure 5.13. Mass of H2 in the storage tank considering rolling horizon approach.

systems and the battery energy storage systems with different duration times:

- Resilience analysis for batteries with 2-hours duration
- Resilience analysis for batteries with 4-hours duration
- Resilience analysis for batteries with 6-hours duration

- Resilience analysis for batteries with 8-hours duration
- Resilience analysis for H2 systems considering round-trip efficiency of 42%

The total load of system during hours 115 till 144 is 84.3 MW, including 28.1 MW critical loads, 11.1 MW moderately-critical loads, and 45.1 MW non-critical loads. Table 5.1 shows the energy not supplied for different load types for the aforementioned scenarios. This table clearly shows that using H2 systems prevents more load curtailment, especially for critical and moderately critical loads. Based on the results, H2 systems supplied 100% of critical loads, and 96.5 % of moderately critical loads, which performs better even with lower efficiencies compared to the battery energy storage systems. To analyze the total served energy, the following resilience index (RI) is used:

$$RI\ (\%) = \Big(\frac{Total\ Load - Curtailed\ Load}{Total\ Load}\Big) \times 100 \tag{5.51}$$

Considering the RI between hours 115 and 144, the worst case scenario is the first one, which is a battery with 2 hours duration and 37.3% served energy; and the best scenario happened when H2 systems are used as backup power sources and long-duration storages, with an index of 80.1%.

H2 Production Cost Analysis in Both Normal and Emergency Operation Modes

The results regarding the H2 production cost including water electrolysis and storage costs are presented in Table 6.5b for both normal and resilient operation modes. As it can be seen, the capacity factor of electrolyzers in resilient operation mode is higher than normal operation mode due to the DR signal imposed by DSO for preparation of extreme event. Additionally, since H2 demand from FCEVs and the amount of H2 produced for grid assistance are different, capacity factors for three H2 systems are different from each other. Additionally, the average H2 production cost in

Table 5.1. Resilience Analysis Between H2 Systems and Batteries with Different Duration

Case Study		1	2	3	4	5
Energy Not Supplied (MWh)	Critical Load	13.92	9.06	4.53	2.11	0
	Moderately Critical Load	7.57	7.57	7.24	6.03	0.38
	Non-Critical Load	31.38	31.38	31.38	30.17	16.41
Total Energy Not Supplied (MWh)		52.87	48.01	43.15	38.31	16.79
RI (%)		37.3	43.1	48.8	54.6	80.1

Table 5.2. H2 Production Cost Analysis in Different Operaton Modes

Operation Mode	Normal Operation			Resilient Operation		
H2 System	HS1	HS2	HS3	HS1	HS2	HS3
Capacity Factor (%)	38.34	39.27	41.73	54.74	53.29	58.11
Water Electrolysis Cost ($/kg)	1.46	1.54	1.59	2.18	2.33	2.53
Storage Cost ($/kg)	0.02	0.02	0.02	0.02	0.02	0.02
H2 Production Cost ($/kg)	1.48	1.57	1.61	2.21	2.35	2.55

normal operation is $1.5/kg. However, in resilient operation mode, the average H2 production cost is $2.3/kg, due to the power consumption of electrolyzers by expensive DGs. It should be noted that H2 production cost is mainly the function of water electrolysis cost, since it depends on hourly consumed prices rather than the storage cost.

Conclusion

In this chapter, a bi-level proactive scheduling framework for H2 systems' operation in integrated distribution and transmission networks was proposed for both normal and emergency operation modes. The goal of the was to minimize the load curtailment based on their priority and importance using H2 systems. Additionally, rolling horizon approach was applied to limit the access of DSO to perfect information regarding the PV, wind, and extreme event time. Additionally, to show the flexibility of H2 systems and preventing from more load curtailment, CBDR signals are modeled for both normal and emergency preparation modes in which DSO asks H2 system owners to fill their storage tank in the case of long-lasting outages (e.g. outages for more than 10 hours). Moreover, realistic costs considering water electrolysis and storage costs are calculated based on the true capacity factor of the electrolyzer.

Simulation results showed that the DSO can exchange power with TSO to minimize the cost by purchasing power from TSO in the case of high wind penetration (which results in lower purchasing prices compared to DGs in distribution system) and selling the excess PV power to TSO. In addition, simulation results showed that DSO can impose CBDR signals in normal and emergency operation modes based on the system needs, and H2 system can follow those signals based on their available electrolyzer, fuel cell, and storage capacity. Moreover, simulation results demonstrated that H2 production cost in the case of emergency operation is higher compared to the normal operation mode, due to the power consumption of electrolyzer from DG units to address the signals imposed by DSO regarding filling the tank with H2 for preparatory operation. Finally, simulation results demonstrate that H2 systems perform better in supplying more loads (higher resilience index) compared to the battery energy storage units with different duration times in the case of long-duration outages. The future work directions can be 1) improving the modeling aspect of H2 systems by considering heat constraints, leakage models, etc.; 2) applying robust techniques to deal

with uncertainties from load, renewable energy, and disruption time; 3) planning of H2 systems in both normal and emergency operation modes for decarbonized and resilient power systems.

CHAPTER 6: P2P ENERGY EXCHANGES FOR LOWERING THE HYDROGEN PRODUCTION COST: TOWARDS ENERGY DECARBONIZATION [1]

Energy decarbonization cannot be achieved without high penetration of renewables (such as wind, solar, etc.). Recently, hydrogen (H2) energy has demonstrated a great potential for decarbonization concerns due to its benefits in energy sector. However, due the land availability and monetary restrictions, as well as battery storage duration (energy) limitation, electric utilities are not capable of increasing the renewable penetration significantly in the transition, unless they consider the role of customer side DERs. The emerging peer-to-peer (P2P) markets can incentivize customers to share energy with each other or grid with lower prices than utility tariffs. Considerable penetration of P2P energy exchanges could result in lowering the net residential demand, increasing the potential capacity of renewable generation without installing utility-scale renewables, lowering the market clearing price, and as a consequence reducing the H2 production cost during the energy transition. Simulation results demonstrate that 1) electrolyzer efficiency changes under different operating conditions which significantly depends on actual cell voltage and current; 2) H2 could be produced at lower costs due to P2P energy exchanges by reducing the peers' electricity demand, providing more available capacity of renewables, and consequently reducing the market clearing price and H2 cost.

Motivated by the net-zero emission policy targets, this chapter aims at exploiting the potential benefits of peer-to-peer (P2P) energy exchanges in lowering the hydrogen (H2) production cost in the active distribution networks. The main contributions of this chapter are:

[1] This chapter is prepared based on the paper that is under review:
Hamed Haggi, Wei Sun, Paul Brooker, and James M. Fenton "Peer-to-Peer Energy Exchanges for Lowering the Hydrogen Production Cost: Towards Energy Decarbonization", *IEEE Transactions on Power Systems*, Under review, 2022.

- Developing a realistic model for grid-integrated electrolyzer based on polarization curve components to address the non-linear conversion efficiency of this device under different operating conditions which significantly affect the actual voltage and current of stack, H2 production rate and consequently stack efficiency.
- Developing a P2P enabled optimization framework for balanced distribution networks. Considerable penetration of P2P energy exchanges could result in lowering the net residential demand, increasing the potential capacity of renewable generation without installing utility-scale renewables, lowering the market clearing price, and as a consequence reducing the H2 production cost during the energy transition

Problem Formulation

This section provides a detailed formulation for electrolyzer stack considering polarization curves and how this model is integrated to a utility-centric P2P energy exchange model.

Water Electrolysis and Storage System Modelling

The electrolyzer electrochemical model is presented in (6.1)-(6.22). Let us define V^{cell}, V^{oc}, V^{ohm}, V^{act}, and V^{con} as electrolyzer cell voltage, open circuit voltage, ohmic voltage, activation overpotential, and concentration voltage. Equation (6.1) refers to electrolyzer cell overpotential which consists of open circuit voltage, ohmic voltage, activation overpotential, and concentration voltage. Equation (6.2) refers to Nernst equation where ΔG, R, T, and F denote as Gibbs free energy of reaction, ideal gas constant, temperature, and Faraday constant, respectively. P_{H_2}, P_{O_2}, and P_{H_2O} are defined as hydrogen, oxygen, and water operating pressures. Equations (6.3)-(6.4) present ohmic overpotential calculation, in which R^{ohm}, I_{cell}, δ, and λ are defined as ohmic resistant, cell

current, material thickness, and membrane water content [50]. Activation overpotentials for anode and cathode are shown in (6.5)-(6.6) where α_a and α_c are defined as charge transfer coefficient at anode and cathode, respectively. Concentration voltage of electrolyzer cell is presented in (6.7) where I_L denotes to limit current density.

$$V^{cell} = V^{oc} + V^{ohm} + V^{act,a} + V^{act,c} + V^{con} \tag{6.1}$$

$$V^{oc} \;=\; E_0 + \frac{R.T}{2.F} \;\times\; Ln\left(\frac{P_{H2}.\sqrt{P_{O2}}}{P_{H_2O}}\right), \;\; E_0 \;=\; \frac{\Delta G}{2.F} \tag{6.2}$$

$$V^{ohm} \;=\; R^{ohm} \,.\, I^{cell}, \quad R^{ohm} \;=\; \frac{\delta}{\sigma} \tag{6.3}$$

$$\sigma \;=\; (0.005139 \,.\, \lambda - 0.00236)\; exp\left[1268(\frac{1}{303} \;-\; \frac{1}{T})\right] \tag{6.4}$$

$$V^{act,a} \;=\; \frac{R.T}{2.\alpha_a.F} \,.\, arcsinh(\frac{I^{cell}}{2.I_{a0}}) \tag{6.5}$$

$$V^{act,c} \;=\; \frac{R.T}{2.\alpha_c.F} \,.\, arcsinh(\frac{I^{cell}}{2.I_{c0}}) \tag{6.6}$$

$$V^{con} \;=\; \frac{R.T}{2.F} \,.\, Ln(\frac{I_L}{I_L - I^{cell}}) \tag{6.7}$$

Activation overpotential equations can be simplified using $arcsinh(x) \;=\; Ln(x \;+\; \sqrt{x^2+1})$ as follows:

$$V^{act,a} \;=\; \frac{R.T}{2.\alpha_a.F} \,.\, Ln(\frac{I^{cell}}{2.I_{a0}} + \sqrt{(\frac{I^{cell}}{2.I_{a0}})^2 + 1}) \tag{6.8}$$

$$V^{act,c} = \frac{R.T}{2.\alpha_c.F} . Ln(\frac{I^{cell}}{2.I_{c0}} + \sqrt{(\frac{I^{cell}}{2.I_{c0}})^2 + 1}) \tag{6.9}$$

Since $I >> I_0$, the updated equations for anode and cathode activation overpotential will be:

$$V^{act,a} = \frac{R.T}{2.\alpha_a.F}.Ln(\frac{I^{cell}}{I_{a0}}) \tag{6.10}$$

$$V^{act,c} = \frac{R.T}{2.\alpha_c.F} . Ln(\frac{I^{cell}}{I_{c0}}) \tag{6.11}$$

Moreover the equation (9) can be rewritten as follows:

$$V^{con} = \frac{R.T}{2.F} . Ln(I_L) - \frac{R.T}{2.F} . Ln(I_L - I^{cell}) \tag{6.12}$$

Electrolyzer power consumption is defined as P^{EL} in (6.13). Considering different designs for electrolyzer stack, equation (6.14) shows the stack voltage and current based on the number of cells which is defined as N_v and N_i. Equations (6.15)-(6.17) show the upper and lower limits of cell current, cell voltage, and power of electrolyzer. Defining M^{EL}, η^{EL}, and HHV as amount of hydrogen produced in kg, electrolyzer efficiency, and higher heating value of hydrogen, equations (6.18)-(6.19) refer to hydrogen production and its limits. Equation (6.20) refer to electrolyzer efficiency in which the $\eta^{Faraday}$ is defined as Faraday efficiency [113]. Finally, H2 mass balance equation and storage tank limits are presented in (6.21)-(6.22) in which M^{dem}, MOH, and λ_{dsp} refer to H2 demand from transportation sector, mass of H2 in the storage tank, and dissipation rate, respectively.

$$P_t^{EL} = V_t^{EL} . I_t^{EL} \tag{6.13}$$

$$V_t^{EL} = N_v \,.\, V_t^{cell}, \quad I^{EL} = N_i \,.\, I_t^{cell} \tag{6.14}$$

$$I^{cell,min} \leq I_t^{cell} \leq I^{cell,Max} \tag{6.15}$$

$$V^{cell,min} \leq V_t^{cell} \leq V^{cell,Max} \tag{6.16}$$

$$P^{EL,min} \leq P_t^{EL} \leq P^{EL,Max} \tag{6.17}$$

$$M_t^{EL} \,.\, HHV = \eta_t^{EL}\, P_t^{EL} \tag{6.18}$$

$$0 \leq M_t^{EL} \leq M^{EL,Max} \tag{6.19}$$

$$\eta_t^{EL} = \eta^{Faraday}.\ \frac{V^{ideal}}{V_t^{cell}} \tag{6.20}$$

$$MOH_t = MOH_{t-1} + (M_t^{EL} - M_t^{dem}) - \lambda_{dsp}.MOH_t \tag{6.21}$$

$$MOH^{min} \leq MOH_t \leq MOH^{max} \tag{6.22}$$

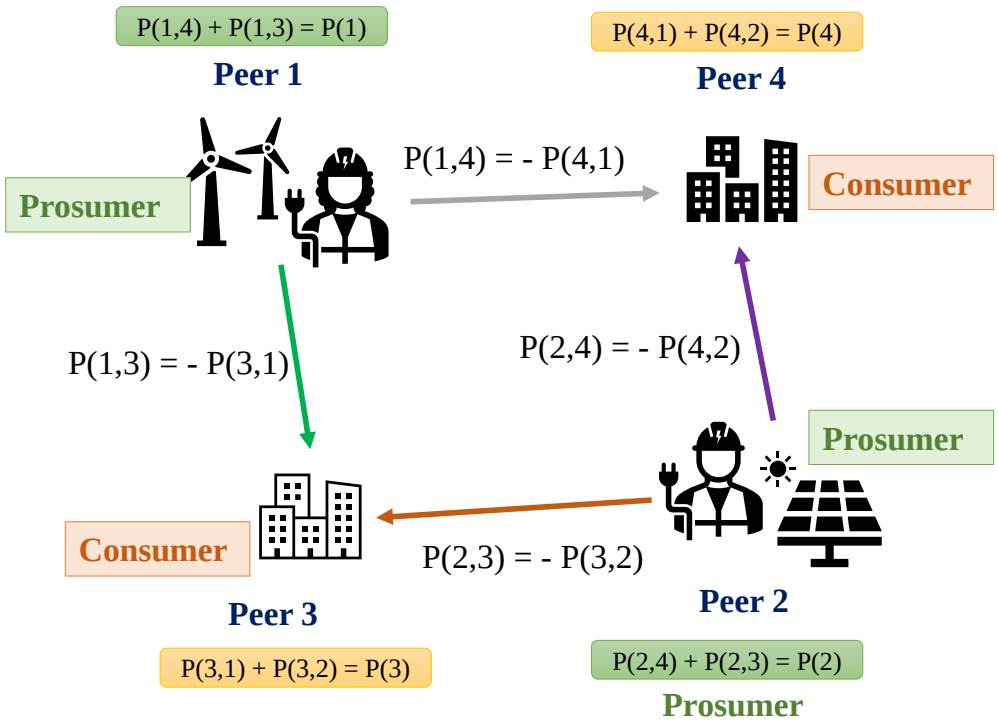

Figure 6.1. Peer-to-Peer energy exchange concept among prosumers and consumers.

Utility-Centric P2P Energy Exchange Model

To begin with optimization based P2P energy exchange formulation, Fig. 6.1 shows the concept of P2P power exchanges among prosumers and consumers. As it can be see, each prosumer shares power to other two consumers and each consumer receives power from the two prosumers. For instance, peer 1 as prosumer exchange power with peer 4 and peer 3 who are consumers. The sold power by prosumers is considered as positive power exchange, and the purchased power by consumers is considered as negative. The sum of all power exchanges of peer 1 with different consumers is considered as final power share of that peer and vice versa.

The problem formulation for utility-centric P2P energy exchange model is presented in equations (6.23)-(6.41). Let us define OC^{P2P} and OC^{Grid} as the operation cost of P2P energy exchanges and

grid in equations (6.24)-(6.25), and consider linear cost terms. $P^p_{t,i}$ and $dem^c_{t,j}$ denote to total traded power of prosumers and total received power by consumers, respectively. Equations (6.27)-(6.28) illustrate the P2P energy exchange among prosumers and consumers in which the sold power by prosumer, P_{nm}, should be equal to the power purchased by consumer P_{mn}. Equations (6.29)-(6.30) express the total sold power from prosumer to consumers, and total purchased power by consumer from other prosumers, respectively. Active power and reactive power (defined as $Q^p_{t,i}$) constraints of prosumers, and general form of elastic demand for all agents are expressed in (6.31)-(6.33). In this chapter it is assumed that the agents' demand is considered as inelastic. Therefore, the upper and lower limits are the same. The inverter capacity S^{inv} constraints of prosumers (e.g. rooftop solar owners) is shown in (6.34). Distflow model is used to model distribution power flow [106] [114]. Let us define OC^{Grid} and $C_i(P^X_{t,i})$ as total operational cost of grid, and cost of purchasing power from upper grid, or operating the DGs, or operation cost of PV. f^p, f^q, P/Q^{load}, R_l, X_l denote to active and reactive power flows, active and reactive electricity demand, and resistance and reactance of distribution system lines. Additionally, P/Q^{UG}, P/Q^{DG}, P/Q^{EL}, S_l, u_l and a_l refer to active and reactive power of upper grid, active and reactive power of DGs, active and reactive power of electrolyzer, apparent power, voltage and current of lines respectively. To this end, equations (6.35)-(6.36) refer to active and reactive power balance equations. The apparent power flow limits and relaxation of second order cone constraint are expressed in (6.37)-(6.39). Voltage drop constraints and current limits are expressed in (6.40)-(6.41).

$$\text{min. } OC^{P2P} + OC^{Grid} \tag{6.23}$$

$$OC^{P2P} = \sum_{t \in T} \Big\{ \sum_{i \in N^p} C_i(P^p_{t,i}) - \sum_{j \in N^c} U_j(dem^c_{t,j}) \Big\} \tag{6.24}$$

$$OC^{Grid} = \sum_{t \in T} \Big\{ \sum_{i \in N^g} C_i(P_{t,i}^{UG}) + \sum_{i \in N^g} C_i(P_{t,i}^{DG}) + \sum_{i \in N^g} C_i(P_{t,i}^{PV}) \Big\} \tag{6.25}$$

$$C_i(P_{t,i}^{X}) = P_{t,i} \ \times \ \Lambda^X \tag{6.26}$$

$$P_{t,i,j}^{nm} \ + \ P_{t,j,i}^{mn} = 0, \quad \forall (i,j) \in (N^p, N^c) \tag{6.27}$$

$$P_{t,i,j}^{nm} \geq 0 \ \ , \ P_{t,j,i}^{mn} \leq 0, \ \forall (i,j) \in (N^p, N^c) \tag{6.28}$$

$$P_{t,i}^{p} = \sum_{j} P_{t,i,j}^{nm}, \quad \forall (i,j) \in (N^p, N^c) \tag{6.29}$$

$$dem_{t,j}^{c} = \sum_{i} P^{mn} t, j, i, \quad \forall (i,j) \in (N^p, N^c) \tag{6.30}$$

$$P^{p,min} \leq P_{t,i}^{p} \leq P^{p,max}, \quad \forall i \in N^p \tag{6.31}$$

$$Q^{p,min} \leq Q_{t,i}^{p} \leq Q^{p,max}, \quad \forall i \in N^p \tag{6.32}$$

$$P^{Load,min} \leq dem_{t,j}^{c} \leq P^{Load,max}, \quad \forall j \in N^c \tag{6.33}$$

$$(P_{t,i}^{p})^2 + (Q_{t,i}^{p})^2 \leq (S^{inv})^2, \quad \forall i \in N^p \tag{6.34}$$

$$f^p_{t,i} = P^{Load}_{t,i} + \sum_{j \to i} f^p_{t,j} + R_l.a_{t,l} - P^{UG}_{t,i} - P^p_{t,i} + P^{EL}_{t,i} \tag{6.35}$$

$$f^q_{t,i} = Q^{Load}_{t,i} + \sum_{j \to i} f^q_{t,j} + X_l.a_{t,l} - Q^{UG}_{t,i} - Q^p_{t,i} + Q^{EL}_{t,i} \tag{6.36}$$

$$(f^p_{t,l})^2 + (f^q_{t,l})^2 \leq (S^l)^2 \tag{6.37}$$

$$(f^p_{t,i} - R_l.a_{t,l})^2 + (f^q_{t,i} - X_l.a_{t,l})^2 \leq (S^l)^2 \tag{6.38}$$

$$\left\| \begin{array}{c} 2f^p_{t,i} \\ 2f^q_{t,i} \\ a_{t,l} - u_{t,i} \end{array} \right\|_2 \leq a_{t,l} + u_{t,i} \tag{6.39}$$

$$u_{t,i} = u_{t,j} - 2(R_l \,.\, f^p_{t,i} + X_l \,.\, f^q_{t,i}) + \widetilde{Z}_l \,.\, a_{t,l} \tag{6.40}$$

$$u^{min} \leq u_{t,i} \leq u^{max} \quad I^{min} \leq a_{t,l} \leq I^{max} \tag{6.41}$$

Simulation Results and Analysis

Fig. 6.2 shows a 33-node distribution network used for validating the results. More details regarding the DGs and PV units can be found in our previous work [103]. Seven prosumers were added to enable P2P energy exchanges among all agents. Additionally, Fig. 6.3a shows normalized hydrogen demand from transportation sector (with maximum demand of 42.4 kg of H2), and PV power profile (both utility and prosumers with capacity of 1.75 MW and 0.2 MW each) [115].

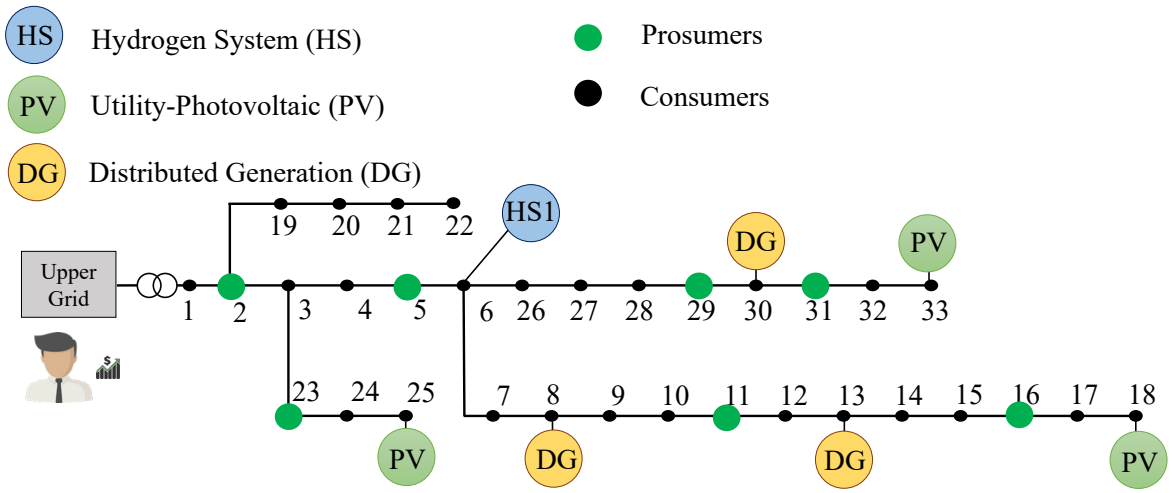

Figure 6.2. P2P integrated active distribution network.

The optimization time horizon is 24 hours with 30 minutes time intervals. All required parameters mentioned in Section 6 can be found in [50], [113], and [116] and electrolyzer capital cost target can be found in [117]. It should be noted that electrolyzer size, temperature, H2 pressure, oxygen and water pressure, and also tank capacity are 3 (MW), 323 (K), 40 barg, 6.9 barg, and 200 (kg). More information can be found in our previous works [118] [119] [120] Finally, the problem is formulated as non-linear program and IPOPT solver is used for solving the problem.

Three case studies are designed to show how P2P energy exchanges can contribute to the 2030 decarbonization targets by lowering the hydrogen production cost: supplying energy 1) without utility PV and P2P markets; 2) with utility PV and without P2P markets; 3) with utility PV and P2P markets. Fig. 6.3b shows the results of polarization curve for cell voltage vs. cell current density. Different operating conditions such as temperature, pressure, resistor, etc. could significantly affect the cell voltage and current, and as a consequence electrolyzer power and its efficiency. Fig. 6.4 shows the electrolyzer efficiency for all three cases. In the first case study, electrolyzer's required energy is supplied by three DG units. Unlike solar power which is available at certain times of a

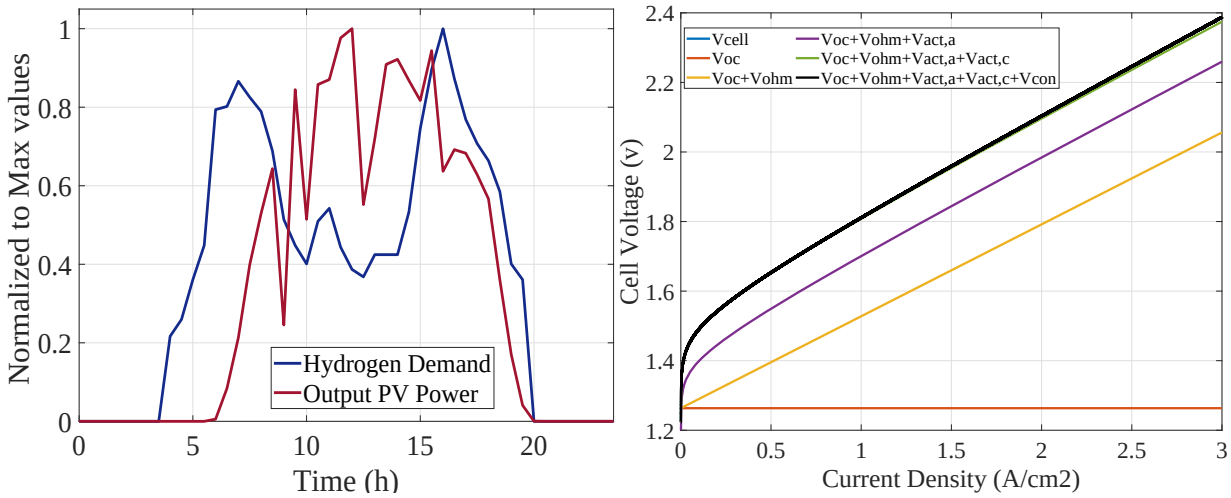

(a) Normalized inputs.

(b) Polarization curve results.

Figure 6.3. Normalized inputs, and electrolyzer polarization curve.

day, all three DGs can generate power and supply the required energy for water electrolysis. Due to available DGs power capacity, the efficiency is almost a flat line. However, in the second case study, due to available utility scale PV power, the electrolyzer is operated with higher current densities to use all available PV power considering the technical and physical network constraints in order to produce cheap H2 (generally the electrolyzers should be operated in lower current densities to have higher efficiencies, but imposed H2 demand make electrolyzers to be operated in higher current densities and this reduces the efficiency significantly and affect the H2 production rate). Operating the electrolyzer in higher current densities results in lower efficiency values, which can be seen clearly during hours 9 am to 4 pm when there is cheap solar energy and H2 system makes low-cost H2 energy. Finally, in the third case study, prosumers exchange their surplus energy (after self supply) with other agents in the P2P market. This results in lowering the residential demand and in some hours, prosumer's surplus power could assist the grid by providing more renewable capacity, which makes electrolyzer to be operated with higher efficiencies compared to second case study and produce cost-effective H2 energy.

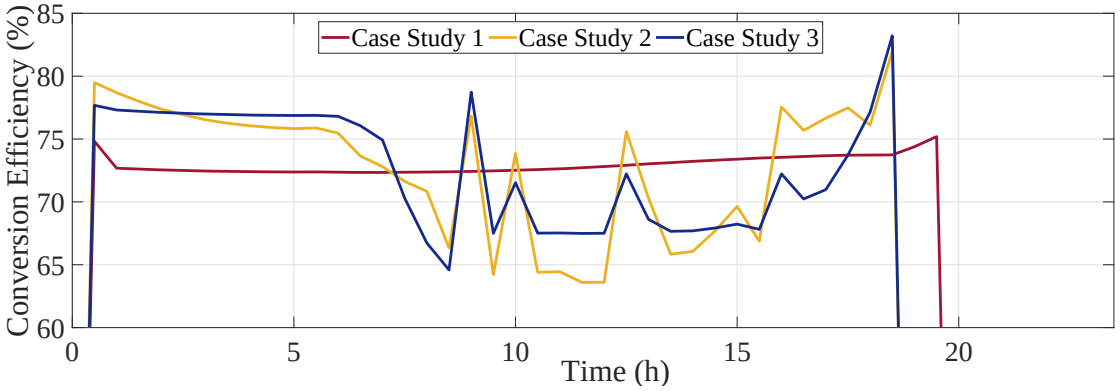

Figure 6.4. Electrolyzer conversion efficiency.

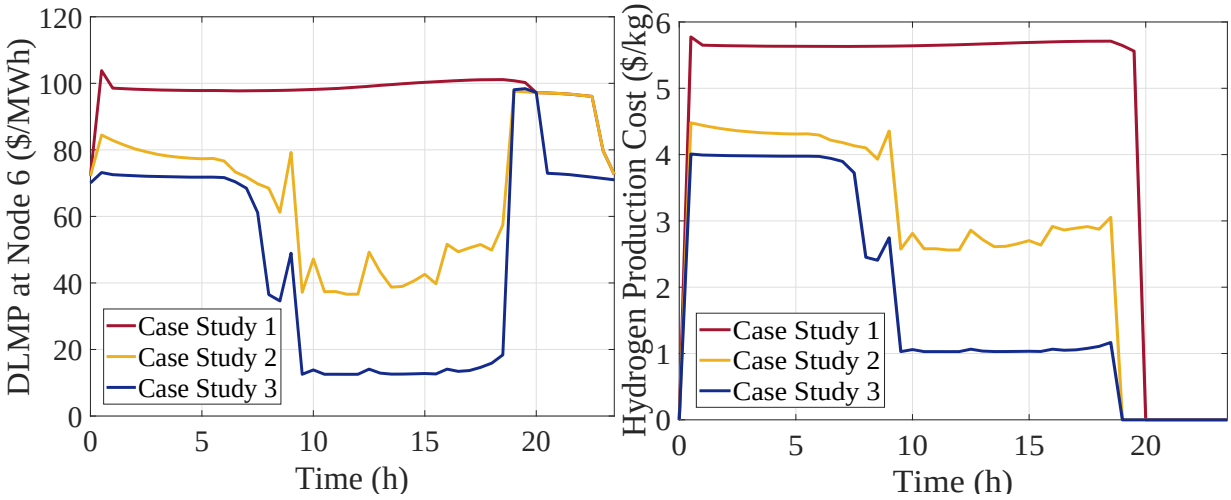

(a) DLMP at node 6.

(b) H2 production cost.

Figure 6.5. Hourly DLMP values and H2 production cost at node 6.

Fig. 6.5a and Fig. 6.5b show the DLMP values of node 6 where H2 system is located, and H2 production cost for all three cases. It shows that the first and third case studies have the highest and lowest DLMP values. Fig. 6.5a shows that utility scale PV units can not significantly lower the DLMP values. However, DLMP values could be lower if prosumers and consumers participate in the P2P market and supply their electricity demand by negotiating with other agents in local

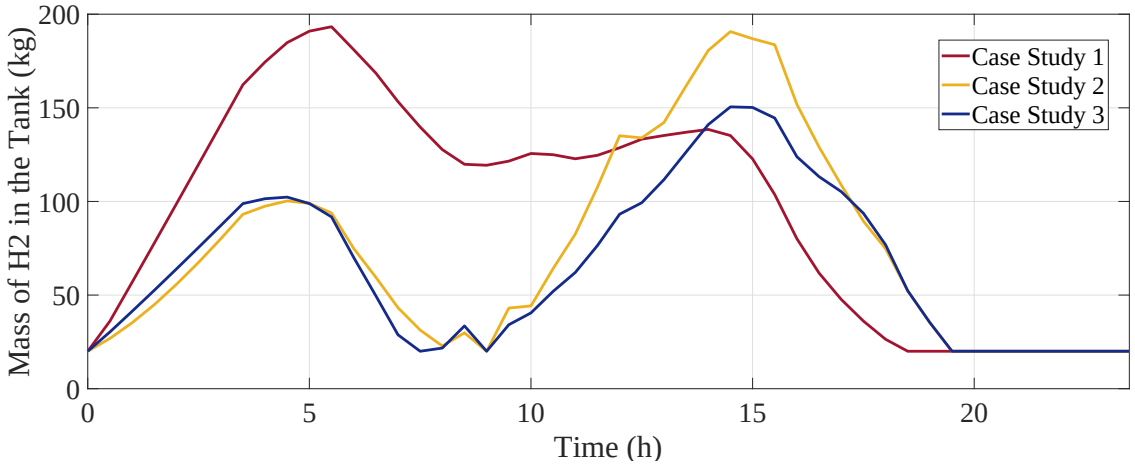

Figure 6.6. Mass of hydrogen in the tank.

markets or inject the surplus generation to the grid and assist the grid to increase the renewable penetration. More P2P interactions results in more available renewable capacity and consequently electrolyzer can be operated by low-cost renewable power which reduces the H2 production cost for other applications such as transportation. This is highlighted in Fig 6.5b that H2 production cost (out of the electrolyzer) could be produced at $1/kg (H2 cost is calculated considering the CAPEX cost, actual capacity factor, lifetime of asset, etc. of the electrolyzer) in the third case study in which both utility PV units and P2P energy exchanges were considered. In addition to the aforementioned results, Fig. 6.6 shows the amount of H2 in the storage tank for three case studies. The mass of H2 in the tank follows the amount of H2 produced by electrolyzer and the H2 demand demand (please see Fig. 6.3a).

To analyze the impact of compressor on H2 cost, compressor efficiency as well as capital cost of this asset is integrated to the aforementioned formulation. Fig. 6.7 shows the sensitivity of H2 cost for the third case study where both utility-scale renewables and P2P energy exchanges were considered. Six different scenarios are considered:

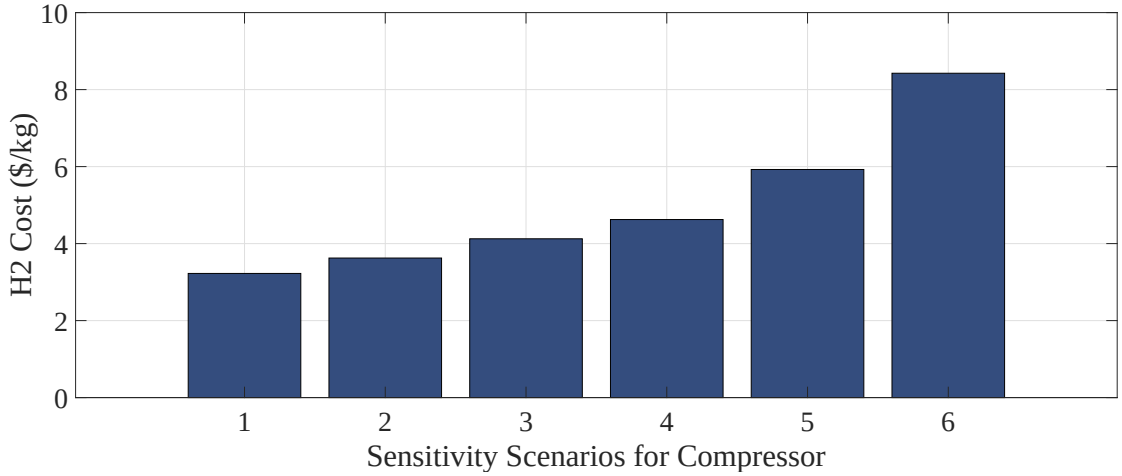

Figure 6.7. H2 cost sensitivity with and without compressor

- Scenario 1: Average H2 cost with no compressor and electrolyzer capital cost of $100/kw
- Scenario 2: Average H2 cost with 100% compressor efficiency and capital cost of $148/kw
- Scenario 3: Average H2 cost with 90% compressor efficiency and capital cost of $148/kw
- Scenario 4: Average H2 cost with 80% compressor efficiency and capital cost of $148/kw
- Scenario 5: Average H2 cost with 70% compressor efficiency and capital cost of $148/kw
- Scenario 6: Average H2 cost with 60% compressor efficiency and capital cost of $148/kw

The average H2 cost for the first scenario is $3.2/kg when there is no compressor. In scenarios 2 to 6, as the compressor efficiency increases, total H2 cost including electrolyzer and compressor CAPEX costs increases as well. The maximum H2 cost value occurs in scenario 6 (with $8.4/kg) since the efficiency of compressor is low and more energy is required to compress the H2. This results in consuming more energy and as a consequence operating DGs even during the time when there are P2P energy exchanges and utility scale PV energy.

Conclusion

This Chapter developed a grid-integrated H2 system model in the P2P-enabled distribution network. A detailed model for H2 system including non-linear conversion efficiency of the electrolyzer based on polarization curves was considered to have realistic H2 production costs. Simulation results highlight that P2P energy exchanges could minimize the operation cost through reducing the peers' electricity demand, providing more available capacity of utility and customer-side renewables for H2 production, and consequently reducing the DLMP and H2 production cost which could play a major role on achieving the net-zero emission targets by the year 2030.

CHAPTER 7: CYBER-PHYSICAL VULNERABILITY ASSESSMENT OF P2P ENERGY EXCHANGES IN ACTIVE DISTRIBUTION NETWORKS[1]

Decreasing costs of DERs and net-zero emission energy production policy are two preeminent factors that motivate utilities to deploy more DERs to enable deep decarbonization of energy production targets [4]. Since energy decarbonization cannot be achieved without high penetration of renewable energy sources, utilities should develop and invest in new business models by considering the price-making role of customer side DERs. However, the current market designs are not able to provide sufficient incentives for small-scale DER owners to share the energy with grid or neighbors. To this end, in order to capture the socio-economic benefits of customer side DERs, peer-to-peer (P2P) energy exchange platforms, including communication, business, and physical layers, are introduced to maximize the green energy harvesting, reducing the bills of customers, etc. However, The large number of peers (prosumers and consumers) equipped with internet of things (IoT) devices have driven the power grids more complex and vulnerable to cyber-physical threats such as natural disasters, cyber intrusions, etc. [70] [47]. Therefore, the motivation of this chapter is to explore the potential cyber-physical threats in P2P markets and analyze the vulnerability of these threats on the real operation of power systems from economic and physical perspectives. To this end, in this chapter, a resilience-oriented P2P energy exchange model is developed considering three phase unbalanced distribution systems. In addition, various scenarios for vulnerability assessment of P2P energy exchanges considering adverse prosumers and consumers, who provide false information regarding the price and quantity with the goal of maximum financial benefit and system operation disruption, are considered. Techno-economic survivability analysis against these attacks are investigated on a IEEE 13-node unbalanced distribution test system. Simulation results

[1]This chapter is prepared based on the paper published at [121]:
Hamed Haggi and Wei Sun "Cyber-Physical Vulnerability Assessment of P2P Energy Exchanges in Active Distribution Networks", *2022 IEEE Kansas Power and Energy Conference (KPEC)*, 2022. [Link]

demonstrate that adverse peers can affect the physical operation of grid, maximize their benefits, and cause financial loss of other agents. P2P energy trading frameworks presented in [46]- [30] are mainly focused on various market mechanisms, while some of them are focused on modeling the physical network constraints and transaction charges in balanced distribution networks. However, the real distribution networks are phase unbalanced, and proper modelling efforts are required to integrate P2P models to unbalanced systems. Moreover, these research studies are only focused on the normal operation of system, and neglect to consider the emergency operation in the case of disruptions such as natural disasters, cyber attacks, etc. Research works presented in [39]- [45] review the potential cyber-physical threats in transactive energy markets. Only in [43–45] the impact of false data injection on HVAC systems is investigated. There is no modelling effort for resilience-oriented P2P interactions in unbalanced network considering the physical constraints such as voltage, line loading, congestion, etc. Motivated by the aforementioned challenges, this chapter proposes a resilience-oriented framework for P2P energy exchanges in unbalanced active distribution networks focusing on both normal and emergency operation modes. In addition, to analyze the vulnerability against cyber-physical attacks, adverse prosumers and consumers who provide false information regarding their surplus renewable energy, demand, and offered price are considered, which results in financial losses of other agents, physical constraint violation, load curtailment, etc.

Proposed P2P Energy Exchange Framework with Cyber-Physical Threats

Fig. 7.1 shows the P2P-enabled distribution system operation including physical, communication, and business layers for agents (including prosumers and consumers that might be equipped with home energy management systems, batteries, etc.). During the time when the prosumers have surplus energy, they can share required information including price and quantity through commu-

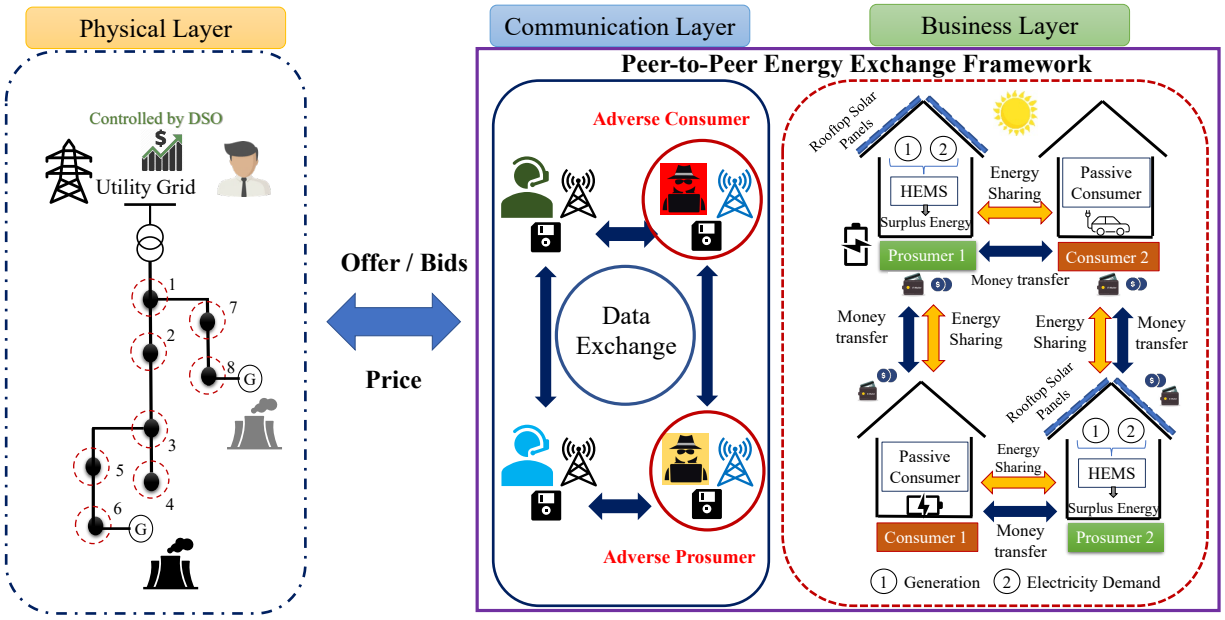

Figure 7.1. Peer-to-Peer enabled distribution system operation with business, physical, and communication layers.

nication layer with consumers to exchange energy based on business layer rules, and increase the monetary benefits while addressing the physical constraints of power grid. However, P2P markets can face with preeminent challenges such as cyber-physical threats due to disruptions in any layers. Natural disasters such as hurricanes, floods, wildfire, etc. and physical attacks on assets in distribution system can impose a threat on the grid-level operation [70, 122]. Moreover, P2P markets create opportunities for cyber attacks at different layers especially communication layer due to large number of IoT devices. Attacks on communication channels (e.g., false data injection, load redistribution attacks, etc.), attacks through adverse users (providing false information to operators and agents), and physical attacks (e.g., on smart metering or distribution lines) are potential threats that P2P energy sharing mechanisms can face [40]. This chapter is focused on prosumers' and consumers' intentional attack as an attacker by providing false information regarding their surplus energy, demand, or even the price of selling or purchasing energy. It should be mentioned that

coordinated attack among prosumers and consumers as adverse agents can significantly affect the normal operation of system from economic and technical perspectives.

Problem Formulation

The proposed resilience-oriented P2P formulation which is integrated to unbalanced distribution network is presented in this section. The distribution network is represented as a graph ($\mathcal{N}$,$\mathcal{L}$), where $\mathcal{N}$ and $\mathcal{L}$ are the set of nodes and lines, respectively. Additionally, the line impedance is expressed as $Z_l = R_l + jX_l$. The set of prosumers' and consumers' nodes are defined as $\mathcal{N}^p$ (indexed by i) and $\mathcal{N}^c$ (indexed by j), correspondingly in which $\mathcal{N}^p \cup \mathcal{N}^c = \mathcal{N}$. Moreover, to make the formulation general, we consider the time index in the formulation and $\mathcal{T}$ represents the set of time steps indexed by t.

P2P Energy Exchange Formulation

Following the P2P concept that was presented in the previously, in this chapter, P2P energy exchange model with the goal of minimizing the total cost of peers (maximizing social welfare) is developed for three phase unbalanced distribution networks and integrated to unbalanced Distflow model as presented in (7.1)-(7.10):

$$\text{min. } OC^{P2P} = \sum_{t \in T} \Big\{ \sum_{i \in N^p} C_i(P^p_{t,i}) - \sum_{j \in N^c} U_j(dem^c_{t,j}) \Big\} \tag{7.1}$$

$$P_{nm}(t,i,j) \; + \; P_{mn}(t,j,i) = 0, \quad \forall (i,j) \in (N^p, N^c) \tag{7.2}$$

$$P_{nm}(t,i,j) \geq 0, \quad \forall (i,j) \in (N^p, N^c) \tag{7.3}$$

$$P_{mn}(t,j,i) \leq 0, \quad \forall (i,j) \in (N^p, N^c) \tag{7.4}$$

$$P^p_{t,i} = \sum_j P_{nm}(t,i,j), \quad \forall (i,j) \in (N^p, N^c) \tag{7.5}$$

$$dem^c_{t,j} = \sum_i P_{mn}(t,j,i), \quad \forall (i,j) \in (N^p, N^c) \tag{7.6}$$

$$P^{p,min} \leq P^p_{t,i} \leq P^{p,max}, \quad \forall i \in N^p \tag{7.7}$$

$$Q^{p,min} \leq Q^p_{t,i} \leq Q^{p,max}, \quad \forall i \in N^p \tag{7.8}$$

$$P^{Load,min} \leq dem^c_{t,j} \leq P^{Load,max}, \quad \forall j \in N^c \tag{7.9}$$

$$(P^p_{t,i})^2 + (Q^p_{t,i})^2 \leq (S^{inv})^2, \quad \forall i \in N^p \tag{7.10}$$

where the objective function in (7.1) includes the prosumers cost and utility of consumers (linear cost curves). $P^p_{t,i}$ and $dem^c_{t,j}$ denote to total traded power of prosumers and total received power by consumers, respectively. Equations (7.2)-(7.4) illustrate the P2P energy exchange among prosumers and consumers in which the sold power by prosumer, P_{nm}, should be equal with the power purchased by consumer P_{mn}. Equation (7.5) and (7.6) express the total sold power from prosumer to consumers, and total purchased power by consumer from other prosumers, respectively. Active

and reactive power (reactive ower is defined as $Q^p_{t,i}$) constraints of prosumers, and general form of elastic demand for all agents are expressed in (7.7)-(7.9). However, in this chapter it is assumed that the agents' demand is considered as inelastic. Therefore, the upper and lower limits are the same. The inverter capacity constraints of prosumers (e.g. rooftop solar owners) is shown in (7.10) which is defined as S^{inv}.

Unbalanced Grid Operation Formulation

To address the business and physical network constraints, the aforementioned P2P model then is developed and integrated to unbalanced convex branch flow [106] model, as shown in (7.11)-(7.22):

$$\text{min. } OC^{Grid} = \sum_{t\in T}\Big\{\sum_{i\in N^g} C_i(P^{UG}_{t,i}) + \sum_{i\in N} C_i(P^{Shd}_{t,i})\Big\} \tag{7.11}$$

$$f^p_{t,i} = P^{Load}_{t,i} + \sum_{j\to i} f^p_{t,j} + R_l.a_{t,l} - P^{UG}_{t,i} - P^p_{t,i} - P^{Shd}_{t,i} \tag{7.12}$$

$$f^q_{t,i} = Q^{Load}_{t,i} + \sum_{j\to i} f^q_{t,j} + X_l.a_{t,l} - Q^{UG}_{t,i} - Q^p_{t,i} - Q^{Shd}_{t,i} \tag{7.13}$$

$$(f^p_{t,l})^2 + (f^q_{t,l})^2 \le (S^l)^2 \tag{7.14}$$

$$(f^p_{t,i} - R_l.a_{t,l})^2 + (f^q_{t,i} - X_l.a_{t,l})^2 \le (S^l)^2 \tag{7.15}$$

$$\left\| \begin{matrix} 2f^p_{t,i} \\ 2f^q_{t,i} \\ a_{t,l} - v_{t,i} \end{matrix} \right\|_2 \le a_{t,l} + v_{t,i} \tag{7.16}$$

$$v_{t,i} = v_{t,j} - 2(\widetilde{R_l} \,.\, f^p_{t,i} + \widetilde{X_l} \,.\, f^q_{t,i}) + \widetilde{Z}_l \,.\, a_{t,l} \tag{7.17}$$

$$(V^{min})^2 \leq v_{t,i} \leq (V^{max})^2 \tag{7.18}$$

$$(I^{min})^2 \leq a_{t,l} \leq (I^{max})^2 \tag{7.19}$$

$$C_i(P^{Shd}_{t,i}) = VOLL.\ P^{Shd}_{t,i} \tag{7.20}$$

$$0 \leq P^{Shd}_{t,i} \leq P^{Load}_{t,i} \tag{7.21}$$

$$Q^{Shd}_{t,i} = P^{Shd}_{t,i} \,.\, \frac{Q^{Load}_{t,i}}{P^{Load}_{t,i}} \tag{7.22}$$

where the objective is to minimize the total purchased power from upper grid, $P^{UG}_{t,i} \in \mathbb{R}^{3\times1}$, and load curtailment, $P^{Shd}_{t,i} \in \mathbb{R}^{3\times1}$, due to cyber-physical threats. Let us denote $f^{p/q}_{t,i} \in \mathbb{R}^{3\times1}$, R_l, X_l, $a_{t,i} \in \mathbb{R}^{3\times1}$, $Q^{Shd}_{t,i} \in \mathbb{R}^{3\times1}$, $Q^{UG}_{t,i} \in \mathbb{R}^{3\times1}$ the active/reactive power flow of distribution lines, line resistant, line reactance, squared current flow of the lines, reactive load curtailment, and reactive power from upper grid. In addition, S^l, $v_{t,i} = \left[\left|v^a_{t,i}\right|, \left|v^b_{t,i}\right|, \left|v^c_{t,i}\right|\right]^T$, $I^{min/max}$, $V^{min/max}$ denote line capacity, squared voltage magnitude, and minimum and maximum limits for the current and voltage magnitudes. Considering the definitions, (7.12) and (7.13) refer to active and reactive power balance of distribution network including the peers demand and surplus energy. The apparent power flow limits and relaxation of second order cone constraint are expressed in (7.14), (7.15), and (7.16). Voltage drop constraints and its maximum and minimum limits as well as current limits are expressed in (7.7)-(7.19). More information regarding the angle relaxation and balanced

voltage, and also distributional locational marginal price (DLMP) can be found in [123] and [14], respectively. Finally, load shedding cost based on the value of loss of load (VOLL) and active and reactive load curtailment constraints are expressed in (7.20)-(7.22).

Considering $\odot$ as element wise product, the following equations are used to calculate $\widetilde{R_l}$, $\widetilde{X_l}$, and $\widetilde{\widetilde{Z}_l}$ [123]:

$$\widetilde{R_l} = Re\{\alpha \odot R_l\} - Img\{\alpha \odot X_l\} \tag{7.23}$$

$$\widetilde{X_l} = Re\{\alpha \odot X_l\} + Img\{\alpha \odot R_l\} \tag{7.24}$$

$$\widetilde{\widetilde{Z}_l} = |Z_l| \odot |Z_l| \tag{7.25}$$

$$\alpha = \begin{bmatrix} 1 & e^{-j2\pi/3} & e^{j2\pi/3} \\ e^{j2\pi/3} & 1 & e^{-j2\pi/3} \\ e^{-j2\pi/3} & e^{j2\pi/3} & 1 \end{bmatrix} \tag{7.26}$$

The final co-optimization between P2P model and distribution system is expressed in (7.27).

$$\begin{aligned} &\text{min. } [\, OC^{P2P} + OC^{Grid} \,] \\ &\quad \text{s.t} \\ &\text{Equations (7.2)-(7.10), (7.12)-(7.26)} \end{aligned} \tag{7.27}$$

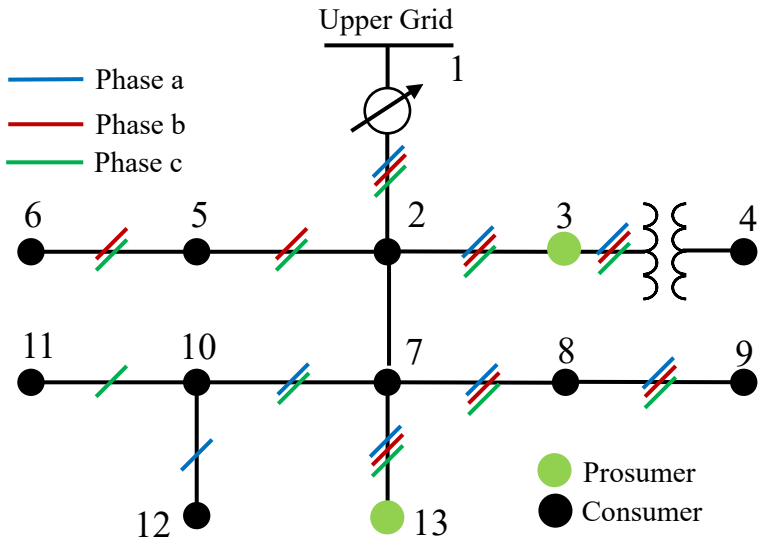

Figure 7.2. Modified IEEE 13-node distribution test system.

Simulation Results and Analysis

The proposed resilience-oriented framework is validated by testing on the modified IEEE-13 node unbalanced distribution system shown in Fig. 7.2. More details regarding the test system can be found in [124]. Nodes 3 and 13 are considered as prosumers (with three-phase connection) with maximum capacity of 650 KVA and offering price of \$35/MWh and \$20/MWh, respectively. Prosumer at node 13 and consumer at node 7 are considered as adverse agents (attackers who provide false information regarding the price and quantity). During the post attack scenario, prosumer at node 13 intentionally increases the price of energy sharing to \$45/MWh and consumer at node 7 reports its demand 25% higher to violate the regular operation of system. Two scenarios for simulation results are considered; 1) Techno-economic survivability analysis before the attack of adverse agents, 2) Post-attack survivability assessment.

Pre- and Post-attack Financial Analysis of Prosumers and Consumers

The normal operation results of P2P energy exchanges for phase c of 13-node system is shown in Fig. 7.3, in which two prosumers exchange power with consumers distributed across the grid. Due to no demand in nodes 2, 3, 5, 6, 10, and 12 [124], there is not any matchings with prosumers in Fig. 7.3. Any prosumer can exchange energy with multiple consumers at grid and vice versa. For instance, considering the phase c, consumer located at node 7 receives 385 kw from both prosumers located at nodes 3 and 13. In addition, DLMP for each phase is calculated and presented in Fig. 7.4a. Before attack, prosumers share correct information with system operator, and the DLMP values are in the range of [$35/MWh-$38/MWh] depending on the location of nodes and voltage regulation, power loss , costs and electricity demand from consumers. During the coordinated attack, prosumer at node 13 and consumer at node 7 intentionally provide false information regarding the offering price and quantity with the goal of maximizing benefit and disruption in normal operation of system. Therefore, the DLMP values are shifted to the range of [$45/MWh-$51/MWh]. In this attack, consumer at node 7 increases the demand by 25%, and the DLMP value at phase b significantly increases due to purchasing power from substation node with price of $50/MWh, which results in more financial losses of consumers compared to phase c.

The final bills of consumers and prosumers for both pre- and post-attack scenarios are calculated based on [76], as presented in Fig. 7.5 and Fig. 7.6. Due to the increase in DLMP in post-attack scenario, the final consumers' bill are increased too. For instance, the final bill of consumer 9 is increased by 35% in the post-attack scenario, and the financial loss is clearly shown in Fig. 7.5. It should be mentioned that node 9 has the highest electricity consumption among the affected consumers and that's why its loss is more than other consumers. Accordingly, the prosumers final revenue is increased in post-attack scenario, as shown in Fig. 7.6. It should also be noted that the total operation cost before and after attack are $88.6 and $144.5, respectively.

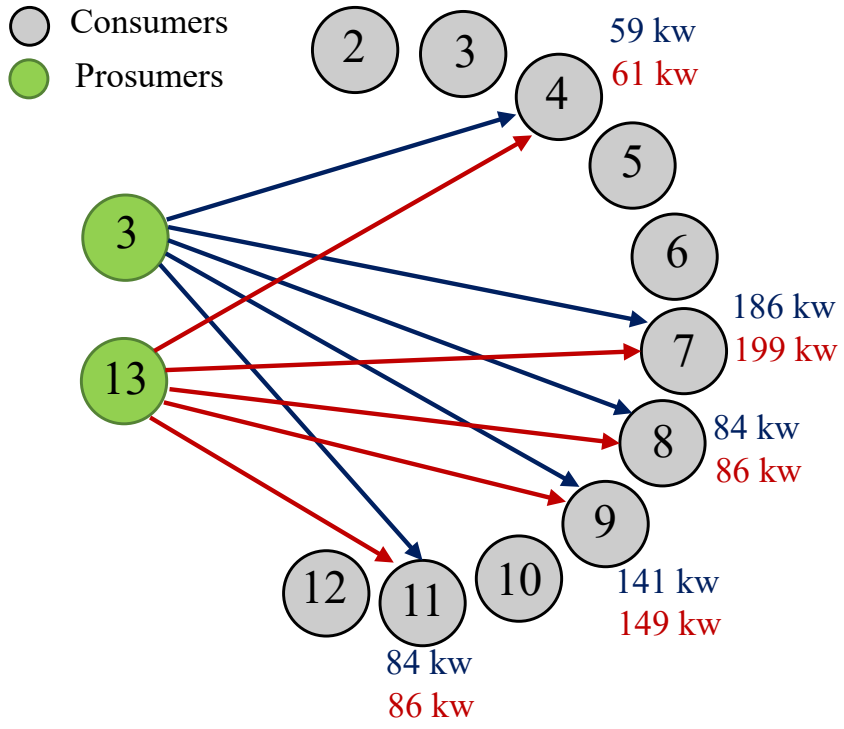

Figure 7.3. Pre-attack P2P matchings among prosumers and consumers (phase c).

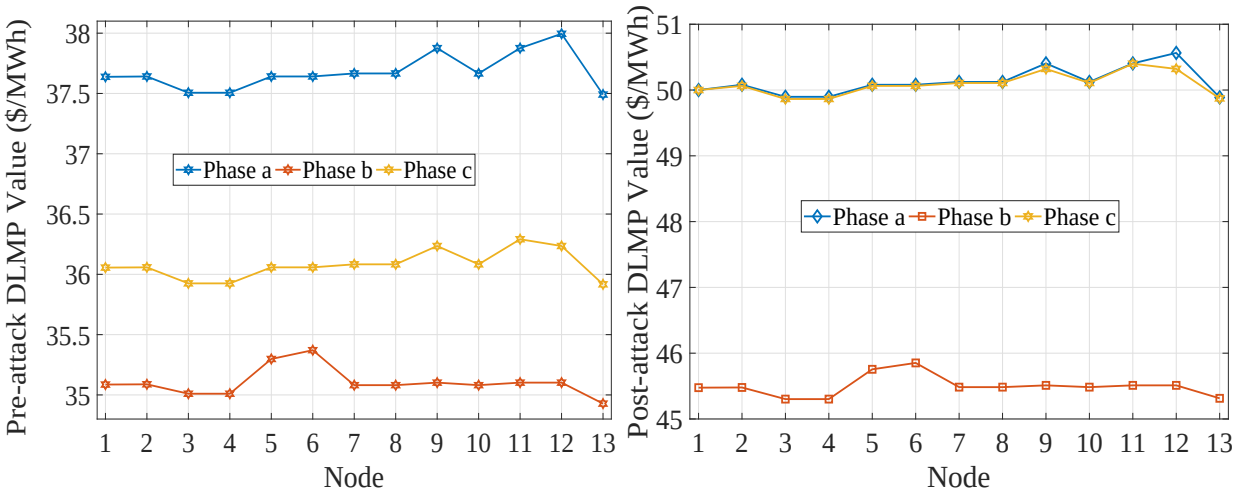

(a) Three phase DLMP before attack

(b) Three phase DLMP after attack

Figure 7.4. IEEE 13-node DLMP values with and without coordinated attack of adverse prosumer and consumer.

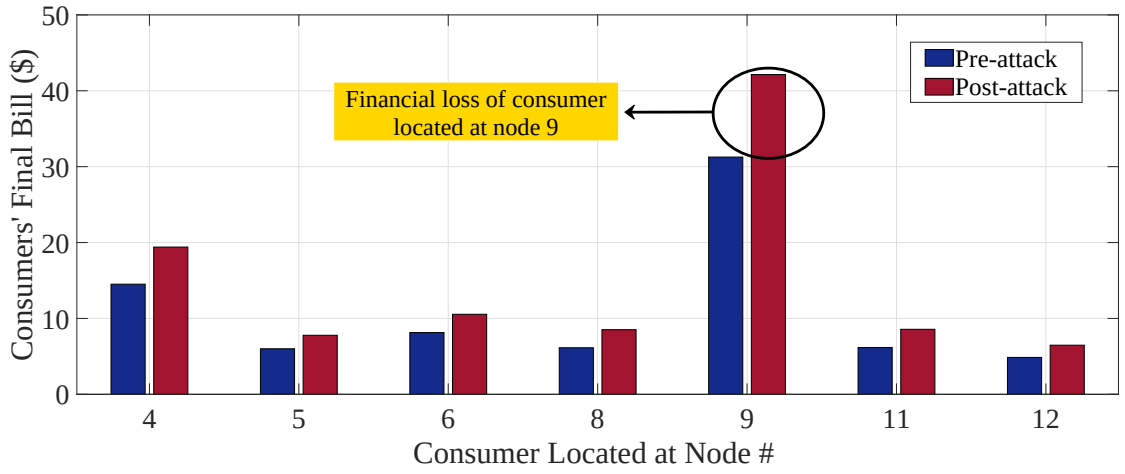

Figure 7.5. Financial loss of affected consumers before and after attack.

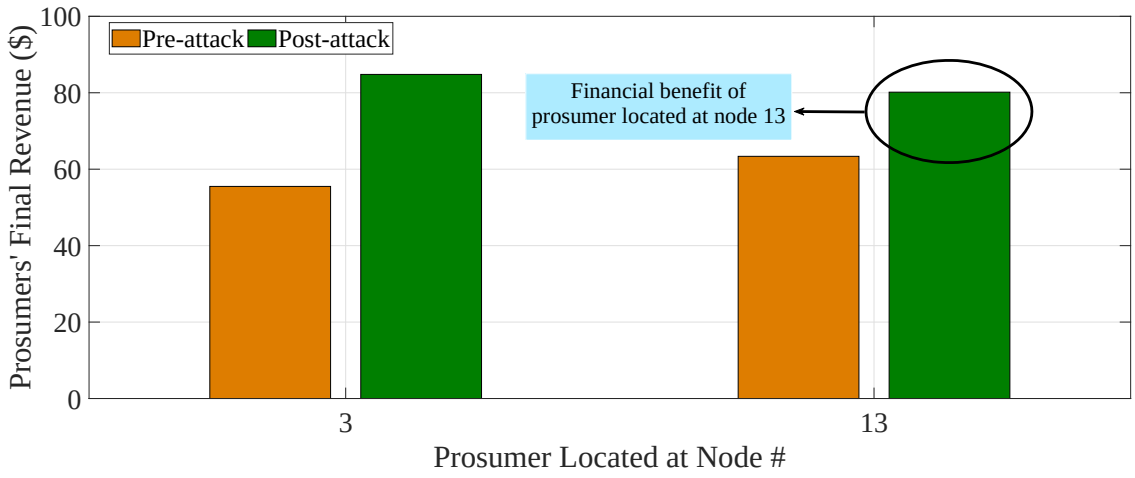

Figure 7.6. Financial benefit of adverse prosumers before and after attack.

Results for Physical Constraints of Distribution Network before and after Attack

Besides financial issues that adverse users can create for business layer of P2P market, they also have the capability of affecting the regular operation of networks. For instance, voltage magnitudes for three phases in both pre- and post-attack scenarios are presented in Fig. 7.7. It can be seen that adverse users can change the optimum voltage set points by providing false information, which

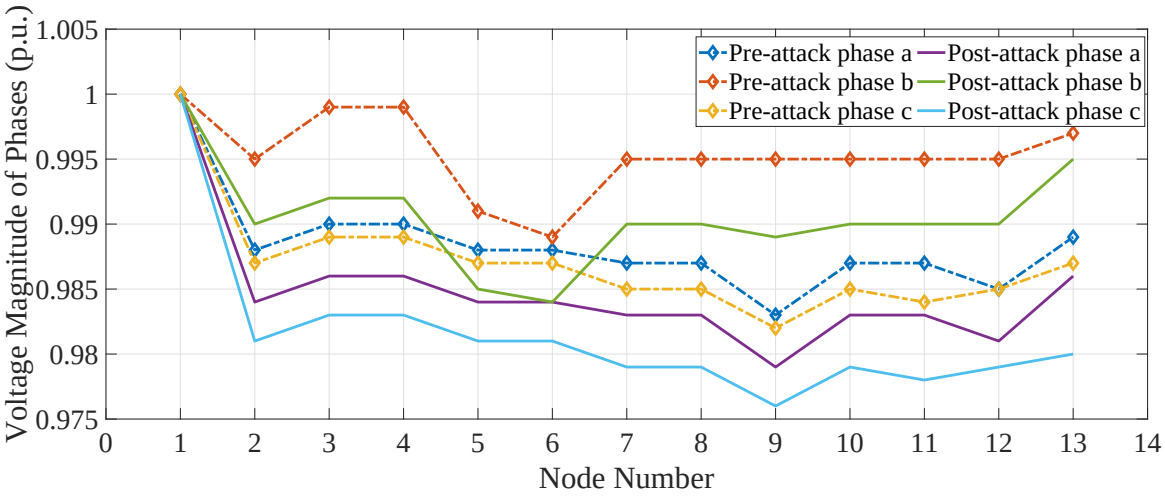

Figure 7.7. Voltage magnitudes before and after attack.

also change the power flow of lines, additional costs, etc. However, since voltage is still within the range, it is hard for system operator to detect this attack. Additionally, prosumer located at node 13 can intentionally damage the line connecting node 2 to 7 (results in line outage) to increase the benefit by selling power to neighboring nodes with a very high price. For instance, if the line between nodes 2 to 7 is attacked to be out of service, the DLMP is increased in nodes 7 to 13 and as a consequence, prosumer 13 (as the only energy provider) can sell all the available power with a very high price such as $VOLL$ and maximize the benefit. Furthermore, this attack can results in 1.8 MW total curtailment in load.

Conclusions

This chapter proposed a resilience-oriented framework for P2P energy exchanges in unbalanced active distribution networks. The problem is formulated to analyze the normal and emergency operation of P2P integrated distribution network operation in the case of cyber-physical threats. Besides analyzing the potential threats in P2P markets, adverse prosumers' and consumers' behaviour

in providing false information regarding the offered price and quantity is considered. Additionally, the impact of this false data provision on market clearing price and physical constraints of network such as voltage is investigated. Simulation results on the IEEE 13-node test feeder demonstrate the effectiveness of the proposed model.

CHAPTER 8: CONCLUSIONS AND FUTURE WORKS

The growth in electricity demand and a continued reliance on fossil fuels for supplying this demand will contribute to the global warming crisis. The rapid and large-scale deployment of renewable energy resources such as wind, solar, and hydrogen due to significant equipment capital cost reduction and net-zero emission energy production policy set by U.S. government are two preeminent factors for power utilities to decarbonize electricity production. While deep decarbonization of electricity production can be achieved with high penetration of renewable energy resources, utilities must consider the role of small-scale DERs in operation and planning policies of distribution power networks to reach the goal of net-zero emission electricity production.

As an important step toward decarbonization of power systems, this dissertation has proposed mathematical models and decision-making tools for power system operation with a high penetration of renewable generation, while incorporating new techno-economic changes induced from the recent transition towards low-carbon power systems. First, a multi-round double auction enabled P2P energy trading framework was proposed in Chapter 3 to provide a novel platform for peers to trade and exchange energy considering the physical constraints and additional costs of distribution networks. Second, in chapter 4, a cooperative operation of PV and hydrogen systems considering the uncertainty and risk level of load, H2 demand, PV power, and market price was proposed to analyze the benefits of H2 systems in normal operation modes. Third, in chapter 5 to analyze the impact of long-duration energy storage in normal and emergency operation mode, a proactive rolling-horizon based bi-level framework operation scheduling of H2 systems considering H2 production cost and emergency capacity based demand response signals was investigated. To analyze the potential benefits of P2P energy exchanges on H2 cost, chapter 6 proposes a detailed model for grid integrated electrolyzer considering non-linear conversion efficiency and polarization curves. Additionally, a P2P optimization framework was developed and integrated to balanced distribution

network. Finally, in chapter 7, cyber-physical vulnerability assessment of P2P energy exchanges in unbalanced distribution networks was investigated by developing a three phase resilience oriented P2P energy sharing model. Cyber attacks from adverse prosumers and adverse consumers as well as physical attacks were considered.

The directions for future research that stem from this dissertation until now are summarized as follows.

- Although P2P energy exchanges bring several opportunities, the challenges of new technologies must be considered in the energy transition. One of the most important aspect of P2P energy exchanges is the privacy of agents. Applying distributed or decentralized methods such as alternating direction method of multipliers (ADMM) algorithms can address this issue. Moreover, to address the uncertainty of customer side DERs (electricity demand, prosumers' generation, etc.), chance constrained, robust, or distributionally robust tools can be applied to the formulation presented in this dissertation as future work.

- Since P2P market models include a lot of IoT devices, cyber attacks might be increased significantly in different layers such as physical, communication, etc. Developing a defender-attacker-defender P2P model to guarantee a safe and reliable operation against cyber-physical attacks, such as false data injection, load redistribution attacks, etc. is required.

- In this dissertation, a detailed model for grid-integrated electrolyzer was developed. However, detailed model for fuel cell is also required to optimally size and operate these systems in active distribution networks. Moreover, natural gas networks as well as water [125] [126] and transportation [127] network modeling can be integrated as extension of H2 related works that are presented in this dissertation.

APPENDIX A: LIST OF PUBLICATIONS

1. **Hamed Haggi** and W. Sun, "Multi-Round Double Auction-enabled Peer-to-Peer Energy Exchange in Active Distribution Networks," *IEEE Transactions on Smart Grid*, Vol. 12, No. 5, pp. 4403-4414, 2021.[Link]

2. **Hamed Haggi**, W. Sun, J. M. Fenton, and P. Brooker "Risk-Averse Cooperative Operation of PV and Hydrogen Systems in Active Distribution Networks ", *IEEE Systems Journal*, 2021. [Link]

3. **Hamed Haggi**, W. Sun, J. M. Fenton, and P. Brooker, "Proactive Rolling Horizon based Scheduling of Hydrogen Systems for Resilient Power Grids", *IEEE Transactions on Industry Applications*, vol. 58, no. 2, pp. 1737-1746, 2022. [Link]

4. **Hamed Haggi**, J. M. Fenton, P. Brooker, and W. Sun "Hydrogen and Battery Storage Technologies for Low Cost Energy Decarbonization in Distribution Networks", *Journal of The Electrochemical Society*, 2022. [Link]

5. **Hamed Haggi**, W. Sun, P. Brooker, and J. M. Fenton "Peer-to-Peer Energy Exchanges for Lowering the Hydrogen Production Cost: Towards Energy Decarbonization", *IEEE Transactions on Power Systems*, Under review, 2022.

6. **Hamed Haggi** and W. Sun "Peer-to-Peer Energy Exchanges for Cyber-Physical Resilience Improvement of Distribution Networks: A Bi-Level Approach", *IEEE Transactions on Smart Grid*, In Preparation, 2022.

7. **Hamed Haggi**, R. R. nejad, M. Song and W. Sun, "A Review of Smart Grid Restoration to Enhance Cyber-Physical System Resilience," *2019 IEEE Innovative Smart Grid Technologies - Asia (ISGT Asia)*, 2019, pp. 4008-4013. (Best paper of 796 accepted papers) [Link]

8. **Hamed Haggi**, W. Sun and J. Qi, "Multi-Objective PMU Allocation for Resilient Power System Monitoring," *2020 IEEE Power and Energy Society General Meeting (PESGM)*,

2020, pp. 1-5.[Link]

9. **Hamed Haggi**, J. M. Fenton, P. Brooker, and W. Sun "Optimal H2 Production and Consumption for Improved Utility Operations: Path to Net-Zero Emission Energy Production", *ECS Meeting Abstracts*, 2021. [Link]

10. **Hamed Haggi**, W. Sun, J. M. Fenton and P. Brooker, "Proactive Scheduling of Hydrogen Systems for Resilience Enhancement of Distribution Networks," *2021 IEEE Kansas Power and Energy Conference (KPEC)*, 2021, pp. 1-5.[Link]

11. **Hamed Haggi**, P. Brooker, W. Sun, and J. M. Fenton "Optimal Dynamic Operation of Grid-Integrated Hydrogen Energy System: A Techno-Economic Analysis", *242nd ECS Meeting Abstracts*, 2022.

12. A. Rahman, X. Gao, J. Xie, I. Alvarez-Fernandez, **Hamed Haggi**, and W. Sun "Challenges and Opportunities in Cyber-Physical Security of Highly DER-Penetrated Power Systems", *2022 IEEE Power and Energy Society General Meeting (PESGM)*, 2022. [Link]

13. **Hamed Haggi** and W. Sun "Cyber-Physical Vulnerability Assessment of P2P Energy Exchanges in Active Distribution Networks", *2022 IEEE Kansas Power and Energy Conference (KPEC)*, 2022. [Link]

14. **Hamed Haggi**, J. M. Fenton, P. Brooker, and W. Sun "Renewable Hydrogen Systems Enabled Deep Energy Decarbonization of Power and Transportation Sectors", *241st ECS Meeting Abstracts*, 2022.

APPENDIX B: LINEARIZATION OF BI-LINEAR TERMS

The DSO objective function is non-linear (multiplying two continuous variables) due to the $\lambda_{t,i}.P_{t,i}^{Exb}$ term, which is defined as NLE. To address the non-linearity, equation (5.46) is used to convert it to a linear equivalent equation:

$$\begin{aligned} NLE = & \sum_{t=1}^{T}(\lambda_{t,i} \,.\, P_{t,i}^{Exb}) = \sum_{t=1}^{T}((\underline{\psi}_{t,i} - \rho_t^b) \,.\, P_{t,i}^{Exb}) = \\ & \sum_{t=1}^{T}(\underline{\psi}_{t,i} \,.\, P_{t,i}^{Exb} - \rho_t^b \,.\, P_{t,i}^{Exb}) \end{aligned} \tag{B.1}$$

Then, by using Karush Kuhn Tucker (KKT) conditions from equation (5.41), the following equation is obtained:

$$\begin{aligned} NLE = & \sum_{t=1}^{T}(\underline{\psi}_{t,i} \,.\, P_{t,i}^{Exb} - \rho_t^b \,.\, P_{t,i}^{Exb}) = \sum_{t=1}^{T}(\underline{\psi}_{t,i} \,.\, P^{UG,max} \\ & - \underline{\psi}_{t,i} \,.\, P^{UG,max} \,.\, U_{i,t} - \rho_t^b \,.\, P_{t,i}^{Exb})) \end{aligned} \tag{B.2}$$

Considering equation (B.2), the term $\underline{\psi}_{t,i}.P^{UG,max}.U_{i,t}$ is the product of binary and continuous variable, which can be linearized based on the big-M method [128] as following:

$$K_{t,i} = \underline{\psi}_{t,i}.P^{UG,max} \tag{B.3}$$

$$-M(1 - U_{t,i}) \leq K_{t,i} - \underline{\psi}_{t,i}.P^{UG,max} \leq M(1 - U_{t,i}) \tag{B.4}$$

$$-M \,.\, U_{t,i} \leq K_{t,i} \leq M \,.\, U_{t,i} \tag{B.5}$$

LIST OF REFERENCES

[1] "Global Energy Transformation: A Roadmap to 2050," [Online].https://www.irena.org.

[2] "H2@scale department of energy (doe)," [Online].https://www.energy.gov/eere/fuelcells/h2scale.

[3] "U.S. Energy Information Administration," [Online].https://www.eia.gov/tools/faqs/faq.php?id=77&t=11.

[4] "International Energy Agency," [Online].https://www.iea.org/reports/net-zero-by-2050.

[5] D. Hsu and D. Ulama, "Building the energy infrastructure necessary for deep decarbonization throughout the united states."

[6] L. J. Vimmerstedt, C. R. Augustine, P. C. Beiter, W. J. Cole, D. J. Feldman, P. Kurup, E. J. Lantz, R. M. Margolis, T. J. Stehly, C. S. Turchi *et al.*, "2018 annual technology baseline (atb)," National Renewable Energy Lab.(NREL), Golden, CO (United States), Tech. Rep., 2018.

[7] H. Haggi, W. Sun, J. M. Fenton, and P. Brooker, "Proactive scheduling of hydrogen systems for resilience enhancement of distribution networks," in *2021 IEEE Kansas Power and Energy Conference (KPEC)*. IEEE, 2021, pp. 1–5.

[8] "Decarbonising society with power-to-x," [Online].https://orsted.com/en/about-us/whitepapers/decarbonising-society-with-power-to-x.

[9] T. Baroche, P. Pinson, R. L. G. Latimier, and H. B. Ahmed, "Exogenous cost allocation in peer-to-peer electricity markets," *IEEE Trans. on Power Syst.*, vol. 34, no. 4, pp. 2553–2564, Jul. 2019.

[10] NRGcoin, “Smart contract for green energy,” https://nrgcoin.org.

[11] Enerchain, “Enerchain decentrally traded decentral energy,” https://enerchain.ponton.de.

[12] P2P3M, “Peer-to-Peer community energy trading,” https://p2pconnecting.wordpress.com/.

[13] T. Sousa, T. Soares, P. Pinson, F. Moret, T. Baroche, and E. Sorin, “Peer-to-peer and community-based markets: A comprehensive review,” *Renew. and Sustain. Energy Reviews*, vol. 104, pp. 367–378, Apr. 2019.

[14] A. Papavasiliou, “Analysis of distribution locational marginal prices,” *IEEE Trans. Smart Grid*, vol. 9, no. 5, pp. 4872–4882, Sep. 2018.

[15] F. Lezama, J. Soares, P. Hernandez-Leal, M. Kaisers, T. Pinto, and Z. Vale, “Local energy markets: Paving the path toward fully transactive energy systems,” *IEEE Transactions on Power Systems*, vol. 34, no. 5, pp. 4081–4088, Jul. 2018.

[16] M. N. Faqiry, L. Edmonds, H. Wu, and A. Pahwa, “Distribution locational marginal price-based transactive day-ahead market with variable renewable generation,” *Applied Energy*, vol. 259, p. 114103, Dec. 2020.

[17] P. Pediaditis, C. Ziras, J. Hu, S. You, and N. Hatziargyriou, “Decentralized dlmps with synergetic resource optimization and convergence acceleration,” *Electric Power Systems Research*, vol. 187, p. 106467, Jul. 2020.

[18] A. Asrari, M. Ansari, J. Khazaei, and P. Fajri, “A market framework for decentralized congestion management in smart distribution grids considering collaboration among electric vehicle aggregators,” *IEEE Transactions on Smart Grid*, vol. 11, no. 2, pp. 1147–1158, Aug. 2019.

[19] S. Hanif, K. Zhang, C. M. Hackl, M. Barati, H. B. Gooi, and T. Hamacher, "Decomposition and equilibrium achieving distribution locational marginal prices using trust-region method," *IEEE Trans. Smart Grid*, vol. 10, no. 3, pp. 3269–3281, May 2019.

[20] K. Zhang, S. Hanif, C. M. Hackl, and T. Hamacher, "A framework for multi-regional real-time pricing in distribution grids," *IEEE Trans. Smart Grid*, Nov. 2019.

[21] T. Morstyn, A. Teytelboym, C. Hepburn, and M. D. McCulloch, "Integrating p2p energy trading with probabilistic distribution locational marginal pricing," *IEEE Trans.actions on Smart Grid*, Jul. 2020.

[22] P. Siano, G. De Marco, A. Rolán, and V. Loia, "A survey and evaluation of the potentials of distributed ledger technology for peer-to-peer transactive energy exchanges in local energy markets," *IEEE Systems Journal*, Sep. 2019.

[23] J. Kang, R. Yu, X. Huang, S. Maharjan, Y. Zhang, and E. Hossain, "Enabling localized peer-to-peer electricity trading among plug-in hybrid electric vehicles using consortium blockchains," *IEEE Trans. Industrial Inform.*, vol. 13, no. 6, pp. 3154–3164, Dec. 2017.

[24] J. Guerrero, A. C. Chapman, and G. Verbič, "Decentralized p2p energy trading under network constraints in a low-voltage network," *IEEE Trans. Smart Grid*, Sep. 2019.

[25] W. Tushar, T. K. Saha, C. Yuen, T. Morstyn, H. V. Poor, R. Bean *et al.*, "Grid influenced peer-to-peer energy trading," *IEEE Trans. Smart Grid*, Aug. 2019.

[26] A. Paudel, K. Chaudhari, C. Long, and H. B. Gooi, "Peer-to-peer energy trading in a prosumer-based community microgrid: A game-theoretic model," *IEEE Trans. on Industrial Electronics*, vol. 66, no. 8, pp. 6087–6097, Aug. 2019.

[27] K. Anoh, S. Maharjan, A. Ikpehai, Y. Zhang, and B. Adebisi, "Energy peer-to-peer trading in virtual microgrids in smart grids: a game-theoretic approach," *IEEE Tran. on Smart Grid*, vol. 11, no. 2, pp. 1264–1275, Mar. 2020.

[28] W. Tushar, T. K. Saha, C. Yuen, T. Morstyn, M. D. McCulloch, H. V. Poor, and K. L. Wood, "A motivational game-theoretic approach for peer-to-peer energy trading in the smart grid," *Applied energy*, vol. 243, pp. 10–20, Jun. 2019.

[29] S. Cui, Y.-W. Wang, Y. Shi, and J.-W. Xiao, "A new and fair peer-to-peer energy sharing framework for energy buildings," *IEEE Trans. on Smart Grid*, Sep. 2020.

[30] W. Tushar, T. K. Saha, C. Yuen, D. Smith, and H. V. Poor, "Peer-to-peer trading in electricity networks: an overview," *IEEE Trans. on Smart Grid*, Jul. 2020.

[31] Z. Li, J. Kang, R. Yu, D. Ye, Q. Deng, and Y. Zhang, "Consortium blockchain for secure energy trading in industrial internet of things," *IEEE transactions on industrial informatics*, vol. 14, no. 8, pp. 3690–3700, Dec. 2017.

[32] T. Zhang, H. Pota, C.-C. Chu, and R. Gadh, "Real-time renewable energy incentive system for electric vehicles using prioritization and cryptocurrency," *Applied energy*, vol. 226, pp. 582–594, Jun. 2018.

[33] J. Kim and Y. Dvorkin, "A p2p-dominant distribution system architecture," *IEEE Trans. on Power Systems*, Jul. 2020.

[34] Z. Zhang, R. Li, and F. Li, "A novel peer-to-peer local electricity market for joint trading of energy and uncertainty," *IEEE Trans. on Smart Grid*, vol. 11, no. 2, pp. 1205–1215, Mar. 2020.

[35] Y. Liu, L. Wu, and J. Li, "Peer-to-peer (p2p) electricity trading in distribution systems of the future," *The Electricity Journal*, vol. 32, no. 4, pp. 2–6, May 2019.

[36] T. Morstyn and M. McCulloch, "Multi-class energy management for peer-to-peer energy trading driven by prosumer preferences," *IEEE Trans. on Power Syst.*, Sep. 2019.

[37] T. Morstyn, A. Teytelboym, and M. D. McCulloch, "Designing decentralized markets for distribution system flexibility," *IEEE Trans. Power Systems*, vol. 34, no. 3, pp. 2128–2139, May 2019.

[38] T. Morstyn, A. Teytelboym, and M. D. Mcculloch, "Bilateral contract networks for peer-to-peer energy trading," *IEEE Trans. Smart Grid*, vol. 10, no. 2, pp. 2026–2035, March 2019.

[39] G. Liang, J. Zhao, F. Luo, S. R. Weller, and Z. Y. Dong, "A review of false data injection attacks against modern power systems," *IEEE Transactions on Smart Grid*, vol. 8, no. 4, pp. 1630–1638, 2016.

[40] R. Dasgupta, A. Sakzad, and C. Rudolph, "Cyber attacks in transactive energy market-based microgrid systems," *Energies*, vol. 14, no. 4, p. 1137, 2021.

[41] D. H. Nguyen, "A cooperative learning approach for decentralized peer-to-peer energy trading markets and its structural robustness against cyberattacks," *IEEE Access*.

[42] C. Barreto, T. Eghtesad, S. Eisele, A. Laszka, A. Dubey, and X. Koutsoukos, "Cyber-attacks and mitigation in blockchain based transactive energy systems," in *2020 IEEE Conference on Industrial Cyberphysical Systems (ICPS)*, vol. 1. IEEE, 2020, pp. 129–136.

[43] Y. Zhang, V. Krishnan, and t. Pi, "Cyber physical security analytics for transactive energy systems," *IEEE Transactions on Smart Grid*, vol. 11, no. 2, pp. 931–941, 2019.

[44] Y. Zhang, S. Eisele, A. Dubey, A. Laszka, and A. K. Srivastava, "Cyber-physical simulation platform for security assessment of transactive energy systems," in *2019 7th Workshop on*

Modeling and Simulation of Cyber-Physical Energy Systems (MSCPES). IEEE, 2019, pp. 1–6.

[45] V. Krishnan, Y. Zhang, K. Kaur, A. Hahn, A. Srivastava, and S. Sindhu, "Cyber-security analysis of transactive energy systems," in *2018 IEEE/PES Transmission and Distribution Conference and Exposition (T&D)*. IEEE, 2018, pp. 1–9.

[46] L. P. M. I. Sampath, A. Paudel, H. D. Nguyen, E. Y. Foo, and H. B. Gooi, "Peer-to-peer energy trading enabled optimal decentralized operation of smart distribution grids," *IEEE Transactions on Smart Grid*, 2021.

[47] A. Rahman, X. Gao, J. Xie, I. Alvarez-Fernandez, H. Haggi, and W. Sun, "Challenges and opportunities in cyber-physical security of highly der-penetrated power systems," *2022 IEEE Power & Energy Society General Meeting (PESGM)*, pp. 1–5, 2022.

[48] R.-H. Lin, Y.-Y. Zhao, and B.-D. Wu, "Toward a hydrogen society: Hydrogen and smart grid integration," *International Journal of Hydrogen Energy*, vol. 45, no. 39, pp. 20 164–20 175, 2020.

[49] A. Buttler and H. Spliethoff, "Current status of water electrolysis for energy storage, grid balancing and sector coupling via power-to-gas and power-to-liquids: A review," *Renewable and Sustainable Energy Reviews*, vol. 82, pp. 2440–2454, 2018.

[50] D. Falcão and A. Pinto, "A review on pem electrolyzer modelling: Guidelines for beginners," *Journal of Cleaner Production*, vol. 261, p. 121184, 2020.

[51] N. A. El-Taweel, H. Khani, and H. E. Farag, "Hydrogen storage optimal scheduling for fuel supply and capacity-based demand response program under dynamic hydrogen pricing," *IEEE Transactions on Smart Grid*, vol. 10, no. 4, pp. 4531–4542, 2018.

[52] A. Kovač, M. Paranos, and D. Marciuš, "Hydrogen in energy transition: A review," *International Journal of Hydrogen Energy*, 2021.

[53] "Road Map to US Hydrogen Economy," [Online].http://www.fchea.org/us-hydrogen-study.html.

[54] H. Khani, N. El-Taweel, and H. E. Z. Farag, "Supervisory scheduling of storage-based hydrogen fueling stations for transportation sector and distributed operating reserve in electricity markets," *IEEE Transactions on Industrial Informatics*, vol. 16, no. 3, pp. 1529–1538, 2019.

[55] H. E. Farag, A. Al-Obaidi, H. Khani, N. El-Taweel, E. El-Saadany, and H. Zeineldin, "Optimal operation management of distributed and centralized electrolysis-based hydrogen generation and storage systems," *Electric Power Systems Research*, vol. 187, p. 106476, 2020.

[56] W. Xiao, Y. Cheng, W.-J. Lee, V. Chen, and S. Charoensri, "Hydrogen filling station design for fuel cell vehicles," *IEEE Transactions on Industry Applications*, vol. 47, no. 1, pp. 245–251, 2010.

[57] G. Taljan, C. Cañizares, M. Fowler, and G. Verbic, "The feasibility of hydrogen storage for mixed wind-nuclear power plants," *IEEE Transactions on Power Systems*, vol. 23, no. 3, pp. 1507–1518, 2008.

[58] M. Eypasch, M. Schimpe, A. Kanwar, T. Hartmann, S. Herzog, T. Frank, and T. Hamacher, "Model-based techno-economic evaluation of an electricity storage system based on liquid organic hydrogen carriers," *Applied energy*, vol. 185, pp. 320–330, 2017.

[59] C. Blazquez-Diaz, "Techno-economic modelling and analysis of hydrogen fuelling stations," *International Journal of Hydrogen Energy*, vol. 44, no. 2, pp. 495–510, 2019.

[60] S. Seyyedeh-Barhagh, M. Majidi, S. Nojavan, and K. Zare, "Optimal scheduling of hydrogen storage under economic and environmental priorities in the presence of renewable units and demand response," *Sustainable Cities and Society*, vol. 46, p. 101406, 2019.

[61] H. Shokouhandeh, M. Ghaharpour, H. G. Lamouki, Y. R. Pashakolaei, F. Rahmani, and M. H. Imani, "Optimal estimation of capacity and location of wind, solar and fuel cell sources in distribution systems considering load changes by lightning search algorithm," in *2020 IEEE Texas Power and Energy Conference (TPEC)*. IEEE, 2020, pp. 1–6.

[62] H. Haggi, W. Sun, J. M. Fenton, and P. Brooker, "Risk-averse cooperative operation of pv and hydrogen systems in active distribution networks," *IEEE Systems Journal*, 2021.

[63] M. Rahmanzadeh, H. Haggi, and M. Aliakbar Golkar, "Optimal energy management of microgrid based on fcchp in the presence of electric and thermal loads considering energy storage systems," 2018.

[64] Y. Xiao, X. Wang, P. Pinson, and X. Wang, "A local energy market for electricity and hydrogen," *IEEE Transactions on Power Systems*, vol. 33, no. 4, pp. 3898–3908, 2017.

[65] M. A. Mirzaei and et.al, "Stochastic security-constrained operation of wind and hydrogen energy storage systems integrated with price-based demand response," *International Journal of Hydrogen Energy*, vol. 44, no. 27, pp. 14 217–14 227, 2019.

[66] D. Yu and e. Wang, "Risk-averse stochastic operation of a power system integrated with hydrogen storage system and wind generation in the presence of demand response program," *International Journal of Hydrogen Energy*, vol. 44, no. 59, pp. 31 204–31 215, 2019.

[67] X. Wu, H. Li, X. Wang, and W. Zhao, "Cooperative operation for wind turbines and hydrogen fueling stations with on-site hydrogen production," *IEEE Transactions on Sustainable Energy*, vol. 11, no. 4, pp. 2775–2789, 2020.

[68] S. R. Khazeiynasab and J. Qi, "Resilience analysis and cascading failure modeling of power systems under extreme temperatures," *Journal of Modern Power Systems and Clean Energy*, vol. 9, no. 6, pp. 1446–1457, 2021.

[69] M. Gilvanejad, M. Goodarzi, and H. Ghadiri, "Introduction of configurational indicators for distribution network optimality based on a zoning methodology," *AUT Journal of Electrical Engineering*, vol. 53, no. 2, pp. 2–2, 2021.

[70] H. Haggi, M. Song, W. Sun *et al.*, "A review of smart grid restoration to enhance cyber-physical system resilience," in *2019 IEEE Innovative Smart Grid Technologies-Asia (ISGT Asia)*, 2019, pp. 4008–4013.

[71] H. T. Nguyen, J. Muhs, and M. Parvania, "Preparatory operation of automated distribution systems for resilience enhancement of critical loads," *IEEE Transactions on Power Delivery*, 2020.

[72] A. Gholami, T. Shekari, and S. Grijalva, "Proactive management of microgrids for resiliency enhancement: An adaptive robust approach," *IEEE Trans. on Sustainable Energy*, vol. 10, no. 1, pp. 470–480, 2017.

[73] A. Hussain, V.-H. Bui, and H.-M. Kim, "A proactive and survivability-constrained operation strategy for enhancing resilience of microgrids using energy storage system," *IEEE Access*, vol. 6, pp. 75 495–75 507, 2018.

[74] M. Amirioun, F. Aminifar, and H. Lesani, "Resilience-oriented proactive management of microgrids against windstorms," *IEEE Transactions on Power Systems*, vol. 33, no. 4, pp. 4275–4284, 2017.

[75] M. H. Amirioun, F. Aminifar, and M. Shahidehpour, "Resilience-promoting proactive scheduling against hurricanes in multiple energy carrier microgrids," *IEEE Transactions on Power Systems*, vol. 34, no. 3, pp. 2160–2168, 2019.

[76] H. Haggi and W. Sun, "Multi-round double auction-enabled peer-to-peer energy exchange in active distribution networks," *IEEE Transactions on Smart Grid*, vol. 12, no. 5, pp. 4403–4414, 2021.

[77] H. Yuan, F. Li, Y. Wei, and J. Zhu, "Novel linearized power flow and linearized opf models for active distribution networks with application in distribution lmp," *IEEE Trans. Smart Grid*, vol. 9, no. 1, pp. 438–448, Jan. 2018.

[78] Z. Wang, X. Yu, Y. Mu, and H. Jia, "A distributed peer-to-peer energy transaction method for diversified prosumers in urban community microgrid system," *Applied Energy*, vol. 260, p. 114327, Feb. 2020.

[79] L. Bai, J. Wang, and C. t. Wang, "Distribution locational marginal pricing (dlmp) for congestion management and voltage support," *IEEE Trans. Power Syst.*, vol. 33, no. 4, pp. 4061–4073, Jul. 2018.

[80] PJM, "Locational marginal pricing in PJM markets," http://pjm.com/markets-and-operations/energy/lmp-model, May 2019.

[81] J. Yang, J. Zhao, and J. t. Qiu, "A distribution market clearing mechanism for renewable generation units with zero marginal costs," *IEEE Trans. Industrial Inform.*, vol. 15, no. 8, pp. 4775–4787, Aug. 2019.

[82] M. E. Baran and F. F. Wu, "Network reconfiguration in distribution systems for loss reduction and load balancing," *IEEE Power Engineering Review*, vol. 9, no. 4, pp. 101–102, Apr. 1989.

[83] H. Khodr, F. Olsina, P. De Oliveira-De Jesus, and J. Yusta, "Maximum savings approach for location and sizing of capacitors in distribution systems," *Electric Power Systems Research*, vol. 78, no. 7, pp. 1192–1203, Dec. 2008.

[84] R. D. Zimmerman, C. E. Murillo-Sánchez, and R. J. Thomas, "Matpower: Steady-state operations, planning, and analysis tools for power systems research and education," *IEEE Transactions on power systems*, vol. 26, no. 1, pp. 12–19, Jun. 2010.

[85] Y. Riffonneau, S. Bacha, F. Barruel, and S. Ploix, "Optimal power flow management for grid connected pv systems with batteries," *IEEE Transactions on sustainable energy*, vol. 2, no. 3, pp. 309–320, 2011.

[86] F. Rahmani, M. A. Robinson, and M. Barzegaran, "Cool roof coating impact on roof-mounted photovoltaic solar modules at texas green power microgrid," *International Journal of Electrical Power & Energy Systems*, vol. 130, p. 106932, 2021.

[87] F. Rahmani, M. S. Mashhadi, H. G. Lamouki, F. Asghari, H. Shokouhandeh, and M. Amoozadeh, "Maximum power point tracking–a study of photovoltaic systems in supplying stand-alone and grid-connected electrical loads," in *2021 International Conference on Applied and Theoretical Electricity (ICATE)*. IEEE, 2021, pp. 1–6.

[88] M. S. Hossan and B. Chowdhury, "Integrated cvr and demand response framework for advanced distribution management systems," *IEEE Transactions on Sustainable Energy*, vol. 11, no. 1, pp. 534–544, 2019.

[89] N. E. M. Association *et al.*, *American National Standard for Electric Power Systems and Equipment-Voltage Ratings (60 Hertz)*. National Electrical Manufacturers Association, 1996.

[90] S. Wang, S. Chen, L. Ge, and L. Wu, "Distributed generation hosting capacity evaluation for distribution systems considering the robust optimal operation of oltc and svc," *IEEE Transactions on Sustainable Energy*, vol. 7, no. 3, pp. 1111–1123, 2016.

[91] H. Ahmadi and J. R. Martı, "Linear current flow equations with application to distribution systems reconfiguration," *IEEE Transactions on Power Systems*, vol. 30, no. 4, pp. 2073–2080, 2014.

[92] P. M. Castro, "Tightening piecewise mccormick relaxations for bilinear problems," *Computers & Chemical Eng.*, vol. 72, pp. 300–311, 2015.

[93] M. E. Khodayar, M. Barati, and M. Shahidehpour, "Integration of high reliability distribution system in microgrid operation," *IEEE Transactions on Smart Grid*, vol. 3, no. 4, pp. 1997–2006, 2012.

[94] B. Vatandoust, A. Ahmadian, M. A. Golkar, A. Elkamel, A. Almansoori, and M. Ghaljehei, "Risk-averse optimal bidding of electric vehicles and energy storage aggregator in day-ahead frequency regulation market," *IEEE Trans. on Power Systems*, vol. 34, no. 3, pp. 2036–2047, 2018.

[95] A. J. Conejo, M. Carrión, J. M. Morales *et al.*, *Decision making under uncertainty in electricity markets*. Springer, 2010, vol. 1.

[96] T. Shekari, S. Golshannavaz, and F. Aminifar, "Techno-economic collaboration of pev fleets in energy management of microgrids," *IEEE Transactions on Power Systems*, vol. 32, no. 5, pp. 3833–3841, 2016.

[97] K. Deb, *Multi-objective optimization using evolutionary algorithms*. John Wiley & Sons, 2001, vol. 16.

[98] R. D. Zimmerman, C. E. Murillo-Sánchez, and R. J. Thomas, "Matpower: Steady-state operations, planning, and analysis tools for power systems research and education," *IEEE Transactions on Power Systems*, vol. 26, no. 1, pp. 12–19, 2011.

[99] R. Mieth and Y. Dvorkin, "Data-driven distributionally robust optimal power flow for distribution systems," *IEEE Control Systems Letters*, vol. 2, no. 3, pp. 363–368, 2018.

[100] "Fuel Cell Electric Vehicle Data," [Online].https://www.fueleconomy.gov/feg/fcv_sbs.shtml.

[101] S. Gharebaghi, A. Safdarian, and M. Lehtonen, "A linear model for ac power flow analysis in distribution networks," *IEEE Systems Journal*, vol. 13, no. 4, pp. 4303–4312, 2019.

[102] S. R. Khazeiynasab, J. Zhao, and N. Duan, "Wecc composite load model parameter identification using deep learning approach," in *2022 IEEE Power & Energy Society General Meeting (PESGM)*. IEEE, 2022, pp. 1–5.

[103] H. Haggi *et al.*, "Proactive rolling-horizon-based scheduling of hydrogen systems for resilient power grids," *IEEE Transactions on Industry Applications*, vol. 58, no. 2, pp. 1737–1746, 2022.

[104] M. A. El-Meligy, M. Sharaf, and A. T. Soliman, "A coordinated scheme for transmission and distribution expansion planning: A tri-level approach," *Electric Power Systems Research*, vol. 196, p. 107274, 2021.

[105] A. Hassan and Y. Dvorkin, "Energy storage siting and sizing in coordinated distribution and transmission systems," *IEEE Transactions on Sustainable Energy*, vol. 9, no. 4, pp. 1692–1701, 2018.

[106] M. Farivar and S. H. Low, "Branch flow model: Relaxations and convexification—part i," *IEEE Trans. Power Systems*, vol. 28, no. 3, pp. 2554–2564, Apr. 2013.

[107] H. Haggi, F. Hasanzad, and M. Golkar, "Security-constrained unit commitment considering large-scale compressed air energy storage (caes) integrated with wind power generation," *International Journal of Smart Electrical Engineering*, vol. 6, no. 04, pp. 127–134, 2017.

[108] J. M. Arroyo, "Bilevel programming applied to power system vulnerability analysis under multiple contingencies," *IET generation, transmission & distribution*, vol. 4, no. 2, pp. 178–190, 2010.

[109] C. Ordoudis, P. Pinson, J. M. Morales, and M. Zugno, "An updated version of the ieee rts 24-bus system for electricity market and power system operation studies," *Technical University of Denmark*, pp. 0885–8950, 2016.

[110] W. Sun, N. Kadel, I. Alvarez-Fernandez, R. R. Nejad, and A. Golshani, "Optimal distribution system restoration using phevs," *IET Smart Grid*, vol. 2, no. 1, pp. 42–49, 2018.

[111] R. Rosenthal, "GAMS-a user's guide, gams release 24.6. 1," 2016.

[112] "Heavy duty fuel cell trucks," [Online].https://www.hydrogen.energy.gov/pdfs/19006_hydrogen_class8_long_haul_truck_targets.pdf.

[113] F. Scheepers *et al.*, "Improving the efficiency of pem electrolyzers through membrane-specific pressure optimization," *Energies*, vol. 13, no. 3, p. 612, 2020.

[114] M. Goodarzi and Q. Li, "Evaluate the capacity of electricity-driven water facilities in small communities as virtual energy storage," *Applied Energy*, vol. 309, p. 118349, 2022.

[115] "California ISO Supply and Demand Data," [Online].http://www.caiso.com/TodaysOutlook/Pages/default.aspx.

[116] Z. Abdin, C. Webb, and E. M. Gray, "Modelling and simulation of a proton exchange membrane (pem) electrolyser cell," *International Journal of Hydrogen Energy*, vol. 40, no. 39, pp. 13 243–13 257, 2015.

[117] "Annual merit review for u.s. department of energy hydrogen and fuel cell technologies office," U.S. Department of Energy, Tech. Rep., 2022.

[118] H. Haggi, J. M. Fenton, P. Brooker, and W. Sun, "Renewable hydrogen systems enable deep energy decarbonization of power and transportation sectors," in *ECS Meeting Abstracts*, no. 39. IOP Publishing, 2022, p. 1785.

[119] H. Haggi, P. Brooker, W. Sun, and J. M. Fenton, "Hydrogen and battery storage technologies for low-cost energy decarbonization in distribution networks," *Journal of The Electrochemical Society*, vol. 169, no. 6, p. 064501, 2022.

[120] H. Haggi, J. M. Fenton, P. Brooker, and W. Sun, "Optimal h2 production and consumption for improved utility operations: Path to net-zero emission energy production," in *ECS Meeting Abstracts*, no. 46. IOP Publishing, 2021, p. 1877.

[121] H. Haggi and W. Sun, "Cyber-physical vulnerability assessment of p2p energy exchanges in active distribution networks," *arXiv preprint arXiv:2204.12081*, 2022.

[122] S. Mehrdad, S. Mousavian, G. Madraki, and Y. Dvorkin, "Cyber-physical resilience of electrical power systems against malicious attacks: A review," *Current Sustainable/Renewable Energy Reports*, vol. 5, no. 1, pp. 14–22, 2018.

[123] R. R. Nejad and W. Sun, "Distributed load restoration in unbalanced active distribution systems," *IEEE Transactions on Smart Grid*, vol. 10, no. 5, pp. 5759–5769, 2019.

[124] "IEEE PES Distribution Test Feeders," [Online].https://cmte.ieee.org/pes-testfeeders/resources/.

[125] M. Goodarzi and Q. Li, "Security-constrained optimal operation of energy-water nexus based on a fast contingency filtering method," *arXiv preprint arXiv:2201.10785*, 2022.

[126] M. Goodarzi, D. Wu, and Q. Li, "Fast security evaluation for operation of water distribution systems against extreme conditions," in *2021 American Control Conference (ACC)*. IEEE, 2021, pp. 3495–3500.

[127] S. Baghali, Z. Guo, W. Wei, and M. Shahidehpour, "Electric vehicles for distribution system load pickup under stressed conditions: A network equilibrium approach," *IEEE Transactions on Power Systems*, 2022.

[128] W. Wu, Z. Tian, and B. Zhang, "An exact linearization method for oltc of transformer in branch flow model," *IEEE Transactions on Power Systems*, vol. 32, no. 3, pp. 2475–2476, 2016.